Exploring miRNAs as Modulators in Retinal Degeneration: Potential Therapeutic Tools for Inherited Retinal Dystrophies

Thesis

Exploring miRNAs as Modulators in Retinal Degeneration:

Potential Therapeutic Tools for Inherited Retinal Dystrophies

Thesis submitted for the Degree of Doctor of Philosophy in

Life, Health & Chemical Sciences

The Open University

Affiliated Research Centre:

Telethon Institute of Genetics and Medicine, Pozzuoli, Italy

PhD student: Irene Guadagnino

Director of studies: Prof. Sandro Banfi

Internal supervisor: Dr Marianthi Karali

External supervisor: Dr Paola Bovolenta

CONTENTS

SUMMARY OF FIGURES

LIST OF ABBREVIATIONS

µg: microgram

µL: microliter

µM: micromolar

AAV: Adeno-associated viral

ac-pre-miRNA: AGO2-cleaved precursor miRNA

AD: Autosomal dominant

adIRDs: Autosomal dominant IRDs

AGO: Argonaute

Aipl1: Aryl hydrocarbon interacting protein-like 1

AMD: Age-related macular degeneration

AMP: Adenosine monophosphate

AMPK: AMP-activated protein kinase

AR: Autosomal recessive

arIRDs: Autosomal recessive IRDs

BDNF: Brain-derived neurotrophic factor

BP: Biological processes

BRB: Blood-retina barrier

CAT: Catalase

CCR4: Carbon catabolite repressor 4

CD: Cone Dystrophies

cGMP: Cyclic guanosine monophosphate

cKO: Conditional Knocking out

CLN: Neuronal ceroid lipofuscinosis

CMV: Cytomegalovirus

CNS: Central nervous system

CNTF: Ciliary neurotrophic factor

CRD: Cone-Rod Dystrophies

DEGs: Differentially Expressed Genes

DGCR8: DiGeorge Syndrome Critical Region 8

DMEM: Dulbecco's modified eagle medium

DMSO: Dimethyl sulfoxide

dsRBP: dsRNA-binding protein

Duox: Dual oxidase

ECL: Enhanced chemiluminescence

ER: Endoplasmic reticulum

ES: Enrichment score

ESCs: Embryonic pluripotent cells

ETC: Electric transport chain

FBS: Fetal Bovine Serum

FDR: False Discovery Rate

GCL: Ganglion cell layer

GCs: Genome copies

GDNF: Glial cell-derived neurotrophic factor

GITs: Gene Independent Therapies

GOEA: Gene Ontology Enrichment Analysis

GS6: Glutamine synthetase

GSH: Glutathione

GSSG: Oxidized glutathione

GW182: Glycine-tryptophan protein of 182 kDa

h: Hours

H_2DCFDA: 2',7'-dichlorodihydrofluorescein diacetate

HCS: High-Content Screening

IFN-γ: Interferon gamma

IGF-1: Insulin-like growth factors

IL-1β: Interleukin-1 beta

IL-6: Interleukin-6

INL: Inner nuclear layer

IPL: Inner plexiform layer

iPSCs: Induced pluripotent stem cells

IRDs: Inherited retinal dystrophies

ISH: In situ hybridization

LCA: Leber Congenital Amaurosis

LPS: Lypopolysaccharide

LRAT: Lecithinretinol acyltransferase

LUC: luciferase

mg: milligram

MHC-II: Major Histocompatibility Complex class II

min: minutes

miRISC: miRNA-induced silencing complex

miRNAs: microRNAs

mL: Milliliter

NAC: N-acetyl cysteine

NADPH: Nicotinamide adenine dinucleotide phosphate

NF: Nerve fiber

ng: Nanogram

NGF: Neurotrophin nerve growth factor

nm: nanometer

nM: nanomolar

NO: Nitric oxide

NOT: Negative regulator of transcription

Nox: NADPH oxidases

NR: Neural retina

nt: Nucleotide

ONL: Outer nuclear layer

OPL: Outer plexiform layer

OS: Outer segment

PDE: Phosphodiesterase

PEDF: Pigment epithelium derived factor

PFA: Paraformaldehyde

PN: Post-natal

pre-miRNA: precursor miRNA

pri-miRNA: primary miRNA

QC: quality control

RCD: Rod-Cone Dystrophies

RdCVF: Rod-derived cone viability factor

Rho: Rhodopsin

RISC: RNA-induced silencing complex

RNA Pol II: RNA polymerase II

RNAase III: Ribonuclease III

ROS: Reactive oxygen species

RP: Retinitis Pigmentosa

RPE: Retinal pigment epithelium

RPE65: RPE-specific 65-kDa protein

RQ: relative quantity

SDS-PAGE: Sodium dodecyl sulphate-polyacrylamide gel electrophoresis

SEM: standard error of the mean

SOD: Superoxide dismutase

SPF: Specific pathogen-free

SSMD: Strictly Standardized Mean Difference

STAT3: Signal transducer and activator of transcription 3

TGF-β1: Transforming growth factor beta 1

TNF-α: Tumor necrosis factor alpha

TNRC6: Trinucleotide repeat containing gene 6

TRBP: Trans-activation-responsive RNA-binding protein

TRP: Transient receptor potential

TSSs: Transcriptional start sites

UPR: Unfolded protein response

UTR: Untranslated region

WT: Wild-type

XPO5: Exportin 5

ABSTRACT

Inherited retinal dystrophies (IRDs) are a large group of genetic diseases that lead to retinal degeneration and represent a major cause of vision impairment or blindness. The high genetic heterogeneity of IRDs hinders a broad application of gene-specific therapies. There is an unmet need for therapies that can target common pathological mechanisms, regardless of the genetic cause. MicroRNAs (miRNAs) are important players in retinal biology and my group has demonstrated that miR-204 has a pathogenic role in human IRDs. Due to their pleiotropic actions, miRNAs represent promising therapeutic tools.

On this basis, I hypothesized that the modulation of miR-204 levels, as well as other miRNAs, could represent a valid approach to tackle retinal degeneration.

The first part of my thesis elucidates the potential of miR-204 administration as a therapeutic approach for IRDs. I found that administration of miR-204 by an adeno-associated viral (AAV) vector at patient-relevant stages of disease progression led to a long-term preservation of retinal function in a mouse model for a dominant form of Retinitis Pigmentosa (RP). Interestingly, transcriptome analysis revealed that miR-204 effect is mediated by dampening pathological processes shared by different IRDs (e.g. innate immune response).

The second part of my work was focused on identifying additional miRNAs that can exert a protective action in IRDs in a gene-independent manner. Using a High Content Screening (HCS) approach I tested 560 miRNAs in a model of oxidative stress-induced retinal degeneration, the light-damage in cone-like cells (661W). As a result, I found that miR-429 significantly preserved 661W viability during photo-stress. Further analysis revealed that miR-429 overexpression increases the activated form of the pro-survival AMP-activated protein kinase (AMPK), recently demonstrated to be protective during retinal degeneration.

Overall, the results of this thesis indicate that modulation of miRNAs can be a promising approach to develop mutation-independent treatments for IRDs.

1 INTRODUCTION

1.1 The retina

The retina is a highly specialized sensory tissue that covers the inner surface of the posterior part of the eye. The function of the retina is to capture light stimuli and process them into neural information sent to the higher visual centers. The retina is considered part of the central nervous system (CNS) considering its neuroectodermal origin. In particular, during embryogenesis, the anterior part of the brain produces a bilateral protrusion, the primary optic vesicles, that invaginate and give rise to a double-walled formation called the optic cup (*1, 2*). The optic cup comprises the layers that will subsequently become the two main components of the retina: the neural retina (NR), which constitutes the sensory part and derives from the inner layer of the optic cup, and the retinal pigment epithelium (RPE), originating from the outer layer of the optic cup (*2*) and consisting of a single layer of melanin-containing cells

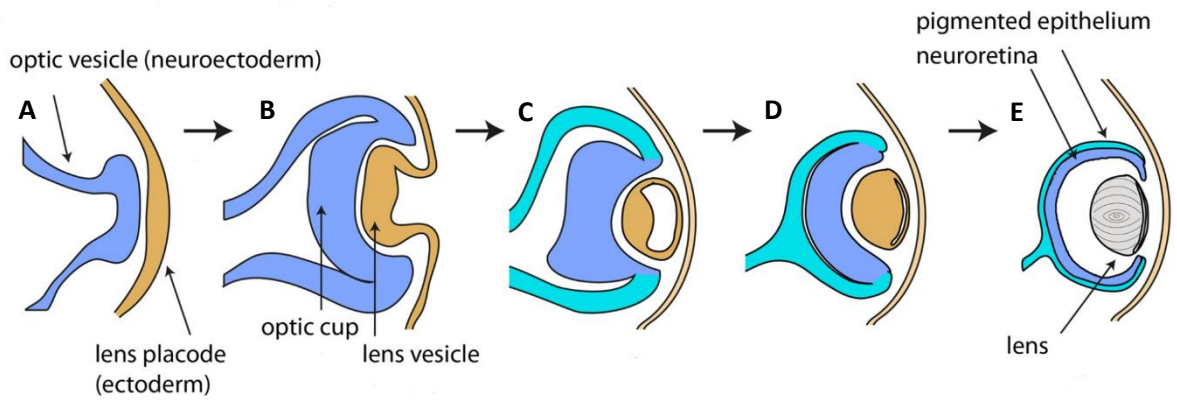

Figure 1. Overview of human eye development during embryogenesis.

The optic vesicles derive from the forebrain neuroectoderm and induce the adjacent ectoderm to form the lens placode (A). The optic vesicle folds in on itself, forming the optic cup, which partially encapsulates the invaginating lens vesicle (interrupted posteriorly by the optic fissure) (B). The optic cup subsequently differentiates into two main layers, the neuroretina and the retinal pigment epithelium, while the lens vesicle thickens and forms the

lens (C,D,E). The neural cells in the neuroretina differentiate from the center to the periphery of the optic disc, leading to the adult retina pattern, which is formed by circumferential zones enriched in specific photoreceptors. Image and caption adapted from Gaspar *et al*.,2018 (*2*).

The sensory neural retina is responsible for the transformation of photons into electric impulses, a process known as phototransduction. These electric signals are then relayed *via* the optic nerve to the visual centers of the brain, where they are further integrated and processed to enable visual perception. Such a specialized function requires a highly organized architecture shaped in different *laminae*. Specifically, the structure of the neural retinal is composed of six major classes of neurons whose cell bodies are organized in three different nuclear layers, the outer nuclear layer (ONL), the inner nuclear layer (INL) and the ganglion cell layer (GCL) that alternate with two layers of synaptic neuropils, the inner and outer plexiform layer (IPL and OPL) (Figure 2).

The ONL contains the cell bodies of the sensory neurons, the photoreceptors (PRs), which transfer the signal to second order neurons, the bipolar cells, whose cell bodies are located in the INL together with the amacrine and horizontal cells. The bipolar cells also communicate with third order neurons, the retinal ganglion cells (RGCs), which reside in the ganglion cell layer (GCL) and are responsible for the transmission of the electric signal outside the retina via the optic nerve.

In the outer plexiform layer (OPL), the axons of photoreceptors make synapses with the dendritic processes of the vertically running bipolar cells and the neurites of the horizontal cells, while in the inner plexiform layer (IPL), the bipolar cells connect with the ganglion cells and amacrine cells. The horizontal and amacrine cells are important to integrate and modulate the synaptic signals.

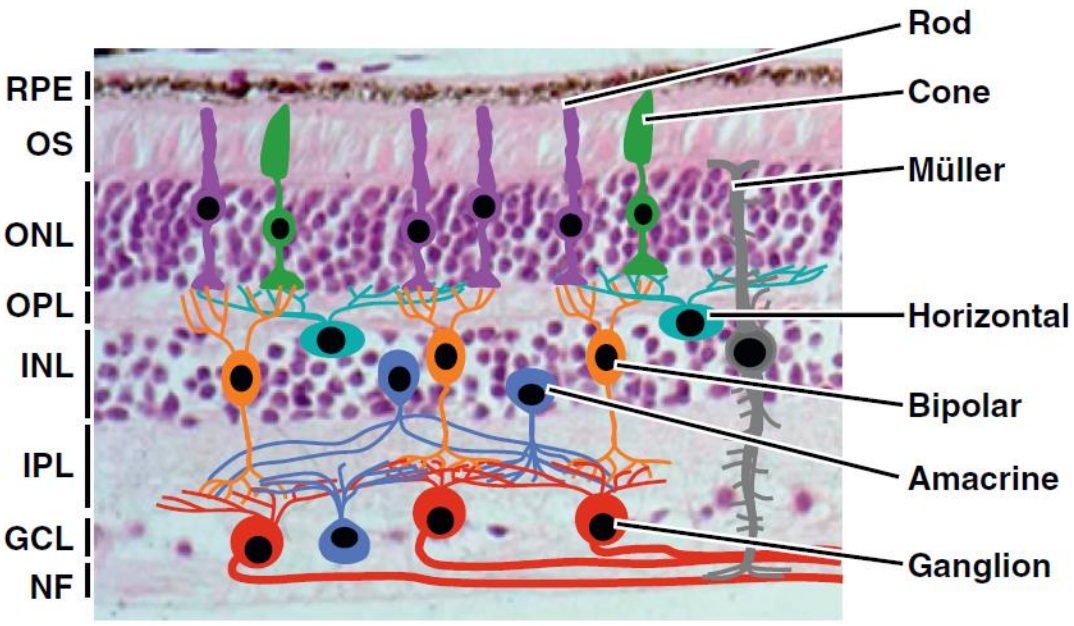

Figure 2. Organization of the vertebrate retina.

Histological image overlaid with a schematic diagram of the mature murine retina structure, as an example of the vertebrate retina. The photoreceptor cell bodies reside in the outer nuclear layer (ONL) and their outer segments (OS) are in contact with the retinal pigment epithelium (RPE). The inner nuclear layer (INL) contains the cell bodies of horizontal, bipolar, and amacrine cells, as well as Müller glia. The ganglion cell layer (GCL) contains the cell bodies of both ganglion and displaced amacrine cells. Connections between the photoreceptor, bipolar, and horizontal cells are found in the outer plexiform layer (OPL), whereas synapses between bipolar, ganglion, and amacrine cells occur in the inner plexiform layer (IPL). The ganglion cell (GC) axons form the nerve fiber (NF) layer. Image and caption from Bassett and Wallace, 2012 (*3*).

In addition to the aforementioned six classes of neurons, the non-neuronal glial cells contribute to the maintenance and functioning of the neural retina. In 1892, Cajal identified three main populations of glial cells in the retina that are now classified as Müller cells, astrocytes and microglia (4). The retinal glial cell types differ both in terms of distribution and function. Müller cells and astrocytes are macroglia cell types. Their processes and end-feet encircle the blood vessel, playing a fundamental role in the formation and maintenance of the

blood-retina barrier (5). While astrocytes are mostly confined to the innermost layers, Müller cells stretch across all the retinal layers (Figure 3). Microglia cells instead are present within the different inner layers, including OPL, INL, IPL, GCL and the nerve fiber layer (NFL), but their spatial distribution changes under pathological conditions as later discussed in the sections 1.4.1 and 3.5.

In terms of function, retina glial cells are important for the maintenance of structural architecture and homeostasis, the provision of nutrients, the modulation of neuronal communication and synaptic connectivity, and the phagocytosis of neuronal debris. Furthermore, microglial cells are the resident macrophages within the CNS and represent the main immune cells in the retina. However, it was shown that also Müller cells and astrocytes can contribute to the retinal response to harmful stimuli (*6*).

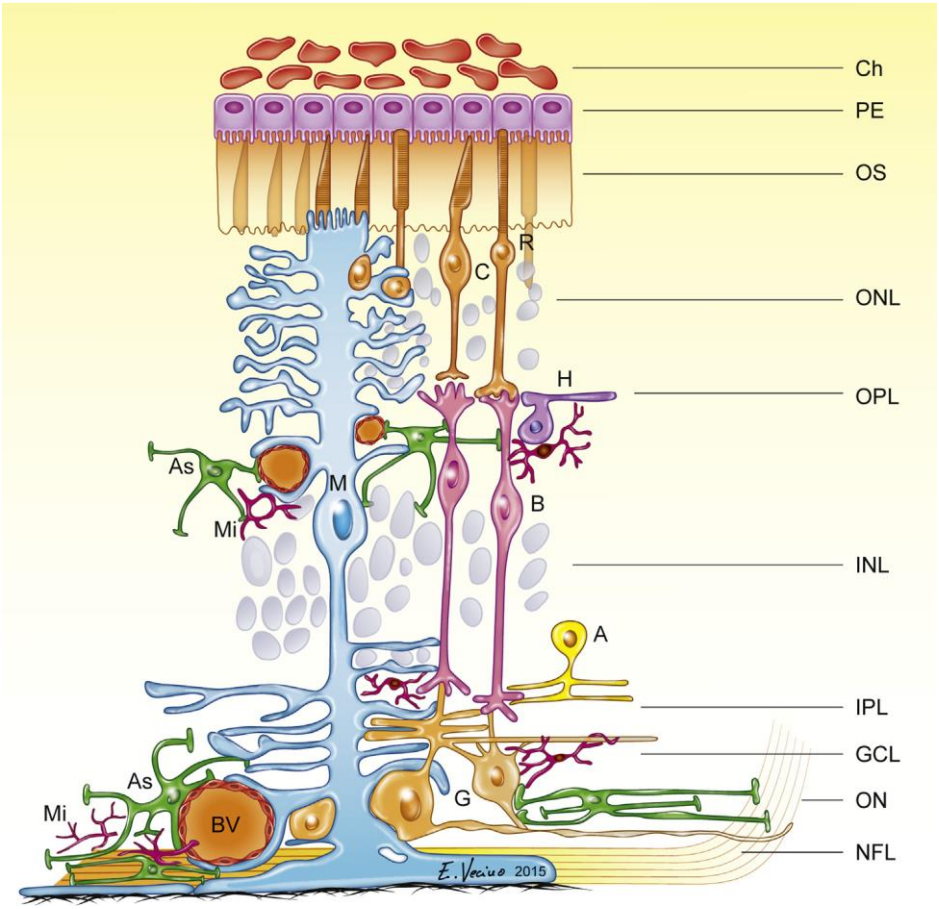

Figure 3. Schematic representation of the glial and neuronal cell types in the mammalian retina.

Müller cells, astrocytes and microglia are the most abundant types of glia in vertebrate retina. Müller cells represent 90% of the retinal glia. They are radially oriented cells and span the entire thickness of the retina. Astrocytes are almost exclusively confined to the innermost retinal layers and their presence and distribution is correlated with the presence and distribution of retina blood vessels. Both Müller cells and astrocytes have the ability to ensheath axons, and to form glial boundaries between the retina and the blood vessels. Microglial cells have a small ovoid-shaped cell body and multiple ramifications in the GCL of the normal retina, and they are organized into a single sheet that is distributed homogeneously. In healthy conditions they are found at variable densities in the different retinal layers, including the NFL, GCL, IPL, INL and OPL. Image from Vacino *et al.*, 2016 (6).

The retinal pigment epithelium (RPE) separates the neural retina from the underlying capillary bed (the choriocapillaris), providing structural, metabolic and functional support to the outer neural retina (*7*). The RPE is important not only for maintaining retinal adhesion but also for

supporting the function and integrity of PRs. The latter is achieved by: 1) the phagocytosis of the PR shed membranes in the outer segment (OS) and the recycling of key elements for the visual cycle; 2) the regulation of the nutrient, molecules and ion flow from the blood to the outer retina and *vice versa (8)*; and 3) by partaking in the process of light absorption and filtering (*9*).

1.2 An overview of Inherited retinal dystrophies (IRDs)

IRDs are a broad group of heterogeneous genetic diseases characterized by degeneration of the retina that ultimately results in loss of vision and blindness. Collectively, IRDs have an estimated incidence of 1:2000 and represent the leading cause of vision loss in people of working-age in the Western world (*10*). The most prevalent form of IRD is Retinitis pigmentosa (RP), which affects 1 in 3000-4000 people worldwide. Leber Congenital Amaurosis (LCA) is considered the most severe form, with an early onset either at birth or in the first years of life (*11*). Overall, IRDs encompass a complex spectrum of diseases with a large clinical and genetic heterogeneity. In this respect, causative mutations have been identified in over 200 genes (RetNet, https://sph.uth.edu/retnet/home.htm) that are mainly expressed in the RPE or photoreceptors cells. These genes encode proteins with diverse functions in the context of the retina; some are structural components of retinal cells, others play important roles in relevant pathways, such as phototransduction and the retinoid cycle, among others. Moreover, mutations in the same gene can be associated with different clinical manifestations, further extending the heterogeneity of IRDs. In some cases, even patients harbouring the same

variants in an IRD gene show different clinical manifestations (*12, 13*), underscoring the complexity of diagnosis and patient management.

IRDs may manifest either as non-syndromic forms, when the disease phenotype affects only the retina, or in the context of syndromic conditions with extraretinal manifestations. An example of the latter form is Usher syndrome, in which RP is combined with hearing loss and, in some cases, vestibular dysfunction. IRDs can also be classified on the basis of the natural history of the disease (progressive or stationary) and the mode of inheritance (autosomal dominant, AD, autosomal recessive, AR, X-linked or mitochondrial). IRDs are also commonly classified according to the retinal cell type that is primarily affected (i.e. rods or cones). On this basis, in Rod-Cone Dystrophies (RCD), such as RP, rods degenerate first and cone demise occurs as a consequence of that. On the other hand, in Cone-Rod Dystrophies (CRD), the degeneration of cone PRs is usually followed by the subsequent death of rods. In Cone Dystrophies (CD) instead, the degeneration of cones does not necessarily impact rod function and viability. At the very early stages of the disease, it is possible to discriminate between these two groups (i.e. RCD or CRD), depending on whether the initial symptoms are impaired night vision (indicative of rod dysfunction) or defects in visual acuity and color vision (due to cone dysfunction). However, as the degeneration progresses, it becomes difficult to distinguish between the primary rod or cone involvement. Finally, the so-called generalised IRDs (e.g. the severe LCA) present the simultaneous degeneration of rods and cones in association with a primary involvement of the RPE.

1.3 Suitable experimental models to test therapeutic approaches for IRDs

1.3.1 Murine models of IRDs

Several animal models, including rodents, dogs and pigs, are available to study the degeneration mechanisms and potential therapeutic approaches for IRDs. Among them, the mouse models have been the most widely employed, also due to the abundance of naturally occurring mutations causing retinal degeneration. Moreover, genetic manipulation (e.g. generation of mutants) is more feasible and affordable in mice compared to larger animals.

In this section, I will introduce some of the most frequently used IRD models and I will mostly focus on those employed or mentioned in the thesis, such as the retinal degeneration 1 (*rd1*) and *rd10* mice, the *Aryl hydrocarbon interacting protein-like 1* (*Aipl1*) and the *RHO*-P347S mouse models.

The naturally occurring *rd1* mouse model was described by Keeler in 1924 (*14*) and represents the first murine strain in which retinal degeneration was identified. In 1990, it was shown that the retinal degeneration in *rd1* is caused by a homozygous nonsense (null) mutation in the *Pde6b* gene (*Pde6b*$^{rd1/rd1}$) encoding the β-subunit of the rod cyclic guanosine monophosphate (cGMP) phosphodiesterase (Pde) 6b, essential for the phototransduction cascade (*15*).). In *rd1* mice, rod PR cell death begins at post-natal (PN) day 9 and is completed by PN18. After this stage, the cones start to degenerate rapidly and by 4 weeks of age only a single layer of cones is left in the outer nuclear layer. The *rd10* mouse is another IRD model due to mutations in *Pde6b* (*Pde6b*$^{rd10/rd10}$). This strain is homozygous for a missense mutation in exon 13 and shows a slower progression of retinal degeneration compared to *rd1*. Specifically, in *rd10* mice, most rods die by PN35 and the majority of cones by PN50 (*16, 17*). Both *rd1* and *rd10* mice are

commonly used models of autosomal recessive forms of RP, since mutations in the *PDE6B* gene have been reported in patients with AR-RP.

The *Aipl1* homozygous null mouse (*Aipl1*$^{-/-}$) is a model with a faster degeneration compared to the *rd1* and *rd10* mice (*18*). The *Aryl hydrocarbon interacting protein-like 1* (*Aipl1*) gene plays a key role in the stabilization of PDE and the survival of photoreceptors. Mutations in the *AIPL1* gene are responsible for LCA in humans, one of the most severe IRD forms with very early onset, leading to complete blindness and loss of electrical responses within the first year of life. Such severity is recapitulated in *Aipl1*$^{-/-}$ mice, which at 4 weeks of age exhibit a complete degeneration of photoreceptors and absence of ERG responses. In this model, the retina develops normally until P12. After this stage, rod and cone PRs quickly degenerate leading to a notable reduction of the ONL thickness, which at P21 comprises only a single row of PR nuclei.

A number of transgenic mice have also been generated to study mutations of particular interest. In that respect, a representative example are mutations of the proline-347 of the Rhodopsin protein, near its carboxyl terminal end. Amino acid substitutions at this position tend to cause severe forms of RP (*19*). This residue is conserved among visual pigments and six different missense mutations have been identified in patients with RP. This indicates that proline-347 is important for the function of Rhodopsin (*20*). The transgenic *RHO*-P347S mouse is a model for autosomal dominant RP caused by the substitution of proline-347 by Serine. This model carries a copy of the human Rhodopsin allele in which the proline 347 is replaced by a serine and represents a useful tool for the study of the early pathogenic events by which this mutation leads to photoreceptor cell death (*20*). The *RHO*-P347S mice show a slow progression of the retinal degeneration without a major perturbation of the phototransduction up to the

early stages of degeneration. Indeed, ERG responses, albeit severely impaired, can be detected up to 2-3 months of age (*20*). This aspect makes the *RHO*-P347S mice a very useful model to assess the retinal function even at late stages as a read-out of therapeutic interventions.

1.3.2 *In vitro* IRD models: the light-induced damage in 661W cells

The investigation of strategies aimed at protecting cone photoreceptors is particularly relevant to advance the therapeutic options for IRD patients. The visual impairment associated with cone degeneration has the most severe impact on patients' life since daylight vision relies on cone functionality. Furthermore, also in rod-cone dystrophies, the death of cone photoreceptors that occurs secondarily to the loss of rods is the most debilitating consequence of the disease. Therefore, therapeutic approaches that tackle the impairment of cones could address the needs of a larger population of patients, regardless of the causative mutation, which may also be unknown.

The use of *in vitro* models of cone damage is particularly useful for the initial identification of cytoprotective compounds because it circumvents the complexity of *in vivo* systems. The study of a therapeutic approach for cone degeneration is even harder in murine models. Being nocturnal animals, rodents have a lower rod:cone ratio (98:2) compared to humans (95:5), and this relative paucity of cones results in rapid cone degenerations in RP models (*21*). Unfortunately, there are very few reliable cellular models of photoreceptors. One of the most commonly used is represented by the 661W, which is a cone-like cell line derived from mouse retinal tumors (*22, 23*). These cells show a neuronal-like morphology with spindle-like processes, express cone photoreceptor markers (i.e. blue and green cone pigments,

transducin, and cone arrestin) and show photoreceptor functions including retinoid processing (*24*). More importantly, these cells are highly susceptible to light-induced stress (*25*).

Light is an environmental risk factor for IRDs and may aggravate the disease progression as seen in various forms of RP (*26*). 661W cells exposed to continuous intense light are extensively used *in vitro* to study the cone photoreceptor damage occurring in human retinal degenerations. This is because key events underlying the light-induced damage in 661W involve pathological mechanisms, such as mitochondrial and oxidative stress among others, which are associated with the secondary degeneration of cones in RP (*27*). Moreover, treatments that enhance the antioxidant cellular response reduce the 661W cell death upon light exposure (*27, 28*). Therefore, the light-induced damage in 661W cells represents a very useful tool to test therapeutic approaches that aim to protect PRs in IRDs irrespectively of the disease causing-mutation, prior to investigating their effect in complex *in vivo* systems.

1.4 Beyond the heterogeneity: common pathological events in IRDs

Several lines of evidence revealed that, besides cell-autonomous mechanisms within mutation-bearing photoreceptors, non-cell autonomous mechanisms contribute to photoreceptor loss in IRDs (*29*). In particular, the involvement of the immune response mediated by microglial hyperactivation was shown to play an important role both in the primary death of rods as well as in the secondary cone degeneration that occurs in RP. Furthermore, oxidative stress and metabolic impairment represent additional pathological changes that take place during rod degeneration and are independent of the causative mutation. These processes seem to be particularly relevant for the secondary death of cones (*30*). Therefore, it is tempting to hypothesize that the modulation of such processes may

impact on the progression of rods degeneration, ultimately preventing or slowing down cone loss regardless of the genetic lesion.

1.4.1 Microglia activation in retinal degeneration

Microglia are the resident immune cells within the brain and retina that mainly mediate inflammation processes. They also maintain the homeostasis of the surrounding neuronal tissues by removing cell debris and regulating the secretion of neurotrophic factors. In the healthy retina, the microglial cells are located in the inner retina (GCL, IPL, OPL) and constantly scan the environment with their highly motile processes. In the presence of harmful stimuli (e.g. pathogens or neurodegeneration), microglial cells rapidly switch from a resting status to a reactive phagocytic status, in which they acquire an amoeboid morphology and migrate towards the insult site to restore the retinal milieu by releasing molecules (such as the Glial cell-derived neurotrophic factor, GDNF; the neurotrophin nerve growth factor, NGF; the brain-derived neurotrophic factor, BDNF) that protect tissues and initiate repair mechanisms (*31, 32*). However, the prolonged or excessive activation of microglia, can also induce damage and exacerbate neurodegeneration due to the increased flow of pro-inflammatory compounds such as nitric oxide (NO), pro-inflammatory cytokines (e.g. Interleukin-1 beta, IL-1β; Tumor necrosis factor alpha, TNF-α; Interferon gamma, IFN-γ; Interleukin-6, IL-6) and reactive oxygen species (ROS) that can damage neighbouring neurons (*33-35*).

Furthermore, activated microglia express several proteins, e.g. Major Histocompatibility Complex class II (MHC-II) and CD68, that are used as markers to determine microglia activity by immunohistochemistry and immunofluorescence-staining procedures (*36*).

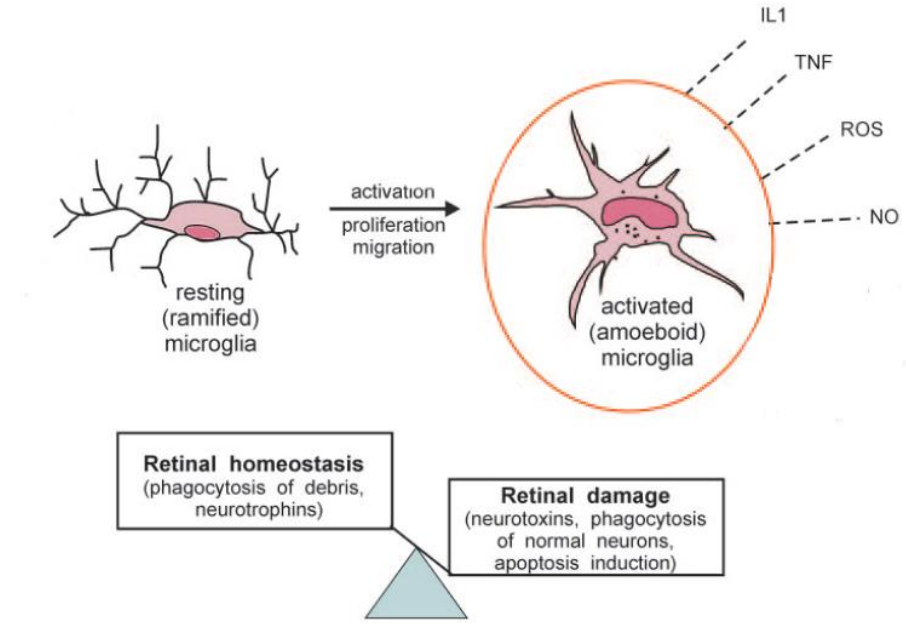

Figure 4. Mechanisms of microglia quiescence and activation related to neuronal degeneration.

Under normal conditions, resting microglia have a ramified morphology and regulate retinal homeostasis. Retinal degeneration triggers microglia activation, proliferation, and migration. Activated microglia adopt an amoeboid microglia shape and secrete various bioactive molecules, initially active in tissue repair. Prolonged microglia activation can lead to excessive responses and consequent retinal damage.

Abbreviations: IL1: Interleukin-1 family; TNF: Tumor necrosis factor; ROS: reactive oxygen species; NO: nitric oxide. Adapted from Langmann *et al.*, 2007 (*36*).

Clinical and laboratory reports demonstrated that the sustained chronic inflammatory response observed in RP is associated with a concomitant activation of microglia cells (*36-41*) and with an increase of inflammatory cytokines (*37, 42*) . In the last years, *in vivo* studies using different models of RP underscored the contribution of retinal microglia in the initiation and exacerbation of retinal degeneration. In particular, it was shown that microglia activation is an early event that can either precede or coincide with photoreceptor degeneration and directly contribute to it (*33, 41, 43, 44*) . Specifically, Zhao *et al.* demonstrated that in *rd10* mice,

activated microglia infiltrate the photoreceptor layer at early stages of degeneration, interact with and phagocytose healthy rods, and become more activated in the process (*41*). The same study provided evidence of microglial phagocytosis of healthy photoreceptors in additional mouse models of RP (e.g. *rd1* and *rd16* mice that harbor different mutations compared to *rd10*) as well as in human histopathological specimens. In support of a key role of microglia activation in the initiation and progression of photoreceptor degeneration in IRDs, different reports show that inhibition or ablation of microglial activation in the context of RP, improves the function and survival of rod photoreceptors (*41, 44, 45*). These improvements were also associated with a reduced production of proinflammatory molecules such as TNF-α and IL-1b. However, it is important to underline that microglia cells are also required to mediate protective effects for photoreceptor survival. In this regard, Wang *et al.* recently reported that the exogenous administration of the transforming growth factor beta 1 (TGF-β1) in different murine models of RP can be beneficial for cone survival and that such a protective effect is disrupted by pharmacologically depleting the 99 % of the microglia (*46*).

Furthermore, Arroba *et al.* showed that *ex vivo* and *in vivo* treatment with insulin-like growth factors (IGF-1) reduced the death of photoreceptors in *rd10* mouse retinas (*47*). Interestingly, the same study also demonstrated that microglia depletion in explants with clodronate-containing liposomes diminished the neuroprotective effect of IGF-1 but also moderately reduced photoreceptor cell death in *rd10* retinas cultured in the absence of IGF-1 (*47*).

Taken together, the above-described studies suggest that microglia have a dual role in the pathogenesis of RP which can be both neuroprotective and neurotoxic.

In light of this evidence, the modulation of microglia activation may represent the basis for the development of mutation-independent therapeutic options that could benefit a wide spectrum of IRDs patients. Obviously, such approaches should not abolish completely the microglia function, but rather modulate it to achieve a fine balance between their beneficial neuroprotective effect while inhibiting excessive pro-inflammatory responses (*48*).

1.4.2 Oxidative stress and IRDs

Oxidative stress is generated by the imbalance between the production of ROS and their detoxification by the physiological anti-oxidant defence mechanisms, resulting in excessive cellular ROS levels. Oxidative stress can lead to structural and functional cellular damage due to the modification of proteins, lipids and DNA, especially in mitochondria, and to the activation of cell-death pathways (*49, 50*).

ROS (e.g. superoxide radical anion ($O^{2\cdot}-$), hydrogen peroxide (H_2O_2), hydroxyl radicals ($^{\cdot}OH$), singlet oxygen ($^1O_2$), nitric oxide radical (NO or $NO^{\cdot}$) and peroxynitrite ($ONOO^-$)) are highly reactive oxidants. Among them, the non-radical H_2O_2 exhibits a lower reactivity, but can still penetrate cell membranes, including the inner and outer membranes of mitochondria. Therefore, H_2O_2 can react with the cellular iron and generate hydroxyl radicals, the most reactive form of oxygen ($^{\cdot}OH$), *via* the Fenton reaction: $H_2O_2 + Fe^{2+} \rightarrow {}^{\cdot}OH + {}^{-}OH + Fe^{3+}$ (*51, 52*)

ROS can be produced upon exposure to environmental stress (e.g. toxins, light) or as by-products of endogenous physiological processes such as the aerobic metabolism in mitochondria and the protein oxidative folding in the endoplasmic reticulum (ER). In particular, the electric transport chain (ETC) reactions in mitochondria are one of the main source of cellular ROS (*53*).

In addition, ROS can be produced by dedicated enzymes, nicotinamide adenine dinucleotide phosphate (NADPH) oxidases (Nox) and their dual oxidase relatives (Duox), which are localized to various cellular membranes (*54*).

ROS have a role in several cellular processes including regulation of gene expression, modulation of enzyme activities and amplification of immune response (*55*). Under physiological conditions, the cells are able to prevent excessive oxidative stress through antioxidant defense mechanisms for ROS scavenging, both non-enzymatic (e.g. ascorbate, carotenoids, glutathione, coenzyme Q10) and enzymatic such as the superoxide dismutase (SOD) enzymes, the peroxidase enzymes (e.g. glutathione (GSH) peroxidase) and the catalase (CAT). In fact, while low levels of ROS can promote cell survival in response to detrimental stimuli, their excessive or prolonged production overwhelms the antioxidant capacity of the cell, eventually leading to cell death (*55, 56*).

An increase of ROS levels has therefore been associated with pathological conditions that are accompanied by decreased antioxidant defenses, excessive energy demand, impairment of oxidative phosphorylation, higher tissue levels of oxygen, inflammation, and chronic induction of the unfolded protein response (UPR) among others (*57-60*). The retina is highly susceptible to oxidative stress. The choroidal blood vessels expose the retina to high levels of oxygen that promote the generation of ROS (*61*). Furthermore, the maintenance of the photoreceptor membrane potential and phototransduction processes require a high metabolic rate which leads to elevated levels of ROS as a consequence of the high mitochondrial metabolism(*29*).

Oxidative stress is a pathogenic event in many retinal neurodegenerative diseases including IRDs, light-induced retinal damage and age-related macular degeneration (AMD) (*62*).

Campochiaro *et al.* reported increased levels of proteins that have been subject to oxidative damage in the aqueous humor of patients with RP compared to control patients. The authors also found a depletion of GSH, a major component of the antioxidant defense, in the aqueous humor of RP patients, leading to a decrease in the ratio of reduced to oxidized glutathione (GSH/GSSG), indicative of ongoing oxidative stress and damage in the eye. Along the same lines, Martinez-Fernandez de la Camara *et al.* had previously reported that patients with RP present low total antioxidant capacity, including reduced SOD3 activity and protein concentration in the aqueous humor (*63*).

The involvement of oxidative stress in IRDs was also shown in studies on animal models of RP either in the primary death of rods (*64*) and its propagation (*65, 66*) as well as the secondary cone cell death (*67, 68*). Moreover, oxidative stress, in particular through the activity of NADPH oxidases, was shown to contribute to the light-induced retinal degeneration in mice (*69*). Finally, oxidative stress contributes significantly also to the non-cell autonomous cone death in RP (*21*). Upon rod photoreceptor death, the consumption of oxygen is drastically reduced. As a result, given that the choroidal flux remains stable, higher levels of oxygen permeate the outer retina (*70, 71*). These changes promote an increased production of ROS, leading to oxidative damage of the surviving cells (mostly cones) and eventually to cell death. A relation between ROS increase and induction of the NADPH oxidase has also been reported (*72*) (Figure 5).

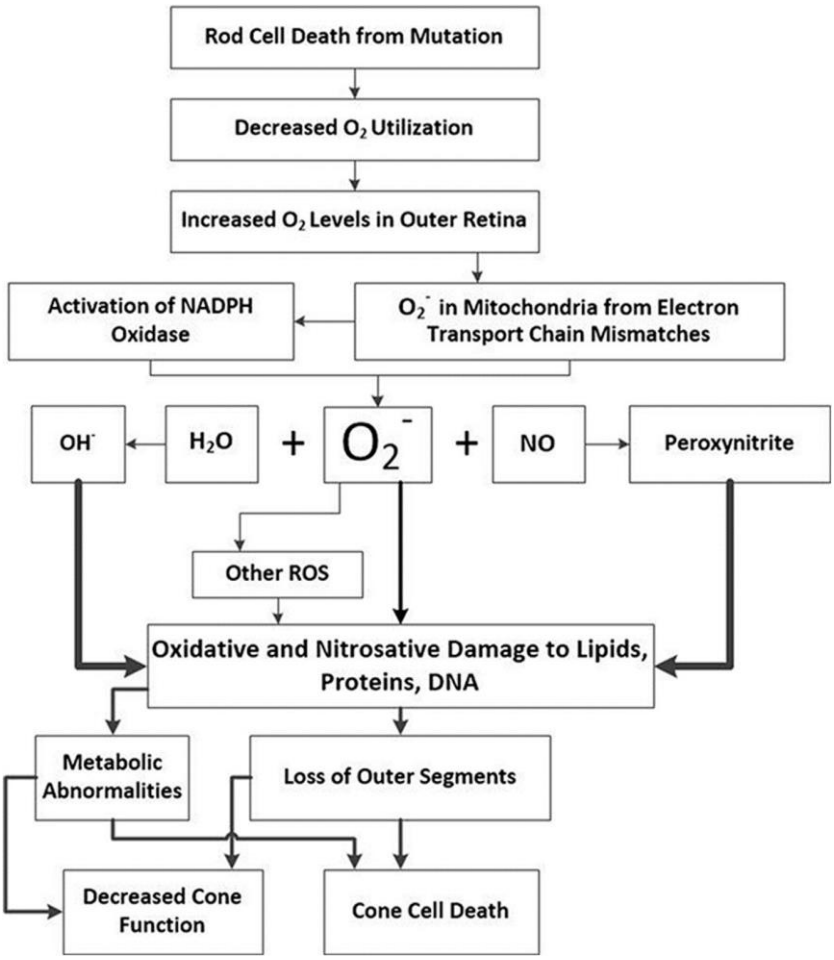

Figure 5. Schematic representation of the mechanism by which oxidative damage can contribute to cone cell death in Retinitis Pigmentosa.

The death of rods reduces oxygen consumption resulting in high tissue levels of oxygen in the outer retina. The excess oxygen stimulates superoxide radical production by mismatches in the electron transport chain in mitochondria and by stimulation of the NADPH oxidase activity in cytoplasm. The high levels of superoxide radicals overwhelm the antioxidant defense system and generate more reactive species including peroxynitrite which is extremely damaging and difficult to detoxify. This results in progressive oxidative damage in cones that contributes to cone cell death and loss of function. Adapted from Campochiaro *et al.*, 2018 (*20*).

Abbreviations: O_2, oxygen; O_2, superoxide radical; H_2O, water; NO, nitric oxide; OH_, hydroxyl radical; ROS, reactive oxygen species.

For all these reasons, therapeutic strategies aimed at reducing oxidative stress, without completely abolishing ROS production and signaling, could delay photoreceptor death and, in

particular, prolong the survival and/or prevent the demise of cones in different forms of IRD regardless of the causative mutation. Promising results in this direction were reported in various mouse models upon treatment with exogenous antioxidants (*73, 74*) or following overexpression of endogenous antioxidant enzymes such as the superoxide dismutase and catalase (*75, 76*).

1.5 Therapeutic approaches for IRDs

The development of treatment options that are suitable for a large number of IRD patients is particularly challenging due to the high genetic and clinical heterogeneity of these conditions, Moreover, delivering therapeutic molecules to the retina is further complicated by the presence of the Blood-Retina Barrier (BRB), an access-limiting barrier that protects the retina from the entry of noxious substances circulating into the blood (e.g. toxin and pathogens), and that maintains tissue homeostasis

To date, only one gene-therapy treatment (LUXTURNA^{TM}) is commercially available for a specific form of LCA associated with biallelic mutations in the *RPE-specific 65-kDa protein* (*RPE65*) gene (*77*). Treatments that are effective for broad populations of patients are currently missing.

Different strategies are under development and their design take into account the subtype of IRD, the stage of the disease, and the knowledge of disease genetics and underlying molecular pathways (Figure 6). Many of these studies are at the preclinical phase or in early clinical development. Nevertheless, there is still an urgent need for neuroprotective therapies to tackle common pathological mechanisms, regardless of the specific disease-causing mutation. The development of such gene-independent approaches has the potential to address the

needs of a larger number of patients compared to gene-based therapies. Gene-independent strategies are especially relevant when considering that almost in one third of cases, the IRD-causing mutations remain unknown (*78, 79*). In particular, protective strategies able to preserve cone viability are of outmost importance for patients' quality of life as daylight vision depends on proper cone function.

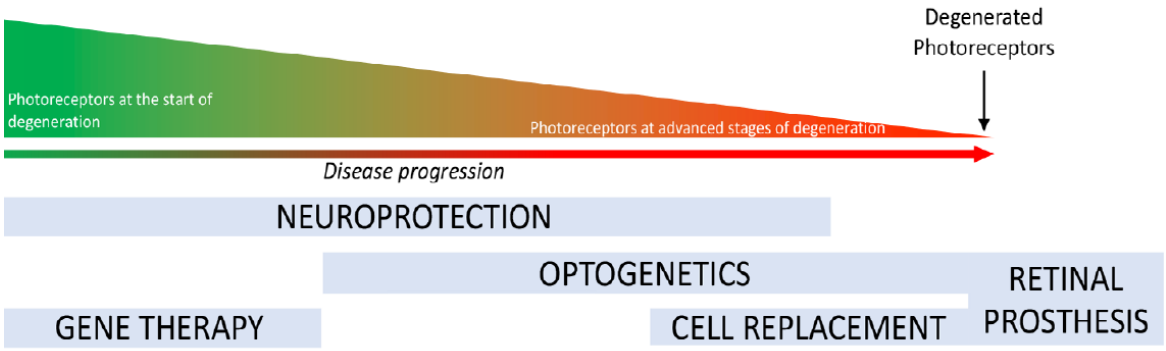

Figure 6. Stages of photoreceptor degeneration and applicable therapies.

Degeneration is represented in a graph showing the reduction in photoreceptors cells during degeneration. The time-windows of different therapeutic options are drawn below. Gene therapy is appropriate for early stages of photoreceptor degeneration and neuroprotective strategies can treat ongoing photoreceptor cell degeneration. Both these treatments act on endogenous photoreceptors. Cell replacement, optogenetics and retinal prosthesis are strategies to treat patients at advanced/late stages of degeneration. Image and caption adapted from Kutluer *et al.,* 2020 (*80*).

1.5.1 Gene replacement/augmentation therapy in IRDs

Gene augmentation is a promising approach for the treatment of IRDs, considering the predominantly monogenic nature of these conditions as well as the advances in deciphering their genetic basis. In addition, the eye is a particularly favourable target organ for molecular therapy. This is because it is an immune-privileged site, thanks to its delimitation by the BRB,

therefore the introduction of foreign antigens, e.g. viral vectors, does not elicit severe inflammatory and immunologic responses (*81*). Moreover, the eye combines accessibility for surgical interventions with non-invasive, follow-up diagnostic procedures.

Gene delivery is usually achieved by the subretinal injection of an AAV vector. This viral system is preferred for the administration of therapeutic molecules to the retina, since specific serotypes were shown to achieve efficient transduction of retinal cells and displayed an excellent safety profile. As a result, AAVs are used in several ongoing clinical trials for other genes (*82*). Moreover, some genes exceed in size the cargo capacity of AAV vectors. This is the case for example of the *USH2A* gene whose mutations are among the most common causes of Usher syndrome and non-syndromic autosomal recessive retinitis pigmentosa. To overcome such a limitation, pre-clinical studies using dual or triple AAV vectors or micro-genes are underway (*83, 84*).

To date the only commercially available treatment for an IRD is a gene therapy-based approach (LUXTURNA^{TM}) for recessive forms of RPE65-LCA. It was approved by the FDA at the end of 2017 and one year later by EMA. This treatment restores RPE65 levels upon delivery of a correct gene copy and improves patients' vision for more than four years post-injection (*77*). Although the number of RPE65-LCA patients that can benefit from such treatment is limited (considering also that the presence of viable photoreceptors is a prerequisite for its application and successful outcome) LUXTURNA^{TM} is a proof that gene therapy holds great promise for IRDs. in order to extend the window for therapeutic interventions beyond the early stages of degeneration and improve its efficacy, it will be important to assess the combination of gene therapy with strategies that block or delay photoreceptor cell death.

Gene replacement/augmentation strategies are effective in the context of autosomal recessive IRDs (arIRDs) in which the mutations give rise to a non-functional gene product (loss-of-function disease-causing mechanism). On the other hand, IRDs with a dominant mode of inheritance (adIRDs) are more frequently associated with gain-of-function mutations, leading to the synthesis of a protein product that can be either toxic to the cells or interfere with the proper function of the WT gene product (*85*). Therefore, therapeutic approaches for adIRDs differ from those designed for arIRDs. Specifically, the former take advantage of the genome editing system to (i) invalidate both alleles, followed by supplementation of the WT gene, (ii) specifically invalidate the mutant allele, with or without gene supplementation, or (iii) to correct the mutant allele (*86*). Strategies of genome editing for IRDs are mostly at a pre-clinical stage and progress has been made towards limiting unwanted off-target effects. The first clinical study of an *in vivo* genome editing approach for IRDs started recently (in 2019). It is based on the CRISPR/Cas9-system (EDIT-101) for the deep intronic variant c.2991+1655A>G in *CEP290*, a mutation associated with LCA type 10 (*87*).

1.5.2 Pharmacotherapy and neuroprotection

Besides gene therapy, other promising approaches for the management of the early stages of some IRDs are neuroprotective strategies, and pharmacotherapy which is able to modulate the affected biochemical pathways. Pharmacotherapy with visual cycle modulators (QLT091001) is under clinical evaluation in patients affected by LCA and RP forms caused by mutations in genes that encode key enzymes of the visual cycle, i.e. RPE65 and lecithinretinol acyltransferase (LRAT). RPE65 and LRAT are responsible for ensuring proper levels of the chromophore 11-cis-retinal, fundamental for the formation of rhodopsin and for rod function.

In previous clinical studies, QLT091001 (9-cis-retinyl-acetate) improved patients' visual function regardless of the underlying genetic cause by acting as a replacement for the lack of 11-cis-retinal and restoring the visual cycle (*88*). Some transient adverse effects have been reported (such as moderate to severe headaches and photophobia) (*88*).

Photoreceptor cell death in IRDs occurs either as the direct result of the causative mutation or due to concomitant, secondary pathological mechanisms such as oxidative stress, metabolic impairment, inflammation or loss of protective factors. Therefore, neuroprotective treatments that increase pro-survival pathways or interfere with cell death mechanisms or secondary detrimental processes could help preserve vision across different forms of IRDs by halting or preventing photoreceptor cell death.

The Rod-derived cone viability factor (RdCVF) is an example of well-studied neuroprotective candidates which sustain cell survival mechanisms. It promotes cone survival accelerating glucose entry into photoreceptors and stimulating aerobic glycolysis (*89*). Exogenous expression of RdCVF was shown to protect photoreceptors, especially cones, in various pre-clinical models of IRDs (*90*), but the study of this molecule has not yet entered the clinical phase. The Pigment epithelium derived factor (PEDF) is another promising neuroprotective candidate that has shown positive effects on photoreceptor survival in several preclinical studies on models of IRDs (*91-93*). Differently from RdCVF, PEDF exerts its protective effect by hindering the increase of intracellular calcium (*94*) and attenuating the related mechanisms that lead to photoreceptor cell death in different forms of IRDs (*21, 95, 96*).

Finally, the modulation of processes that are detrimental for photoreceptor cells during retinal degeneration (*21, 65, 67*), such as oxidative stress, was shown to promote cone survival in pre-clinical studies (*73*). For example, the antioxidant N-acetyl cysteine (NAC) demonstrated a good

safety/efficacy profile also in the initial phase of a clinical evaluation that was recently completed (*97*).

1.5.3 Optogenetic therapy, stem cell transplantation and retinal prosthesis

Optogenetic therapy, stem cell transplantation and retinal prostheses are the approaches under development for the late stages of IRDs when the majority of photoreceptor cells have been irreversibly damaged and lost (*80*). Optogenetic therapies aim to restore light perception by delivering genes encoding light-sensitive proteins in retinal neurons, such as ganglion or bipolar cells. Viral vectors are used to deliver the genes encoding for opsins, which are the major optogenetic tool (*98*). Two types of opsin have been described—microbial opsins (type I) acting as light-sensitive ions channels or pumps, and animal opsins (type II) which are G protein–coupled receptors (*99*). The type-I opsins (channelrhodopsins, halorhodopsins and archaerhodopsins) show a better kinetics compared to the type-II opsins (rhodopsin and melanopsin) which present instead a higher light sensitivity. Interestingly, it was recently found that the use of a mammalian cone opsin, MW-opsin, provide a combination of speed and sensitivity (*100*). Currently, two clinical studies that uses optogenetic approaches are underway but results are not yet available (*101*).

Stem cells-based therapies aim at restoring or preserving vision by replacing retinal cells when photoreceptors degeneration is already advanced. A potential strategy is based on induced pluripotent stem cells (iPSCs). iPSCs are obtained by reprogramming somatic cells at the stage of pluripotent cells obtained from patients. The latter could generate both RPE or PR cells to reimplant in patients. Gene editing tools should also be applied to correct patient-specific mutations. Embryonic pluripotent cells (ESCs) have also been investigated as source of

pluripotent cells. ESCs have a high differentiation capacity and would not require gene editing, however their use raises ethical concerns. Several protocols have been developed to differentiate rod-like cells from iPSCs (*102*), ECSs (*103*) and also adult retinal stem cells (*104, 105*). However, PRs transplantation strategies are still at the pre-clinical stage and require optimization to achieve an efficient integration of engrafted PRs in the host retina.

On the other hand, clinical testing for RPE cell-therapy is ongoing with promising results (*106*). In any case, further efforts are required for the optimization of protocols in order to obtain clinical-grade products and reproducible results.

Retinal implants can partially restore vision (i.e. identification of large objects, better navigation and orientation) in patients with advanced retinal degeneration in which the inner retina has retained the ability of signal transmission (*86*). Four retinal prosthesis have so far received market approval in the United States and/or Europe. Briefly, images are captured by a video camera and converted by a specialized processor to the stimulation patterns that are subsequently delivered to the implanted stimulator chip (*87*). To date, epiretinal and subretinal devices are the most widely documented prostheses. The epiretinal devices are implanted on the surface of the neurosensory retina, adjacent to the nerve fiber and ganglion cell layers, while subretinal prostheses are placed between the degenerated photoreceptor layer and the RPE generating a vision similar to the one that is physiologically generated in the eye (*86*). Argus II, an epiretinal device, is the most widely-used and it has been implanted in more than 250 patients to date with encouraging results (*88*). Finally, for patients with a completely degenerated retina the direct stimulation of the cortical cortex by a cortical implant could be an option. Its development is in the pre-clinical phase (*89*).

1.6 microRNAs

microRNAs (miRNAs) are endogenous, small non-coding RNAs with an average length of 22 nt that direct the post-transcriptional silencing of target mRNAs. The first example of a miRNA was *lin-4*, described in *C. elegans* in 1993 (*90*). Since then miRNAs have been recognized as essential regulatory molecules of gene expression, highly conserved across species, and potentially involved in all biological processes (*107*).

miRNAs originate from DNA sequences that either lie within protein-coding or non-coding genes (intragenic miRNAs) or are located in intergenic regions (intergenic miRNAs), possess their own promoters and are independently transcribed (*108-110*). Intragenic miRNAs are mostly located within introns even though a few exonic miRNAs have also been reported. Intronic miRNAs tend to be transcribed along with their host genes, using their transcriptional start sites (TSSs) to initiate transcription (*111*). However, it has been shown that about 30% of intronic miRNA sequences have their own promoters and the transcription is independent from their host gene (*112*). In many cases miRNA-coding regions form clusters, transcribed as a single sequence and processed in single miRNAs (*113*).

The prevalent mechanism of miRNA biogenesis is termed canonical and involves several different steps starting with the transcription of miRNA-coding DNA sequences into primary miRNAs (pri-miRNAs) which are then processed into precursor miRNAs (pre-miRNAs) and finally into the mature form (Figure 7). The majority of miRNAs are transcribed by RNA polymerase II (RNA Pol II) (*91*). The generated primary miRNAs (pri-miRNAs) contain a 5’ cap and a polyA tail (*92*), like other Pol ll transcripts, and form a stem-loop structure encoding the miRNA sequences in the arm of the imperfectly paired double-stranded stem. They are processed into pre-miRNAs by the microprocessor complex, which consists of an RNA binding

protein, DiGeorge Syndrome Critical Region 8 (DGCR8), and a ribonuclease III (RNAase III) enzyme, Drosha (27). DGCR8 recognises various motifs within the pri-miRNA structure (28) and guides the positioning of Drosha that cleaves the pri-miRNA duplex about 11 bases from the stem base, generating a two nucleotide (nt) overhang at the 3' end. The result of such processing is the so-called precursor miRNA or pre-miRNA, consisting in a hairpin-shaped RNA molecule of 70–100 bases.

The pre-miRNAs are then exported to the cytoplasm by the exportin 5 (XPO5)/RanGTP complex where they undergo further processing by the RNase III Dicer. Dicer recognises the 5' end and/or the 2-nt 3' overhang of the pre-miRNA and cleaves ~22 nt away from the 5' end (*93, 94*). In humans, Dicer functions together with the dsRBP trans-activation-responsive RNA-binding protein (TRBP). The Dicer cleavage removes the loop and generates a double stranded RNA of 22 bases in length (*95*). The miRNA duplex contains two forms of miRNAs, one deriving from the 5' end of the pre-miRNA hairpin and named 5p strand and a strand originating from the 3' end named 3p. Finally, in a process termed RNA-induced silencing complex (RISC) loading, the double-stranded miRNA produced by Dicer is handed over to a member of the Argonaute (AGO) protein family, which selects one strand to become the mature miRNA (also known as guide strand) and discards the other strand (passenger strand; also known as miRNA*) (*96, 97*). AGO proteins loaded with miRNAs dissociate from Dicer and form the miRNA-induced silencing complex (miRISC) (*96*).

For any given miRNA, the proportion of AGO-loaded 5p or 3p strand varies greatly depending on the cell type or cellular environment, ranging from near equal proportions to predominantly one or the other (*98*). The selection of the 5p or 3p strand is based in part on the thermodynamic stability at the 5' ends of the miRNA duplex or a 5' U at nucleotide position 1

(*99*). Generally, the strand with lower 5′ stability or 5′ uracil is preferentially loaded into AGO, and is deemed the guide strand (*100*).

Upon loading of mature miRNAs onto the miRISC complex, the miRNA guides RISC to complementary sequences located mainly in the 3‘ untranslated region (UTR) of its target mRNAs. However, miRNA target sites have also been detected in other mRNA regions including the 5′ UTR and coding sequence (*114-116*). The miRNA sequence between nucleotides 2 and 7 at the 5′ end contains the so-called seed sequence that is considered particularly important for target-recognition (*101*). Additional nucleotides (particularly nucleotide 8) and paring at the 3′ end of miRNAs contribute to the stability and specificity of the miRNA-target interaction (*116, 117*).

The degree of complementarity between the miRNA and its target leads to the mRNA degradation and/or translational suppression (*118, 119*). In animals, the majority of miRNA-target interaction contain mismatches. A full complementarity is more likely to induce target degradation, through stabilization of the interaction with AGO2. In animals, the majority of miRNA-target interactions contain central mismatches that results in inhibition of protein synthesis by miRISC either repressing translation or promoting mRNA deadenylation and decay (*120, 121*). Besides the mature miRNA and the AGO protein that directly bind the miRNA, glycine-tryptophan protein of 182 kDa (GW182) proteins (in mammals, the trinucleotide repeat containing gene 6 (TNRC6) proteins) are key components of the miRISCs, acting as downstream effectors in the repression (*122*). Specifically, they mediate the interaction with other effector proteins, such as deadenylase complexes poly(A)-specific ribonuclease 2 (PARN2)–PARN3 or carbon catabolite repressor 4 (CCR4)–negative regulator of transcription (NOT), which shorten the poly(A) tail of the mRNA. Shortening of the mRNA poly(A) tail triggers

the removal of the 5’ cap of the mRNA (decapping), allowing for a rapid 5’−3’ degradation by exoribonuclease 1 (XRN1) (*121*).

The CCR4-NOT complex may also induce translational repression but the repression may also involve the release of other factors (*123*).

The processes described above are illustrated in Figure 7. This figure also shows an example of an alternative, Drosha-independent processing of miRNAs that occurs for mirtrons. The latter are very short introns and their corresponding pre-miRNA is directly released by splicing and debranching (*118*).

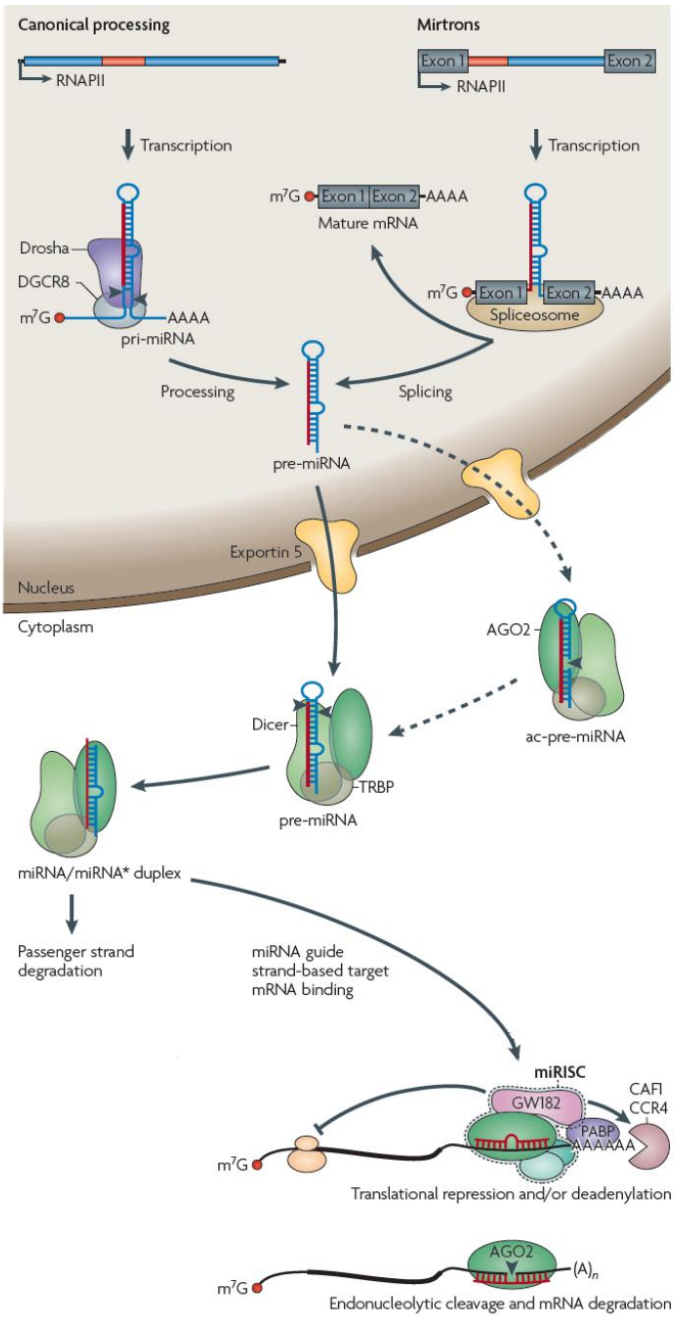

Figure 7. miRNA processing.

MicroRNAs (miRNAs) are processed from RNA polymerase II generated transcripts. In the canonical pathway, primary precursor (pri-miRNA) processing occurs in two steps catalysed by Drosha and Dicer that operate in complexes with dsRNA-binding proteins (dsRBPs) (i.e. DGCR8 and transactivation-responsive (TAR) RNA-binding protein (TRBP) in mammals). The Drosha–DGCR8 complex processes the pri-miRNA into an ~70-nucleotide

precursor hairpin (pre-miRNA), which is exported to the cytoplasm. Some pre-miRNAs are produced from very short introns (mirtrons) as a result of splicing and debranching, thereby bypassing the Drosha-DGCR8 step. In either case, cleavage by Dicer, assisted by TRBP, in the cytoplasm yields an ~20-bp miRNA/miRNA* duplex. In mammals, Argonaute 2 (AGO2), which has RNaseH-like endonuclease activity, supports Dicer processing by cleaving the 3' arm of some pre-miRNAs, thus forming an additional processing intermediate called AGO2-cleaved precursor miRNA (ac-pre-miRNA). Following processing, one strand of the miRNA/miRNA* duplex (the guide strand) is preferentially incorporated into a miRNA-induced silencing complex (miRISC), whereas the other strand (passenger or miRNA*) is released and degraded (not shown). Image and caption modified from Krol *et al.* 2010 (*118*)

Although miRNAs influence gene expression mainly by post-transcriptional inhibition, some studies also report a miRNA-mediated translational activation that seems to occur under specific conditions. This activation was observed in quiescent cells such as oocytes (*124*), or during cell-cycle arrest (*125*) as well as during amino acid starvation (*126*), upon binding of miRNAs to the 5' UTR of mRNAs encoding ribosomal proteins. However, the specific conditions that elicit this miRNA-mediated activation of translation are not yet fully elucidated.

A single miRNA can bind multiple mRNA targets (*127*), possibly modulating entire signaling pathways. In that respect, miRNAs act as pleiotropic molecules that fine-tune gene networks and stabilize them against aberrant fluctuations due to cellular stress (*128, 129*). In this complex regulatory network, miRNAs can regulate at least 30% of the human genes (*107, 130*) involved in nearly all physiological processes (e.g. developmental timing (*131*), circadian rhythm (*132*), cell proliferation (*133*), differentiation (*134*) and death (*135*), haematopoiesis (*136*), patterning of the nervous system (*137*) , etc.). Importantly, aberrant or altered expression of miRNAs and their pathways is implicated in the pathogenesis of many human conditions (*138*) including cancer, inflammatory, cardiovascular, neurodegenerative and genetic diseases (*139*).

Furthermore, miRNAs have been proposed also as prognostic and diagnostic biomarkers for several diseases (*140*), including retinal degenerations (*141*). Although miRNAs are mainly expressed within the cells, several studies have reported their presence in the extracellular space. These extracellular or circulating miRNAs were detected in a wide range of biological fluids such as plasma (*142*) and serum, cerebrospinal fluid (*143*), saliva, urine (*144*), and vitreous and aqueous humor in the eye (*145*). Interestingly, their expression seems to follow specific patterns in relation to different physio-pathological conditions, thus suggesting that circulating miRNAs can be useful biomarkers (*146*).

1.6.1 miRNAs in the eye

Over the past years, expression analyses demonstrated that a number of miRNAs are significantly expressed in the retina. This suggested that miRNAs have an important role in the retina, which is exposed to high environmental stress (*147*) and, therefore, requires a tight regulation of gene expression.

Notably, my research team generated the first high-resolution expression atlas showing the spatiotemporal distribution of miRNAs in the developing and adult WT mouse eye (*148*). In addition to expression analysis based on microarrays, they performed RNA *in situ* hybridization (ISH) experiments for more than 220 miRNAs, and showed their distribution in the retinal layers at different developmental stages (*148*).

More recently, they also generated the most comprehensive high-resolution analysis of the human retina miRNome by Next Generation Sequencing (NGS) procedures that led to the identification of novel retina-specific candidate miRNAs as well as to the recognition of a high number of sequence variants (isomiRs) (*149*).

Several studies showed that miRNAs have a key role in retinal development and function. (*147*). Some of these studies relied on the disruption of Dicer, the enzyme that is fundamental for miRNAs maturation. The constitutive deletion of Dicer in mice leads to early embryonic lethality (*150*). The conditional Knock out (cKO) of key miRNA-processing enzymes allowed instead to study the effect of global perturbation of miRNA levels in a tissue-specific manner. This approach was used in mice to characterize the influence of miRNA-mediated regulation in the mammalian eye (*151-153*). In this regard, mice that were cKO of Dicer in the developing eye displayed an impaired development of the retina, lens, cornea and optic chiasm (*152, 154, 155*), indicating a crucial role of miRNAs in the developing eye.

miRNAs also play a fundamental role in the homeostasis and functioning of the mature retina. In particular, the effect of miRNA deficiency on photoreceptor cells has been investigated by generating mice with rod- and cone-specific cKO of miRNA-processing enzymes (i.e. Dicer and/or Dgcr8). These models were designed in such a way, so that impairment of miRNA processing occurred exclusively in mature and differentiated photoreceptor cells (*156*). Disruption of global miRNA levels in the rods of Dicer cKO mice was associated with a disorganization of the outer segments followed by retinal degeneration (*157*). During the pre-degenerative phase, the mice did not exhibit impairment of the photo-transduction and visual cycle, thus suggesting a primary role of miRNA-mediated regulation in rod survival (*157*). The cKO of *Dgcr8* in cones resulted in outer segment loss and functional impairment (*158*). The conditional loss of Dicer in cones was associated with a more severe phenotype, characterised by enhanced cone death and structural disorganization (*159*). Collectively, the above-mentioned studies provided strong evidence of the importance of miRNAs for photoreceptor homeostasis, function, and survival (*156*).

Besides the study of global miRNA perturbation, also the modulation of specific miRNAs revealed the important contribution of individual or clustered miRNAs in mammalian eye development, function and homeostasis. For example, let-7, miR-125, and miR-9 have been identified as key regulators of the early to late developmental transition in retinal progenitors (*160*).

Another miRNA that is highly abundant in the retina and the CNS is miR-124 (*161*). Deletion of the locus encoding miR-124a-1, the paralog that is predominantly expressed in the developing retina, severely interfered with the maturation and survival of cones (*162*).

The miR-183/96/182 cluster has an important role in multiple sensory tissues and is particularly abundant in photoreceptors. Studies based on the inactivation of miR-183/96/182 in mice suggested that these miRNAs are important for the differentiation and morphogenesis of photoreceptors, for the phototransduction pathway, as well as for the regulation of key genes of the synaptogenesis and synaptic function (*163*). Zhu *et al.* generated a transgenic mouse model expressing a miRNA sponge for all three miRNAs of the miR-183/96/182 cluster in mature rods (*164*). The resulting sequestration of miR-183/96/182 did not produce detectable morphologic or functional differences compared to the WT. However, the disruption of miR-183/96/182 activity sensitized the transgenic mice to retinal damage upon light exposure, indicating that this cluster protects rods under stress conditions (*164*). Along the same line, the delivery of miR-182 and miR-183 in Dgcr8 cKO cones, i.e. cones depleted of all miRNAs, was reported to prevent loss of cone outer segments (*156, 158*).

Finally, miR-204 is another abundant and well-studied retinal miRNA. It is essential for key aspects of retinal development and function and is described in detail in paragraph 1.6.3.

1.6.2 miRNAs and retinal degenerations

Several studies have reported altered miRNA expression in human and animal models of retinal dysfunction, suggesting that miRNAs participate to the pathogenesis of retinal diseases including diabetic retinopathy (*165*), macular degeneration and inherited retinal dystrophies (*166*). In that respect, Loscher *et al.* reported the down-regulation of miR-96, miR-182, and miR-183, and the up-regulation of miR-1, miR-133, and miR-142 as a common pattern in four models of RP with different underlying mutations and inheritance patterns (*167*). Specifically, this was shown in two rhodopsin (*Rho*) mutant mice models ($Rho^{-/-}$ and transgenic *RHO*-P347S) and in two RDS/Peripherin mutants ($rds^{-/-}$ and transgenic RDS–Δ307). This study suggested that aberrantly expressed miRNAs are involved in RP regardless of the nature of the causative mutation.

The miRNA expression profile in early retinal degeneration was recently studied in the *rd10* mouse, a commonly used model of autosomal recessive RP (*166*). The expression profiles of 1900 miRNAs were analysed by microarray (*168*). miR-6240, miR-6937-5p, miR-3473b, and miR-7035-5p were differentially expressed at P15, a stage that immediately precedes photoreceptor death, prompting the authors to suggest that these miRNAs are likely to be involved in the onset of the disease (*168*).

Furthermore, miR-9, miR-23a, miR-27a, miR-34a, miR-146a and miR-155 have been proposed as potential biomarkers for AMD, a multifactorial and progressive retinal degeneration with late onset. The dysregulation of their expression was indeed confirmed in the serum of AMD patients (*141*).

Although multiple studies reported miRNAs whose aberrant expression is associated with retinal degenerations, a direct causative role of a miRNA in the pathogenesis of IRDs in humans was shown only for miR-204 (*169*).

1.6.3 miR-204

In the human genome, miR-204 is located within intron 8 of the transient receptor potential (TRP) channel gene, *TRPM3*, on chromosome 9q21.12.

Mir-204 is predominantly expressed in the eye, especially in the RPE, neural retina, lens and ciliary body (*161, 170*) and its expression pattern is evolutionary conserved across fish, mouse and humans (*149, 161, 169, 171, 172*). In particular, within the neuroretina, miR-204 is expressed in the retinal ganglion cell layer, inner nuclear layer, and in photoreceptors (*169*). In mammals, miR-204 has a closely related paralog, the miR-211. Their sequences differ by one or two nucleotides, depending on the species, but display the same seed sequence thereby they most likely target common pathways.

Over the past years, the Banfi's group has extensively characterized the role of miR-204 in the eye. By using the medaka fish (*Oryzias latipes*) model organism, they showed that the fish homolog of miR-204 influences multiple events of eye formation, such as lens differentiation and optic cup development (*172, 173*). Furthermore, they demonstrated that miR-204 is necessary for photoreceptor cell function and survival (*169*). Importantly, they identified a point mutation in the seed region of miR-204 and demonstrated that it is responsible for an autosomal dominant form of retinal dystrophy in patients, accompanied by eye coloboma, a genetic developmental disorder characterized by keyhole-shaped defects in various eye structures (*169*). Furthermore, the authors of the latter study hypothesized that the effects of

the mutated miR-204 are mainly mediated by a gain-of-function mechanism consisting in the aberrant recognition of novel targets. This study (*169*) represents the first report of a causative relation between a miRNA and a form of IRDs in humans.

Given its key role in retina development, function and disease, miR-204 emerged as an attractive target in therapeutic approaches for retinal degeneration.

AIM OF THE THESIS

MiRNAs are fine modulators of gene expression that act as pleiotropic molecules able to influence functionally coordinated pathways. This feature makes miRNAs attractive therapeutic targets to counteract multiple pathological processes that underlie human diseases. Recent evidence supported a role of the miRNA miR-204 in the pathogenesis of IRDs. However, it has not yet been explored whether modulating miRNA expression can have a protective effect in IRDs.

IRDs are characterised by high genetic heterogeneity and the availability of therapies for a large number of patients is still challenging. The general aim of my thesis project was to address this issue by exploring the ability of miRNAs to counteract disease-exacerbating processes that accompany IRDs regardless of the specific diseases-causing mutation. I also aimed to better understand the role exerted by miRNAs in retinal degeneration, and explore their potential as molecular tools in Gene Independent Therapies (GITs) for IRDs. The work consists of two main parts:

- *Exploring the translational potential of a miR-204-based therapeutic approach*

  Encouraging data about a beneficial role of miR-204 in IRDs were generated by Banfi's group. Early (PN4) subretinal delivery of miR-204 in two different preclinical models of IRDs yielded a protective effect, suggesting that this miRNA could act in a gene-independent manner. The models were the transgenic *RHO*-P347S mice that recapitulates an autosomal dominant form of RP, and the *Aipl1* $^{-/-}$ mice, model of a recessive form of LCA. In the first part of my thesis work, I used the *RHO*-P347S mouse model to investigate whether miR-204 delivery was able to counteract retinal

degeneration at advanced postnatal ages which better represent patient-relevant disease stages. I also characterized the possible mechanisms underlying its effect.

- *Screening of miRNAs able to target pathological process common to different forms of IRDs*

  In the second part of my thesis work, I sought to identify additional miRNAs able to protect PRs against the damage induced by processes that contribute to disease-progression but are independent of the causative mutation. This is the case, for example, of the oxidative stress, which has a key role in the secondary death of cones in RP. Cone dysfunction and loss leads to the most debilitating visual impairment and occurs in almost all forms of RP, even though the disease-causing mutation may affect genes with rod-specific expression. I used the light-induced damage in the 661W cells as an in vitro model of PR cell degeneration, particularly cone degeneration, which is related to oxidative stress and is independent of specific mutations. The HCS approach has allowed me to simultaneously test over 500 of the most conserved miRNAs.

2 MATERIALS AND METHODS

2.1 Animal Models and Procedures

For subretinal injections in the *RHO*-P347S background, pups were obtained by crossing the *RHO*-P347S transgenic (*20*) with C57BL/6 mice. The C57BL/6 strain was used as a wild-type (WT) control line. Studies were conducted in accordance with the institutional guidelines for animal research and approved by the Italian Ministry of Health (D.L. 116/92 art. 7; protocol number: 650/2018-PR). Mice were maintained under specific pathogen-free (SPF)-like conditions at the TIGEM Animal Facility. Surgical procedures were performed under anesthesia, and all efforts were made to minimize suffering. Viral vectors were delivered subretinally in the dorsal retinal areas *via* a trans-scleral transchoroidal approach (*174*). Eyes were injected with 1 microliter (µL) of an AAV vector/vector mix (specified in each figure) containing a total of 1.1 X 10^9 viral GCs.

2.2 Electroretinography

Electrophysiological recordings were performed as previously described (*175*). Mice were dark adapted for 3 hours (h) and accommodated in a stereotaxic apparatus under dim red light. Pupils were dilated with a drop of 1% tropicamide (Alcon Laboratories, Fort Worth, TX, USA), and the body temperature was maintained at 37.5°C. ERGs were evoked by 10-ms flashes of different light intensities ranging from 10^{-4} to 20 cd·s/m2, generated through a Ganzfeld stimulator (CSO, Florence, Italy). To minimize the noise, three different responses evoked by light were averaged for each luminance step (the time interval between light stimuli was 4–5 min). Electrophysiological signals were recorded with gold-plated electrodes inserted under

the lower eyelids in contact with the cornea. Electrodes in each eye were referred to a needle electrode inserted subcutaneously at the level of the corresponding frontal region. The different electrodes were connected to a two-channel amplifier. Amplitudes of a- and b-waves were plotted as a function of increasing light intensities. After completion of responses obtained in dark-adapted conditions (scotopic), the recording session proceeded to dissect the cone pathway mediating the light response (photopic). To this end, ERG responses to light of 20 cd·s/m2 were recorded in the presence of a continuous background light (set at 50 cd·s/m2). For each group, the mean a- and b-wave amplitude was plotted as a function of luminance (transfer curve) under scotopic and photopic conditions.

2.3 AAV production

Recombinant AAV2/8 viruses were produced by the TIGEM Vector Core as reported (*176*) Physical titers (genome copies [GCs] per milliliter [GC/mL]) of each viral preparation were determined by TaqMan PCR quantification.

2.4 Plasmid construction

The AAV.CMV.miR204 and AAV.CMV.miR204MUT plasmids were previously generated in Banfi's laboratory (*177*). Recombinant AAV vectors containing the murine precursor sequence of miR-204 under the cytomegalovirus (CMV) promoter were constructed by a two-step cloning protocol.

Initially, the cassette containing the precursor of miR-204 was amplified from mouse genomic DNA using the following set of oligonucleotides: 5'-ATAAGAATGCGGCCGCCTGTTCAGGACTTGGCTAAG-3' and 5'-

CGCGGATCCAACATGGGGTTGTTAATCTG-3' for miR-204. The obtained amplimers were subcloned in the TOPO TA Cloning Vector (Invitrogen) and released following digestion with *NotI* and *BamHI*. The fragment was then cloned into the *NotI–BamHI* sites of the pAAV2.1-CMV-EGFP plasmid (*178*) and used for the production of AAV2/8 vectors. The control vector bearing the precursor of miR-204 with a mutated seed sequence was generated by purine-pyrimidine changes in both arms of the precursor to maintain the same complementarity and hairpin structure as shown in Figure 8.

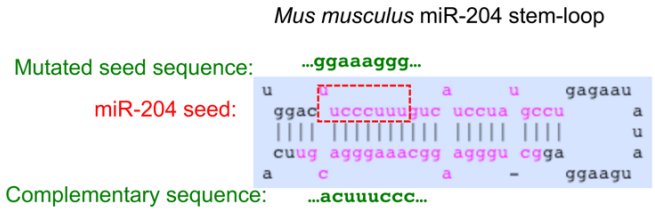

Figure 8. Scheme of the mutated miR-204 seed sequence contained in the pAAV.CMV.miR204 plasmid used to generate the AAV.CMV.miR204MUT.

Sequence of the miR-204 stem-loop in *Mus musculus* (blue box). The sequence of the mature miR-204-5p (upper strand) and miR-204-3p (lower strand) is in purple. The seed region of miR-204-5p is in a red frame. The sequence introduced by site-directed mutagenesis to generate the AAV.CMV.miR204MUT control vector is in green. Karali *et al*., 2020 (*177*).

This was achieved with two sequential steps of site-directed mutagenesis using primer extension. The first reaction introduced the modified seed sequence of the mature miRNA (5'-GGAAAGGG-3' instead of 5'-TTCCCTTT-3' at chr19: 22,750,610–22,750,617) and the second introduced a sequence complementary to the newly mutated seed at the 3p arm of the precursor hairpin (5'-CCCTTTCA-3' instead of 5'-AAAGGGAC-3' at chr19: 22,750,660–22,750,667) (Figure 8). The internal primer pairs containing the desired mutation and complementary ends were 5'-CGTGGACGGAAAGGGGTCATCCTATGCCTG-3', 5'-

GGATGACCCCTTTCCGTCCACGAGTCACATG-3' and 5'-GGAAGGCCCCTTTCAGTTCAATTGTCATCAC-3', 5'-ATTGAACTGAAAGGGGCCTTCCCAGCCTCC-3'. The external flanking primers, used in combination with the internal mutagenic primers, were the ones described above for the amplification of the miR-204 precursor.

The vector bearing the precursor miR-204 under the control of a photoreceptor-specific promoter (pAAV.RHO.miR204) was generated by exchanging the CMV promoter of pAAV.CMV.miR204 with the human RHO promoter sequence (*179*) Briefly, the sequence corresponding to the human *RHO* promoter was released from the pAAV2.1-RHO-EGFP plasmid (*178*) by restriction with *Nhe I* and *Not I* and was cloned in the pAAV.CMV.miR204 backbone, previously digested with the same enzymes.

For the Luciferase assay the 3' UTR sequences of *Xaf1* and *Siglec1* were amplified by PCR from mouse genomic DNA using the following sets of oligonucleotides that included tags for the *SpeI* restriction site: Forward 5'-GGACTAGTCCCAGATCCCACTAGCTTC-3' and Reverse 5'-GGACTAGTATGACGATTGCCCTTCTAAC-3' for *Xaf1*; Forward 5'-GGACTAGTCAACTCAGGTGCTGTGAAC-3' and Reverse 5'-GGACTAGTCCCTTTCAGCATGGTATGTTTATG-3'. The control vector bearing the mutated recognition site for the miR-204 seed sequence was generated by PCR site-directed mutagenesis to introduce the CGCATAC sequence instead of AAAGGGA at position 1180-1186 of *Xaf1* 3' UTR, and the GCTATCG and CGCTATC instead of AAGGGAA and AAAGGG, respectively, at the positions 567-573 and 671-676 of the *Siglec1* 3' UTR. The digested PCR products were then inserted in the pGL3-tk-LUC vector.

For the transfection of miR-204 in the BV-2 microglial cell-line, the precursor of miR-204 as well as that bearing the mutated seed sequence were cloned in the psiUx expressing vector which is particularly effective for the production of small non-coding RNAs (*180*). The precursor sequences were amplified from the AAV.CMV.miR204 and AAV.CMV.miR204MUT plasmids, respectively, and cloned in the *BglII-XhoI* restricted psiUx plasmid.

2.5 RNA Extraction, Library Preparation, Deep Sequencing, and Computational Analysis

Total RNA was extracted from mouse retinas using the miRNeasy kit (QIAGEN, Hilden, Germany). RNA-seq library preparation and sequencing were performed as previously described (*181*). The RNA-seq data are deposited in NCBI's Gene Expression Omnibus (GEO: GSE121785). Data analysis was performed as reported (*181*). The threshold for statistical significance was FDR <0.1.

2.6 Gene Ontology Enrichment Analysis (GOEA)

GOEA (*182*) was performed on the list of up-regulated and down-regulated genes, separately. The Database for Annotation, Visualization and Integrated

Discovery (DAVID) online tool (v. 6.7) was used by restricting the output to BP (BP_FAT) and Cellular Component (CC_FAT) terms, with a significance threshold of FDR <10% and ES >1.5.

Redundant terms and commonly encountered categories were eliminated. The visualization of GO-term interconnections was performed using GOView (http://www.webgestalt.org/GOView/).

2.7 Luciferase assay

To test the direct regulation of target genes by miR-204, the vectors bearing the 3' UTR of selected genes or the mutated form (as described in 2.4) were co-transfected with a synthetic miR-204 mimic in HeLa cells. HeLa cells were seeded at a density of 40000 cells/well in a 24-multi-well plate. The cells were cultured overnight at 37°C and 5% CO_2 in DMEM supplemented with fetal bovine serum (FBS, 10%), penicillin (100 U/ml) and streptomycin (50 milligram [mg]/mL). The next morning the cells were transfected with 370 nanogram (ng) of plasmid DNA using the PolyFect transfection reagent (Qiagen) according to the manufacturer's instructions. A Renilla expressing vector was also transfected to allow normalization of the transfection efficiency. The transfection was performed in triplicate for each condition. Six hours later, the cells were transfected with 50 of negative mimic or miR-204 mimic (Dharmacon) using INTERFERIN (Polyplus) according to the manufacturer's instructions. The luciferase activity was detected 48 hours after the first transfection using the Dual-Luciferase Reporter Assay System (Promega).

2.8 Immunostaining

Immunostaining for retinal and microglial markers was performed as reported (*183*). Frozen retinal sections were washed once with PBS and then fixed for 10 min in 4% paraformaldehyde (PFA). Sections were then permeabilized for 15 min in PBS containing 1% IGEPAL CA-630 (Sigma-Aldrich, St. Louis, MO, USA. Permeabilization and blocking of sections for anti-Iba1, anti-CD68 staining were performed for 1 h in 0.3% Triton/4% normal goat serum. Antibodies were then incubated overnight at 4°C in 0.1% Triton/2% normal goat serum (for dilutions and providers, see below). DAPI (Vectashield; Vector Labs, Peterborough, UK) was used for nuclei

counterstaining. Sections were photographed using Zeiss (LSM 710) confocal microscopy (Carl Zeiss, Oberkochen, Germany).

The primary antibodies used were anti-Iba1 (1:300; 019-19741; Fujifilm Wako Pure Chemical, Osaka, Japan) and anti-CD68 (1:500; MCA1957T; Bio-Rad, Hercules, CA, USA).

2.9 BV-2 microglial cells and lypopolysaccharide (LPS)-mediated activation

BV-2 are an immortalised murine microglial cell line. BV-2 cells were maintained in Dulbecco's modified eagle medium (DMEM; Life Technologies) supplemented with 10% heat-inactivated FBS (Euroclone), L-glutamine at a final concentration of 2 mM and 1% penicillin/streptomycin. An incubator with humidified atmosphere of 5% CO_2 at 37°C was used to culture the cells.

The BV-2 cells were transfected with the vector containing the miR-204 precursor and the vector containing the precursor of miR-204 bearing a mutation in the seed sequence. After transfection (6 h), the cells were incubated overnight with fresh normal medium. Cells were subsequently treated with LPS (100 ng/ml; Lipopolysaccharides from *E. coli* O111:B4; L4391; Sigma-Aldrich) for 24 h.

2.10 Real-Time PCR (qPCR)

Total RNA was extracted from BV-2 cells using the miRNeasy kit (QIAGEN). cDNAs were then generated by the Quantitect kit for the qRT-PCR analysis (QIAGEN) according to manufacturer's instructions. Quantitative PCR were performed using SYBR Green Master Mix (Roche) and run in triplicate on a Light Cycler 480 instrument (Roche).

The primer sequence used were: TNFα-Forward: 5'-GCCTCTTCTCATTCCTGCTTG-3'; TNFα-Reverse: 5'-CTGATGAGAGGGAGGCCATT-3'; iNOS-Forward: 5'-CTTTGCCACGGACGAGAC-3'; iNOS-Reverse: 5'-TCATTGTACTCTGAGGGCTGA-3'; ATP5B, forward primer 5'-GGCACAATGCAGGAAAGG-3', reverse primer 5'-TCAGCAGGCACATAGATAGCC-3' (*184*).

2.11 661W cells

661W cells are a transformed murine cone cell line derived from mouse retinal tumors that was kindly provided to us by Dr. Muayyad R. Al-Ubaidi (Department of Cell Biology, University of Oklahoma, USA) (*22*). The cells were validated by IF staining for S- and M-opsin proteins using respectively anti-Opn1mw (anti-M opsin; 1:200; AB5405; Millipore, Burlington, MA, USA) and anti-Opn1sw (anti-S opsin; 1:200; AB5407; Millipore, Burlington, MA, USA).

661W cells were maintained in high-glucose (4.5 mg/mL) Dulbecco's modified Eagle's medium (DMEM High-glucose; Life Technologies) supplemented with 10% heat-inactivated fetal bovine serum (FBS; Euroclone), L-glutamine at a final concentration of 2 mM, 100 U/ml penicillin and 100 microgram (µg)/mL streptomycin. Cells were not exposed to direct light during feeding or passaging and were cultured in a humidified atmosphere of 5% CO_2 at 37°C. For the HCS experiments the medium was replaced with serum-free High-glucose DMEM before light exposure, to sensitize the cell to light-induced damage, as previously reported (*185*). For the MTT and western-blot experiments the 661W were exposed to light in high-glucose DMEM containing FBS 1% for 4 h or 6 h, respectively.

2.12 MTT Cell Viability Assay

For the pilot and hit confirmation experiments of the HCS, the light-induced damage in 661W cells was assessed by using the MTT [3-(4, 5-dimethylthiazole-2-yl)-2, 5-diphenyltetrazolium bromide] assay as indicator of cell viability. In fact, viable cells reduce MTT to form purple formazan crystals. Following light exposure, the MTT solution was added to the cells at a final concentration of 0.5 mg/mL and the plate was placed in the incubator. After 3.5 h the medium was carefully removed, the formazan precipitates were dissolved in dimethyl sulfoxide (DMSO) and after 30 min of shaking the absorbance was read at 560 nanometer (nm). 661W that underwent light exposure were compared with dark control cells. The cell viability (%) was calculated by averaging the ratios of absorbance readings of light exposed cells to the dark control cells considered as 100% viable.

2.13 High-Content Screening (HCS)

HCS was used to identify miRNAs able to protect the 661W cells from light-induced damage. The strategy and workflow of the HCS is described in the Results section 3.8. The human miRIDIAN miRNA Mimic Library (384-well format) was used as a source of miRNA mimics. The library contains the 2503 human miRNAs reported in the miRBase sequence database, version 21.0. The miRNA mimic stock solution (1 micromolar [µM]) was dispensed in the test plate (ViewPlate-384 Black with Optically Clear Bottom; PerkinElmer) by using the STAR-let liquid handling system (Hamilton, Reno, NV, USA). For the reverse transfection, a mix of Opti-MEM reduced serum media (ThermoFisher) and the transfection reagent Interferin (Polyplus) were used according to manufacturer's instructions. The 661W cells in DMEM (~650 cells/well) were

added subsequently using the E1-ClipTip™ Bluetooth™ Electronic Multichannel Pipettes (ThermoFisher). Before placing the plate in the incubator, cells were let to recover under the cell culture hood for 5-10 min. After transfection (~60 h), the cells were exposed to white LED light (~15000 lux) for 6 h. Following light exposure, Hoechst 33342 was added to the media. After 15 min the cells were imaged by using the Opera live imaging system (PerkinElmer). The Columbus software was then used for the automated analysis of the images as described in the Results section 3.8.2. The experiment was performed in three replicates, carried out on different days.

2.14 Detection of cellular ROS

I used CM-H_2DCFDA (ThermoFisher), a chloromethyl derivative of the 2',7'-dichlorodihydrofluorescein diacetate (H_2DCFDA) as an indicator of cellular ROS in 661W. This reagent passively diffuses into the cells where it undergoes cleavage by the intracellular esterase. Subsequent oxidation generates a green fluorescent compound that is retained inside the cell. Briefly, the transfection mix containing the miRNA mimics was spotted at the bottom of a 96-well plate for imaging and 661W cells were seeded to allow reverse transfection (3000 cells/well). After 48 h, the cells were treated with H_2O_2 (200 µM in DMEM, 10% FBS) for 3 h and 15 min. The media was subsequently removed and the cells were washed gently with PBS and incubated for 30 min with a medium containing 5 µM CM-H_2DCFDA in the dark at 37˚C, 5% CO_2. After rinsing with PBS, the labelled cells were visualized by fluorescence microscopy using the Operetta live imaging system with a 20X objective and a standard GFP filter, maintaining a low excitation intensity and a short time of exposure (~10 min for the image acquisition of the whole plate). The fluorescence intensity and spatial distribution of the

green signal were analysed with the Columbus software and verified by visual inspection. The total fluorescence was then calculated by correcting for the background.

2.15 Western Blot

To obtain whole cell lysates, the 661W were homogenized in cold RIPA lysis buffer supplemented with protease inhibitor cocktail (Sigma-Aldrich) and phosphatase inhibitors tablets (PhosSTOP, Roche), and then incubated for 20 minutes in ice. After centrifugation (13 000 rpm) for 10 min at 4° C, the supernatants, containing the total protein extract, were collected and used for the experiments. Total protein concentration was determined by using the Pierce BCA assay (Thermo Scientific). Each sample contained protein extract corresponding to 15 µg of proteins and Loading buffer (SDS, Tris HCL pH6.8, Glycerol, Bromophenol Blu, Dithiothreitol-DTT). Proteins were separated by sodium dodecyl sulphate-polyacrylamide gel electrophoresis (SDS-PAGE) which was performed using a 7.5% polyacrylamide gel in Tris-Glycine running buffer.

The proteins were then transferred from the gel to hydrophobic polyvinylidene fluoride membranes (Immobilon-P PVDF Membrane, Millipore) that were subsequently incubated with the primary antibodies overnight at 4 °C or for 2 h at room temperature (for dilutions and providers, see below). Proteins of interest were detected with horseradish peroxidase conjugated goat anti-mouse or anti-rabbit IgG antibody (1:3,000, GE Healthcare) and visualized using Pierce enhanced chemiluminescence (ECL) Western Blotting Substrate (Thermo Scientific) or SuperSignal West Femto Maximum Sensitivity Substrate (Thermo Scientific). Western blot images were acquired using the ChemiDoc-It imaging system (UVP).

Densitometric analyses of the western blot bands were performed using the Image J Software (National Institutes of Health, Bethesda, Maryland, USA).

The primary antibodies used were anti-Phospho-AMPKα (Thr172) (1:1000, #2531, Cell Signaling Technology-CST), anti-AMPKα (1:1000, #2532, Cell Signaling Technology-CST) and anti-p115 (1:1000, sc-48363, Santa Cruz Biotechnology).

3 RESULTS

Exploring the translational potential of miR-204 overexpression as a therapeutic approach for IRDs.

Over the past years, the Banfi's research group has produced significant evidence indicating a fundamental role of miR-204 in eye development and function. Notably, they found that a mutation within the miR-204 seed sequence is responsible for a familial form of retinal degeneration in humans. They then explored the effect of miR-204 overexpression in animal models of IRDs at early post-natal stages (i.e. at PN4). To this aim, they cloned the precursor sequence of miR-204 under the control of the CMV constitutive promoter in an AAV vector of the 2/8 serotype (AAV-miR-204). This serotype transduces efficiently the RPE and PRs upon subretinal administration in several species, including mice (*178, 186*). Following subretinal injection of the AAV-miR-204 vector in WT mice, miR-204 was correctly processed and expressed, without evident changes in retinal structure and function (*177*). In addition, the subretinal injection of the miR-204 AAV vector in different IRD models (namely, the *Aipl1*$^{-/-}$ and the *RHO*-P347S mouse lines) at PN4 was associated with a significant reduction of retinal degeneration (*177*). These data suggested that miR-204 could exert a protective effect on IRDs in a gene-independent manner.

With the first part of my thesis work, I contributed to the study of the protective effect of miR-204 in IRDs. I hypothesized that miR-204 overexpression could slow down the progression of retinal degeneration upon administration at later stages. In that respect, the data produced on mice at PN4 represented encouraging premises. However, such an early stage (i.e. PN4) does not correspond to a time of intervention that can be relevant in humans. Therefore, my work focused on exploring the effect of miR-204 overexpression at later postnatal time-points

that better represent the patient-relevant disease stages. The retinal degeneration proceeds more slowly in the *RHO*-P347S model compared to *Aipl1*$^{-/-}$ mice and visual activity can be recorded in *RHO*-P347S up to 3 months after birth. The fast degeneration occurring in the retina of *Aipl1*$^{-/-}$ mice does not allow an effective analysis of interventions at later time-points. I therefore used the *RHO*-P347S mice to further investigate the translational potential of miR-204 as a therapeutic approach for IRDs because the rate of degeneration in this model allows an appropriate window of therapeutic intervention starting from post-developmental stages.

3.1 Subretinal injection of pre-miR204 at PN14 preserves visual function in *RHO*-P347S mice at PN30 and PN60

To explore whether miR-204 overexpression could impact IRD progression upon delivery at more clinically relevant stages, I assessed the functional effect of the AAV-miR204 administration at later postnatal timepoints in *RHO*-P347S mice exploiting the moderate rate of retinal degeneration in this model. I first tested the effect of miR-204 overexpression at PN14, when the mouse retina is fully differentiated but signs of degeneration are not yet evident. These experiments were performed in collaboration with Prof Enrico Maria Surace and Elena Marrocco. A group of *RHO*-P347S mice was treated according to the injection scheme shown in Figure 9. Specifically, we injected one eye with 1x10^9 GC of AAV.CMV.miR204 and the contralateral one with a control vector mix containing 1x10^9 GC AAV.CMV.miR204MUT, a control vector that drives expression of the miR-204 precursor sequence with a mutated seed sequence (*177*). An EGFP-expressing vector (AAV.CMV.EGFP)

was co-injected in either eye at a 1:10 ratio (i.e. $1x10^8$ GC) to assess virus distribution. We then recorded retinal function by electroretinogram (ERG) at PN30 (n=18) and PN60 (n=13).

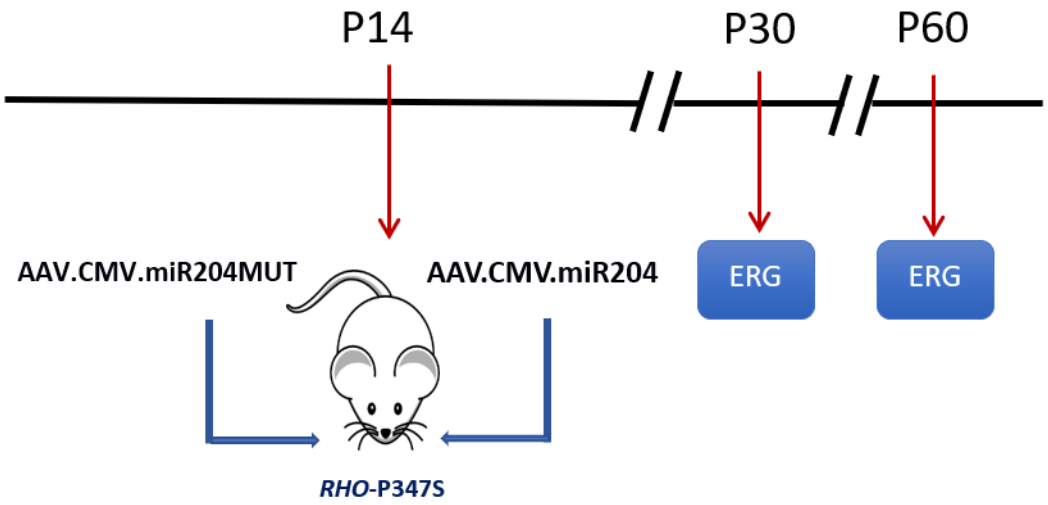

Figure 9. Schematic representation of the experimental design.

The ERG detects the electric signal generated by the retina in response to a light stimulus. Specifically, it consists in measuring the amplitude of the a- and b-wave. The a-wave reflects the electrical activity deriving from the initial photoreceptor response. The b-wave indicates the activity of the downstream bipolar-Müller cell complex, whose light response is initiated by synapses with photoreceptors (*187*), and constitutes the most prominent component of the ERG response. The amplitudes of the a- and b-waves are plotted against the light intensities, both in dark-adapted scotopic conditions, in which the response is mediated by rods, as well as in light conditions which evoke cones response.

I observed a significant increase of the b-wave amplitude and a trend of preservation of the a-wave amplitude in the miR-204 treated eyes compared to the control eyes at PN30 (Figure

10A). In particular, the difference is evident and statistically significant for the b-wave component in response to the highest luminances (i.e. 10 and 20 cd.s/m^2) under scotopic conditions (Figure 10A, right panel). Under these conditions, the ERG response is related to a mixed rod-cone activity. These results indicate that the overall retinal function of *RHO*-P347S mice is significantly preserved upon overexpression of miR-204 by subretinal injection at PN14. Noteworthy, the protective effect of AAV-miR-204 injection persisted up to six weeks post-injection, as shown by the fact that an improved ERG response was still observed at PN60 both for the a-wave and b-wave components (Figure 10B). Taken together, these results suggested that miR-204 overexpression at early stages of the disease is able to preserve visual function in preclinical models of IRD, similarly to what has been observed with injections at PN4.

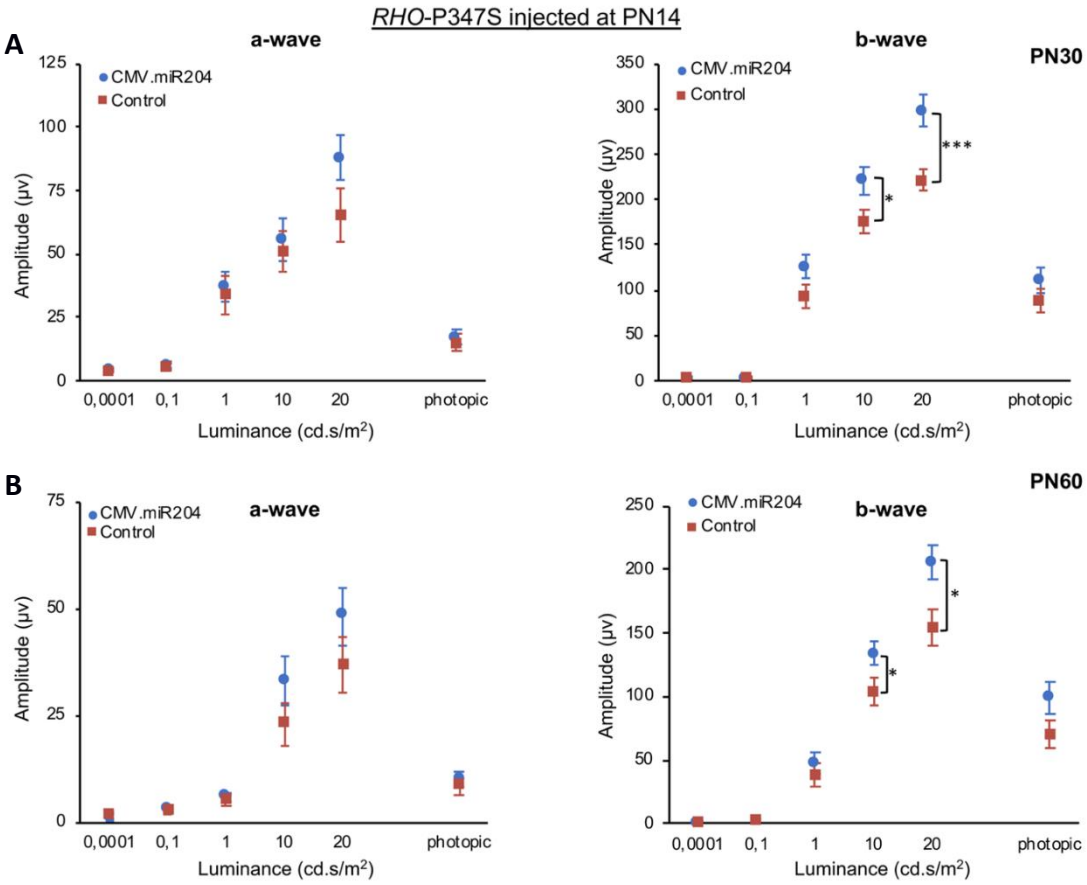

Figure 10. Protective effect of miR-204 injection at PN14 in *RHO*-P347S mice.

ERG analysis of *RHO*-P347S mice injected with the AAV.CMV.miR204 and control vector at PN14. Retinal function was better preserved in miR-204 treated eyes vs contralateral eyes injected with the control vector at PN30 (A, n=18) and PN60 (B, n=13), as indicated by a statistically significant increase in b-wave amplitudes at a light stimulus of 10 and 20 cd.s/m2

* p<0.05, ***p<0.001, unpaired Student's t-test

3.2 Subretinal injection of pre-miR204 at a stage of advanced degeneration (PN24) preserves visual function in *RHO*-P347S mice

In order to explore the translational potential of miR-204 overexpression as a therapeutic approach for IRDs, I assessed the effect of miR-204 delivery at later postnatal stages that would recapitulate more closely those exploitable for clinical applications in human patients. To this end, in collaboration with Prof Enrico Maria Surace and Elena Marrocco, we administered the AAV-miR204 vector in *RHO*-P347S mice at PN24, which is a stage of advanced retinal degeneration. Subretinal injections were performed using the above-mentioned viral doses and injection scheme. We recorded the ERG responses directly at PN60 to allow adequate time for the AAV vector to effectively transduce the retinal cells before assessing possible outcomes. Consistently with the experiments conducted at earlier timepoints, I observed an increased amplitude of the scotopic ERG response at high luminances in mice treated with the AAV-miR204 vector compared to those injected with the control. Notably, this difference was statistically significant for both a-wave and b-wave amplitudes recorded at the highest luminance of 20 cd.s/m^2, and for the b-wave also at 10 cd.s/m^2 (Figure 11). These results indicate that miR-204 overexpression exerts a protective effect in *RHO*-P347S mice even when the vector is administered at a stage in which the degeneration is ongoing. Taken together, these data strongly corroborate my initial hypothesis that miR-204 overexpression by subretinal injection may represent a promising therapeutic approach for IRDs.

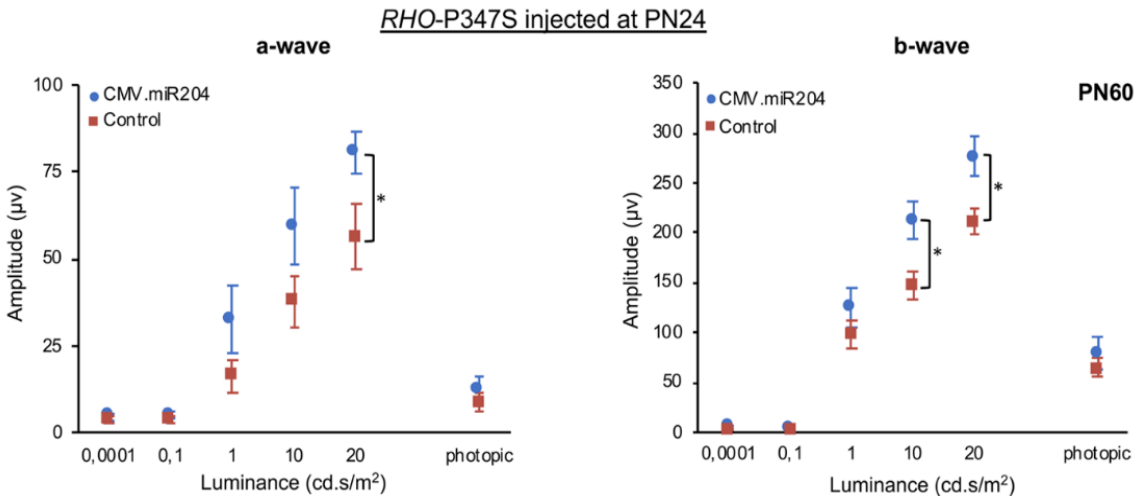

Figure 11. Protective effect of miR-204 subretinal injection at PN24 in *RHO*-P347S mice.

ERG analysis at PN60 of *RHO*-P347S mice (n=11) injected subretinally at PN24 with the AAV.CMV.miR204 and control vector. Significantly improved a- and b-wave responses were recorded in the miR204-treated eyes compared to controls. * p<0.05, ***p<0.001, unpaired Student's t-test

Dissection of the molecular and cellular mechanisms underlying the protective effect of miR-204 overexpression in *RHO*-P347S mice

Histological analysis was previously performed at PN30 on retinas of both *Aipl1*$^{-/-}$ and *RHO*-P347S mice injected with AAV.CMV.miR204 at PN4 to determine the structural and cellular changes associated with the observed protective effect (*177*). These experiments revealed a preservation of photoreceptor structures in the eyes injected with AAV.CMV.miR204 compared to the contralateral control eyes, as assessed by immunolabelling for photoreceptor markers (i.e. Rhodopsin, Cone arrestin, M- and S-opsin) (*177*). In parallel, TUNEL staining revealed a significant decrease in the number of apoptotic cells in the outer nuclear layer (ONL, containing the nuclei of cone and rod photoreceptors) of miR-204-treated eyes. Moreover,

there was a reduction in gliosis as indicated by immunolabelling for glutamine synthetase (GS6), which is a commonly used marker for Müller glia cells (*177*).

Photoreceptor cell death and reactive gliosis are tightly linked with the pathogenesis and progression of IRDs, even though their precise contribution is not fully elucidated. In particular, microglia activation is triggered by PR death in order to promote restoration of the retinal milieu. However, if the harmful stimulus is severe or sustained, activated microglia exceed the homeostatic activity and contribute to the worsening of the degeneration(*188*). Microglia activation was also shown at pre-degenerative stages (*41, 189*) indicating a possible role in the initiation of retinal degeneration processes.

In this respect, the preservation of retinal function that we observed in *RHO*-P347S mice upon overexpression of miR-204 under the ubiquitous CMV promoter could derive either from a direct protective effect of miR-204 on PR cells or an indirect protection of PRs following the reduction of glial activation, or a combination of the above. To elucidate the mechanism by which miR-204 overexpression exerts its protective effect in *RHO*-P347S retinas, I sought to dissect the underlying molecular pathways and cellular processes.

3.3 Transcriptome analysis of AAV.miR204-injected *RHO*-P347S mice

To decipher the pathways that primarily mediate the protective effect observed upon subretinal administration of miR-204 in *RHO*-P347S mice, I carried out a transcriptome analysis in collaboration with the bioinformatic core at TIGEM. The *RHO*-P347S mice (n=3) were injected at PN4 that was shown to be an effective timepoint of injection. In each animal, one eye was injected with the AAV.CMV.miR204 and the contralateral eye was injected with the control vectors. Total RNA was collected from injected retinas at PN12 and was analysed by

RNASeq. I chose to carry out this experiment at PN12 in order to get insights into the early gene expression changes associated with miR-204 overexpression and avoid readouts of secondary effects that may merely reflect the differential evolution of the degeneration processes in *RHO*-P347S mice.

Analysis of the transcriptomic data revealed a total of 420 Differentially Expressed Genes (DEGs) (based on a False Discovery Rate (FDR)<0.1) between the miR-204-injected eye versus the contralateral one. Of those, 104 genes were up-regulated and 316 genes were down-regulated. A Gene Ontology Enrichment Analysis (GOEA) analysis was conducted on the DEGs, focusing on the biological processes (BP) terms (GOTERM_BP_FAT) with an enrichment score (ES) > 1.5 and FDR < 0.1.

The top statistically significant enriched terms were mostly associated with the down-regulated genes. Specifically, more than half of enriched terms were related to immune response, innate immune response, and inflammatory responses (Figure 12). On the other hand, there was significant enrichment for terms associated with visual perception among the up-regulated genes. This was in agreement with the improvement of ERG responses and the preservation of PRs morphology that I observed in the functional and histological analysis described in the above paragraph.

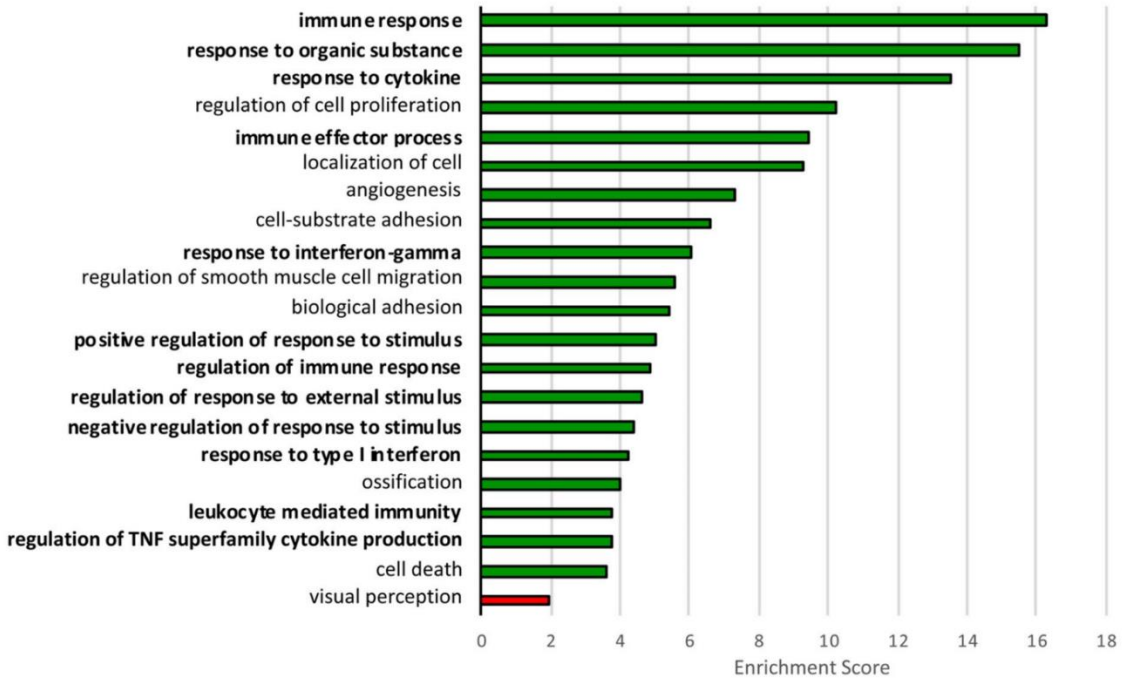

Figure 12. Top enriched biological processes (BPs) in *RHO*-P347S retinas injected with AAV.CMV.miR204.

Among the differentially expressed genes up-regulated genes are significantly enriched for the visual perception BP (red). Down-regulated genes are significantly enriched for BPs related to innate immune response, inflammatory response, defense response, and cell death, among others (green). Terms that are directly related to the ancestor terms of "immune system process" (GO:0002376) and "response to stimulus" (GO: 0050896; ancestor of inflammatory response-related terms) are indicated in bold fonts. Terms are ranked according to the enrichment score of each cluster (plotted on the x axis)

Interestingly, previous transcriptomic analyses of retinas from WT (C57BL/6) and *RHO*-P347S mice had shown that the pathways of innate immune response, inflammatory responses and cell death are associated with the early pathogenic events in *RHO*-P347S mice (M. Karali, personal communication).

Taken together, these results strongly indicate that the subretinal administration of AAV.miR204 exerts a protective effect in *RHO*-P347S mice by reducing the activation of

processes such as immune response and cell death which are both associated with the onset and progression of retinal degeneration in this model.

3.4 Identification and *in vitro* validation of mRNA targets underlying the protective effect of miR-204 in *RHO*-P347S mice: *Siglec1* and *Xaf1*

In order to uncover the possible direct mediators of the protective activity exerted by miR-204 in *RHO*-P347S mice, I filtered the significantly down-regulated DEGs for genes that are predicted targets of miR-204.

Several bioinformatic tools have been developed to predict miRNA-mRNA interactions (*190*). Most target prediction tools take into account common features of miRNA target recognition such as: a) a match between the seed sequence of a given miRNA and the 3' UTR sequence in the mRNA of the putative target gene; b) the conservation across species of the regions of interest in the miRNA and mRNA sequences; c) the stability of the predicted miRNA-mRNA binding (assessed in terms of free energy, ΔG) and d) how easily the miRNA can access the interaction site of the target mRNA, given the secondary structure acquired by the mRNA (*190*). Based on these criteria, putative mRNA targets for a given miRNA are listed in databases (e.g. microTCDS (*191*), http://diana.imis.athenainnovation.gr/DianaTools/index.php?r=microT_CDS/index ; TargetScan (*192*), http://www.targetscan.org/). Other co-expression-based tools for systematic miRNA target recognition, such as HOCTAR (*193*) and Co-expression Meta-analysis of miRNA Targets (CoMeTa) (*194*), allow a more comprehensive and accurate prediction of miRNA targets.

I combined the miR-204 predicted targets from sequence-based miRNA target-prediction databases (e.g. microTCDS and TargetScan) and co-expression-based tools (e.g. Cometa), and identified a list of putative miR-204 targets among the genes that were down-regulated upon miR-204 administration in *RHO*-P347S. I then focused my attention on genes that were reported in literature to be associated with retinal degeneration and that were significantly up-regulated in *RHO*-P347S mice compared to WT mice, according to the transcriptomic analysis that was previously performed by our research group (see above). In particular, I selected two candidate genes, namely *Siglec1* and *Xaf1*, and performed a luciferase assay to test whether miR-204 is able to directly target their 3' UTR.

Siglec1 is a predicted target of miR-204 (according to both microTCDS and TargetScan) and was up-regulated in retinas of *RHO*-P347S compared to WT mice. Upon miR-204 administration in *RHO*-P347S, *Siglec1* was significantly down-regulated compared to the control-treated eye. *Siglec1* encodes for Sialoadhesin (Sn or CD169), a cell adhesion receptor expressed on the membrane of macrophages and activated monocytes (*195, 196*). *Siglec1* was recently shown to promote the neuroinflammation associated with the progression of neurodegenerative diseases and its up-regulation was related to the pathogenesis of neuronal ceroid lipofuscinosis (CLN) (*197*). Consistently, *Siglec1* inactivation in a CLN mouse model resulted in a significant reduction of the neuron loss and the retinal thinning associated with the disease (*197*). Based on this evidence, I hypothesized that miR-204 may exert a beneficial effect on retinal degeneration, in part, by modulating *Siglec1* expression.

Xaf1 (XIAP-associated factor 1) is another predicted target of miR-204 that drew my attention. XAF1 is a proapoptotic factor that can sensitise cells to death by inhibiting the anti-apoptotic action of XIAP (*198, 199*) or sensitising the cell todeath triggers such as TNF-alpha, independently of its interaction with XIAP (*199*). Notably, XIAP is reported to be a protective factor in mouse models of IRDs (*200, 201*). I therefore hypothesized that the reduction of *Xaf1* levels could be a direct mechanism underlying the protective effect of miR-204 in *RHO*-P347S mice. Indeed, *Xaf1* levels are higher in *RHO*-P347S compared to WT retinas, suggesting its involvement in retinal degeneration, similar to what had been observed for *Siglec1*.

To test the direct binding of miR-204 to the 3'UTR of *Siglec1* and *Xaf1* I performed a luciferase assay which is routinely used to study the post-transcriptional activity of miRNAs on target genes (*202*). This assay consists in using the firefly luciferase (LUC) as a bioluminescent reporter gene fused with the 3' UTR of the miRNA putative target gene. The engineered vector is then co-transfected with the test miRNA or negative controls in an *in vitro* cellular system. A reduced bioluminescence in the cells transfected with the test miRNA compared to those receiving the negative control miRNAs will indicate that the miRNA can bind to the 3' UTR of engineered luciferase vector and regulate its expression.

For this purpose, the 3' UTR sequences of *Siglec1* and *Xaf1* were amplified by PCR from mouse genomic DNA and cloned downstream of the luciferase coding sequence in the luciferase reporter constructs. The so-engineered reporter construct was then co-transfected with the miR-204 mimic duplex into HeLa cells. Non-targeting miRNA mimics (negative mimic) were used in parallel as negative controls. In each experiment, a reporter construct containing the 3' UTR with the mutated predicted binding site of the miR-204 seed were used as control for

the specificity of the binding between the 3' UTR and the miRNA mimics (Figure 13B). The presence of the mutated binding site should prevent the targeting of the 3' UTR by the miRNA under investigation and consequently the reduction of luciferase activity.

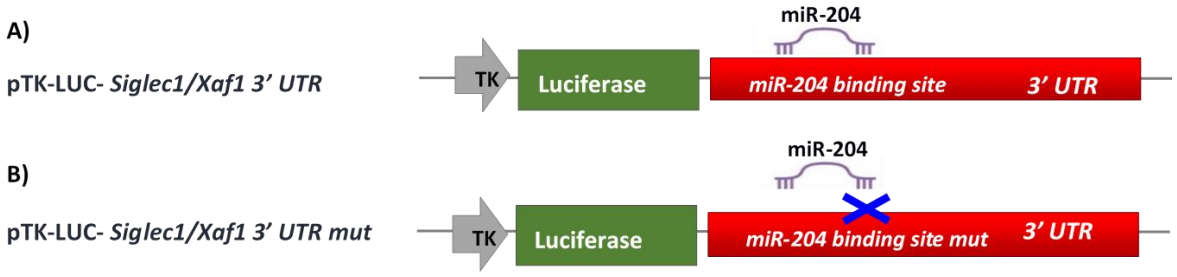

Figure 13. Schematic representation of the luciferase reporter vectors used for the transfection of HeLa cells and interaction with miR-204.

A) The 3' UTR of the putative target gene is inserted in the LUC vector. The direct binding between miR-204 and the miR-204 binding site in the 3' UTR will lead to a reduced LUC expression and activity in the cells co-transfected with the luciferase (LUC) vector bearing the WT 3' UTR of the gene and miR-204 mimics compared with the control cells (transfected with the engineered LUC vector and negative mimic). The intensity of the cellular bioluminiscent signal is used as a read-out of the LUC activity.

B) To demonstrate the specificity of the binding between the 3' UTR and the miR-204 mimics, together with miR-204 or control miRNAs, the cells are transfected with a LUC vector bearing the 3'UTR of the putative target gene mutated for the miR-204 binding site. The specific binding between miR-204 and its binding site will be prevented and the LUC expression and activity will be comparable with that of control cells.

I observed a significant reduction of luciferase activity of nearly 40% in the case of *Siglec1* and 50% for *Xaf1* when the reporter vectors containing the 3' UTR of *Siglec1* or *Xaf1* were co-transfected with the miR-204 mimics, compared to the negative control non-targeting mimics (Figure 14 and Figure 15, bars on the left hand-side). Furthermore, the specificity of the miRNA seed:target site binding was confirmed by the fact that the luciferase activity was not reduced upon co-transfection of the mimics with the reporter vectors containing the mutagenized 3'UTR of the gene of interest (Figure 14 and Figure 15, bars on the right hand-side). These

results confirmed both *Siglec1* and *Xaf1* as direct targets of miR-204. Therefore, it is plausible that the down-regulation of these two genes contributes to the protective effect exerted by miR-204 administration in *RHO*-P347S mice. In particular, the modulation of *Xaf1* levels and its downstream impact on anti-apoptotic processes may account for an early protective effect exerted by miR-204 on photoreceptor survival directly.

Moreover, the validation of *Siglec1* as a target of miR-204 is in agreement with the early modulation of pathways related to inflammation and immune response observed in miR-204 treated *RHO*-P347S mice. Together, these observations support a possible direct effect of miR-204 on inflammatory processes such as microglial activation, which was shown to contribute to retinal degeneration even prior to PRs cell death (*41*). A direct modulation of this detrimental response may account for an additional, non PR-autonomous, mechanism underlying the neuroprotective effect of miR-204.

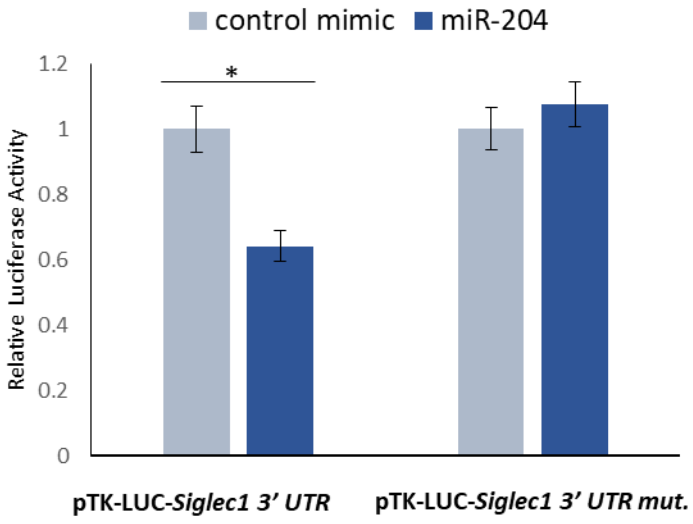

Figure 14. miR-204 binds directly the 3' UTR of *Siglec1*.

Luciferase assay confirms the direct binding of miR-204 to the 3' UTR of *Siglec1.* miR-204 mimics (bars on the left hand-side) and negative control mimics (bars on the right hand-side) were transfected in HeLa cells together with the indicated luciferase reporter plasmids carrying either the WT *Siglec1* 3' UTR (pTK-LUC-*Siglec1* 3'UTR) or the mutated binding site of the miR-204 seed (pTK-LUC-*Siglec1* 3' UTR mut). Relative luciferase activity is reported as fold change to the cells transfected with control or miR-204 mimic. A two-way ANOVA was used to compare the groups. Data are represented as mean ± standard error of the mean (SEM). n=6 observations with * p<0.05

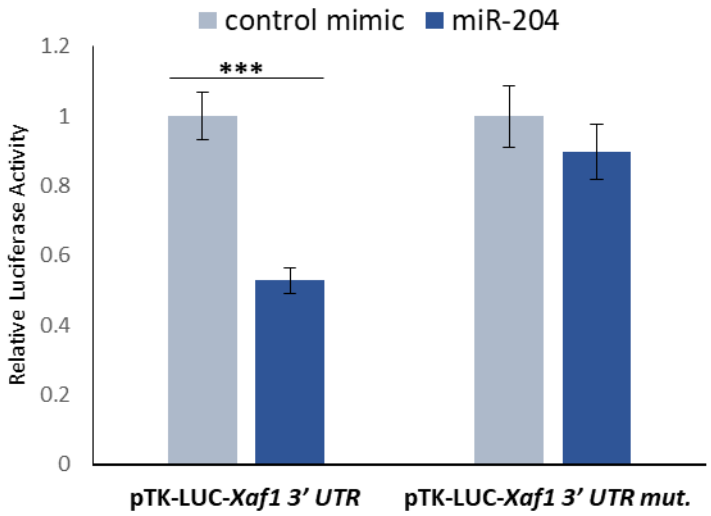

Figure 15. miR-204 binds directly the 3' UTR of *Xaf1.*

Luciferase assay confirms the direct binding of miR-204 to the 3' UTR of *Xaf1.* miR-204 mimics (bars on the left hand-side) and negative control mimics (bars on the right hand-side) were transfected in HeLa cells together with the indicated luciferase reporter plasmids carrying either the WT *Xaf1* 3' UTR (pTK-LUC-*Xaf1* 3' UTR) or the mutated binding site of the miR-204 seed (pTK-LUC-*Xaf1* 3' UTR mut). Relative luciferase activity is reported as fold change to the cells transfected with control or miR-204 mimic. A two-way ANOVA was used to compare the groups. Data are represented as mean ± SEM. n=6 observations with * p<0.05

3.5 miR-204 overexpression dampens microglia activation *in vivo* and *in vitro*

The transcriptomic analysis described in section 3.3 revealed an extensive effect of miR-204 on biological processes related to inflammatory and innate immune responses in *RHO*-P347S retinas. Resident microglia are the main effector cells of the innate immune system in the

retina, as elsewhere in the CNS (*203*). Resting microglia are mainly located in the inner retina and have a highly ramified morphology. Upon harmful stimuli such as oxidative stress, high intensity light and inherited mutations in retinal genes (*48*), microglia are activated, acquire a less ramified, amoeboid shape and migrate to the site of damage. Activated microglia have an enhanced phagocytic capacity, which is important for the removal of cell debris, and release pro-inflammatory cytokines, ROS and reactive nitrogen species (RNS) as well as neuromodulatory factors promoting tissue repair (*32, 203*). However, under excessive or prolonged pathological stimuli, activated microglia exceed their homeostatic function secreting a large amount of pro-inflammatory and potentially cytotoxic compounds (e.g. TNF-α, IL-1β, ROS, NO) (*36, 203*). Several lines of evidence suggest that a prolonged or excessive microglial activation can contribute to the initiation and/or exacerbation of retinal degeneration in IRDs. For example, in a mouse model of RP, microglia were shown to infiltrate the ONL early during degeneration and phagocytose non-apoptotic, living rod photoreceptors thus accelerating photoreceptor loss and disease progression (*41, 189*).

Based on these observations, I assessed whether miR-204 overexpression modulates microglia activation. I looked at the activation status of microglia by IF in PN30 retinas of *RHO*-P374S mice injected at PN4 with the AAV.CMV.miR204 vector. I performed a double-immunolabeling for the microglial marker Iba1 (Ionised calcium binding adaptor molecule 1), which marks both resting and activated microglia, and the CD68 lysosomal marker which is expressed at high levels in activated microglia. Immunolabeling of Iba1 in control-treated eyes revealed that the majority of microglial cells had an amoeboid shape and were mostly located in proximity to the photoreceptor outer segment (PR OS) (Figure 16, upper panels). Moreover, these bloated cells (arrowheads in Figure 16) close to the PR OS stained positive for CD68. Both the

morphology, spatial location and CD68-positivity indicated that these cells were mostly activated mononuclear phagocytes. On the contrary, the majority of microglial cells in miR-204-treated eyes were ramified, confined to the inner retinal layer and stained weakly for CD68, suggesting that microglial activation was reduced compared to control-treated eyes. These results suggest that the administration of miR-204 in *RHO*-P347S mice dampens microglia activation and are in agreement with the transcriptomic analysis (paragraph 3.3) that had indicated an early impact of miR-204 on immune responses. Nevertheless, I cannot ascertain whether the effect of miR-204 on microglial cells is direct.

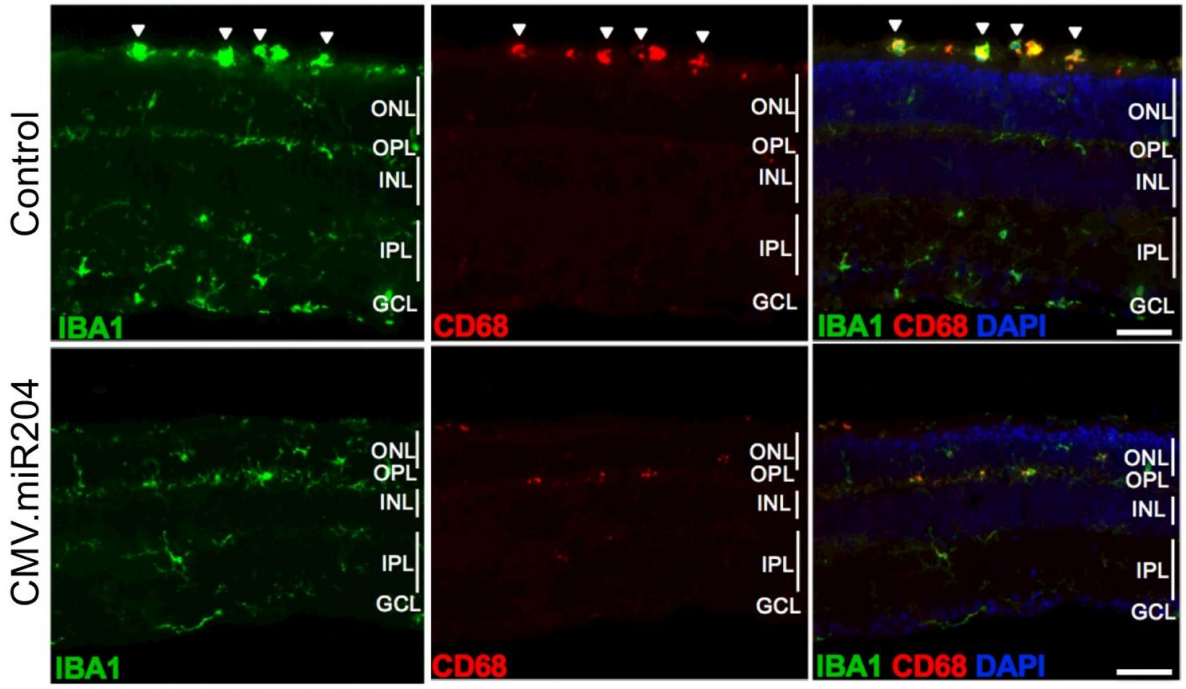

Figure 16. AAV-Mediated Delivery of miR-204 reduces microglia activation in *RHO*-P347S mice.

Immunofluorescence staining for the microglia markers Iba1 (green) and CD68 (red) on PN30 retinal sections of *RHO*-P347S mice injected with AAV.CMV.miR204 vector mix (1 x 10^9 GC AAV.CMV.miR204 and 1 x 10^8 GC AAV.CMV.EGFP) at PN4. The contralateral eye was injected with the AAV.CMV.EGFP control vector (1.1 x 10^9 GC). Iba1-positive and CD68-positive, large-bodied amoeboid mononuclear phagocytes at the proximity of the photoreceptor outer segments are marked by arrowheads.

To determine whether miR-204 is able to directly modulate microglial activation at the cellular level, I employed an *in vitro* approach based on the LPS-activated BV-2 microglial cells. BV-2 cells are an immortalised murine microglia cell line and their activation by the bacterial endotoxin LPS is a widely used *in vitro* model to study neuroinflammation. The suitability of this model was corroborated by transcriptional analyses that showed a striking correlation between the BV-2 response to LPS and the *in vivo* LPS-mediated microglia activation (*204*). Overall, this cell line exhibits a response to inflammatory stimuli (like the LPS-induced one) and cytokines (e.g. interferon) that resembles the response of primary microglia (*204*). In particular, activated BV-2 cells show a normal regulatory response of the production of nitric oxide (NO), which is a key trigger of neuronal death in neurodegenerative processes (*34*). To get insights into the role of miR-204 in microglia activation, I assessed the effect of miR-204 overexpression on the response of BV-2 cells to LPS treatment. For the cellular delivery of miR-204, I generated two constructs using as backbone the psiUx expressing vector, which is particularly effective for the production of small non-coding RNAs (*180*). One vector, referred to as 'miR-204' in Figure 17 and 18, carried the precursor sequence of miR-204. The other vector, referred to as 'miR-204-mut' in Figure 17 and 18 contained the precursor of miR-204 bearing a mutation in the seed sequence.

Briefly, as shown in Figure 17, I transfected the BV-2 cells with the miR-204 and miR-204-mut constructs and then measured by qPCR in the LPS-activated BV-2 cells the levels of the inducible nitric oxide synthase (*iNOS*) that produces the potentially toxic NO.

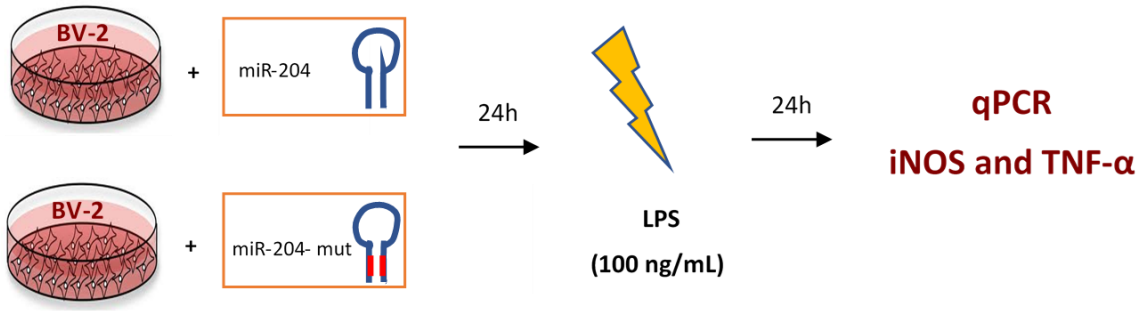

Figure 17. Experimental set-up to test the effect of miR-204 delivery on the LPS-mediated microglia activation.

Following LPS-induced activation for 24 h, *iNOS* was up-regulated seven-fold compared to untreated cells. I observed a statistically significant reduction of almost 50% in the mRNA levels of *iNOS* in cells transfected with miR-204 compared to those transfected with the control vector (Figure 18A). Across the experiments, I also observed a consistent, albeit not statistically significant, trend of reduction in the levels of *TNF-α*, a fundamental molecule for the induction and maintenance of inflammatory immune responses (*33*) (Figure 18B).

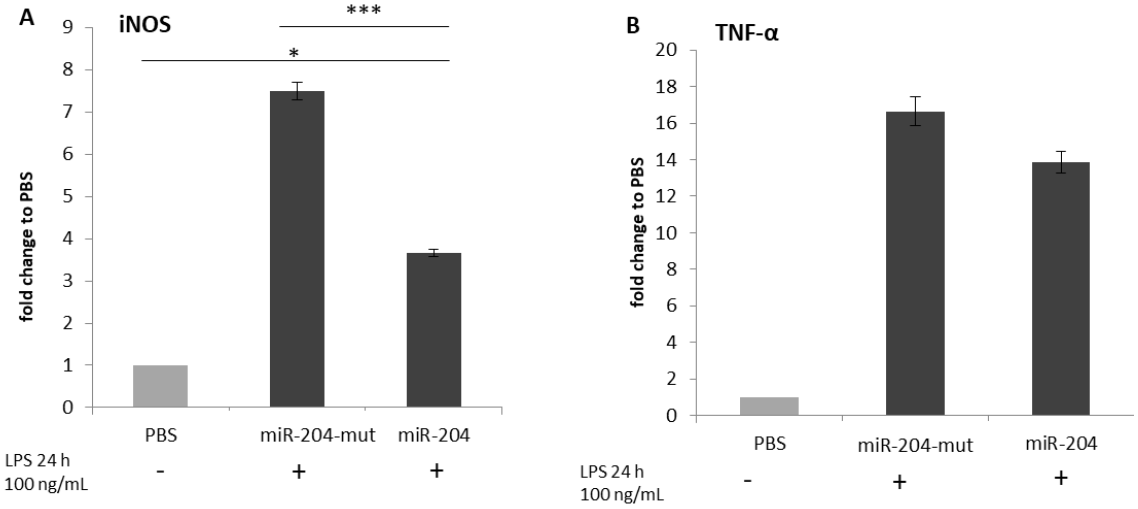

Figure 18. Expression levels of inflammatory mediators following LPS-mediated activation in BV-2 cells transfected with miR-204.

The expression level of *TNF-α* and *iNOS* was determined by quantitative real-time PCR and calculated as relative quantity (RQ) using as calibrator condition the untreated cells (light grey bars). A decrease in the expression was

observed in BV-2 cells transfected with the pre-miR204 vector (labelled 'miR-204') and activated with LPS compared to BV-2 transfected with pre-miR204-mutated vector (labelled 'miR-204 -mut') and activated with LPS. A one-way ANOVA followed by Tukey post-hoc analysis was used for within-groups analysis. Data are mean RQ ± SEM. * p<0.03 ***p<0.001. n=4 observations.

This finding indicates that miR-204 delivery reduces the production of the aforementioned pro-inflammatory mediators, probably by dampening the microglial activation that instead induces it. This observation is particularly relevant since both the free radical NO, which is produced by *iNOS*, and TNF-α are detrimental factors that contribute to retinal degeneration (*33, 34, 48*). In fact, treatments able to reduce their expression were shown to ameliorate photoreceptor death (*34, 205*). Therefore, it is plausible that the neuroprotection exerted by miR-204 in *RHO*-P347S may be mediated in part by a reduction of the inflammatory mediators produced by reactive microglia that, in turn, exacerbate photoreceptor damage (*37*). In light of the above, it will be interesting to test whether the microglial-specific delivery of miR-204 in *RHO*-P347S retinas improves retinal function. However, transduction of microglial cells by AAV vectors is still particularly challenging with only one study reporting a successful outcome (*206*).

3.6 Photoreceptor-specific delivery of miR-204 partially preserves visual function in *RHO*-P347S mice

To understand whether miR-204 preserves visual function in *RHO*-P347S mice by acting directly on PRs, I assessed the effect of delivering miR-204 using a rod-specific promoter. To this end, I generated the pAAV.RHO.miR204 vector by replacing the CMV promoter in pAAV.CMV.miR204 (used in the previous experiments) with the human *RHO* promoter sequence which directs transgene expression primarily to rod photoreceptors. I then used the

pAAV.RHO.miR204 construct to generate the corresponding AAV vector (AAV.RHO.miR204) in the 2/8 serotype, similar to what described for AAV.CMV.miR204. In this set of experiments, *RHO*-P347S mice were injected with the RHO.miR204 vector mix (1 x 10^9 GC AAV.RHO.miR204 and 1 x 10^8 GC AAV.RHO.EGFP) in one eye, while the contralateral eye was injected with the control vector AAV.RHO.EGFP (1.1 x 10^9 GC). The subretinal injections were performed at PN4 and PN14. Retinal function was assessed by ERG at PN30 and PN60.

We recorded a significantly improved b-wave amplitude, both at PN30 and PN60, following injection of AAV.RHO.miR204 in the *RHO*-P347S mice at PN4. In particular, the b-wave amplitude of both scotopic and photopic ERG responses at PN30 was significantly higher in AAV.RHO.miR204-treated mice compared to those injected with the control (Figure 19B). Similar levels of retinal function persisted up to 2 months post-injection in miR-204 treated eyes and were significantly different compared to those of control eyes at most luminance stimuli applied (Figure 19CD). A-wave amplitudes also showed a trend of improvement in miR204-treated eyes, but without statistical significance.

On the contrary, the subretinal delivery of AAV.RHO.miR204 at PN14 did not preserve significantly ERG responses at PN30 or PN60 (Figure 20), indicating that a PR-autonomous mechanism may not represent the primary mechanism underlying the protective effect exerted by miR-204 in *RHO*-P347S mice at later stages of intervention.

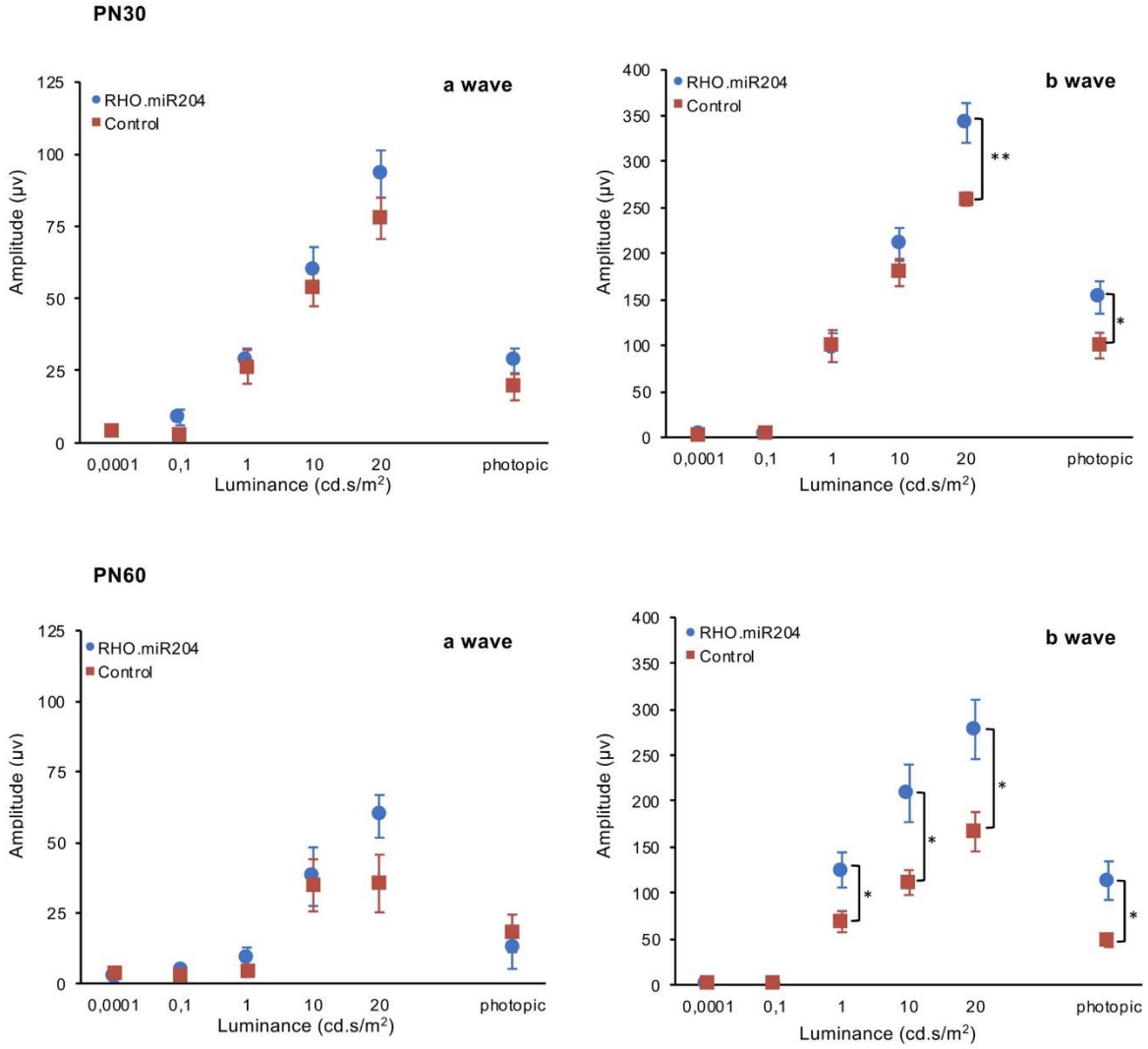

Figure 19. Rod-specific delivery of AAV-miR-204 in the retina of *RHO*-P347S mice at PN4 improves ERG responses.

ERG responses of *RHO*-P347S mice injected with AAV.RHO.miR204 or AAV.RHO.EGFP at PN4. Mice were recorded at PN30 (n = 19; A and B) and PN60 (n = 11; C and D). Subretinal injection of RHO.miR204 results in a statistically significant increase of b-wave amplitudes in miR204-treated eyes compared to control-injected contralateral eyes. Statistical significance (p value), calculated using an unpaired t test against control vector values, is indicated with asterisks (*$p < 0.05$; **$p < 0.01$).

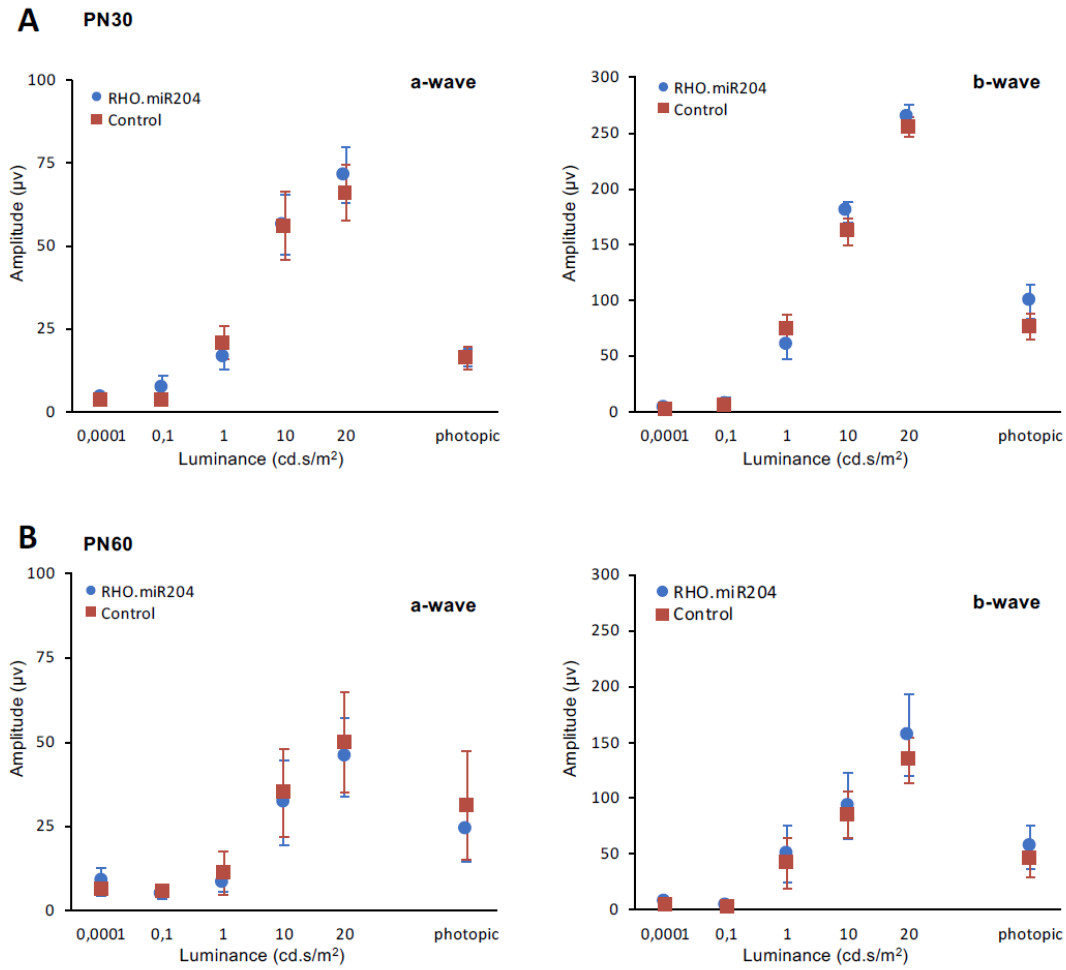

Figure 20. AAV-mediated delivery of miR-204 using a photoreceptor-specific promoter at PN14 does not improve ERG responses in *RHO*-P347S mice.

ERG responses of RHO-P347S mice injected with the AAV.RHO.miR204 and the control vector (AAV.RHO.EGFP) at PN14. ERGs were recorded at PN30 (n=17; A) and PN60 (n=5; B). No statistically significant improvement of a- and b-wave amplitudes was recorded at PN30 and PN60 in RHO.miR204-treated vs contralateral control eyes. Vector doses were: 1x109 GC AAV.RHO.miR204, 1x108 GC AAV.RHO.EGFP per eye; 1.1x109 GC AAV.RHO.EGFP per control eye.

In summary, the miR-204 overexpression under a rod-specific promoter at PN4 preserved retinal function in *RHO*-P347S mice, yet to a lesser extent than the one achieved upon the widespread delivery of miR-204 using the ubiquitous CMV promoter. Furthermore, IF analysis

and TUNEL assays did not reveal evident differences in the expression of PR markers (i.e. cone arrestin, Rhodopsin, M-opsin, S-opsin) and in the extent of cell death between RHO.miR204-injected and control eyes (data not shown). Taken together, these data suggest that the protective effect exerted by AAV-miR204 delivery in *RHO*-P347S mice is only partially mediated by cell-autonomous mechanisms in photoreceptor cells. Instead, it is plausible that miR-204 targets additional cell processes related to the pathogenesis of retinal degeneration in *RHO*-P347S mice. In this respect, I did not detect any significant change in microglia activation (IF with anti-CD68 and anti-Iba1; data not shown) following RHO.miR204 delivery between miR204-treated and control eyes. This observation supports our interpretation that the dampening of immune responses in CMV.miR204-treated eyes is likely to be due to the direct effect of miR-204 on innate immune effector cells.

In vitro study to identify candidate miRNAs with a protective action on retinal degeneration

3.7 Light-induced damage in 661W cells as an *in vitro* model of retinal degeneration

To expand my investigation on the potential role of miRNAs in Gene Independent Therapies (GITs) for IRDs, I decided to identify additional candidates that can counteract retinal degeneration processes regardless of the disease-causing mutation. To this aim, I used an *in vitro* model based on light-induced damage in the 661W cone-like cells (*23, 207*) which has been widely used to study photoreceptor degeneration (*185*). In order to test the activity of several miRNAs in parallel, I designed a high-throughput approach.

First, I determined the most appropriate conditions for our experimental needs, such as the ratio between cell seeding density and final concentration of miRNAs, and illumination. For the pilot experiments, I used 96-multiwell plates which are easier to handle, and transfected non-targeting mimics (negative mimics) which I then used as controls for the actual screening. I initially tested 25 nM and 50 nM of mimics, and opted for the lower concentration to gain a fine modulation without overloading the miRNA processing machinery. To set up the system, I exposed the 661W cells to intense white LED light (15000 lux) for 4 h in a dedicated incubator and assessed cell viability using the 3-(4,5-dimethylthiazol-2-yl)-2,5-diphenyltetrazolium bromide tetrazolium (MTT) assay according to published protocols (*185*). I also verified that the temperature of the cell culture medium remained stable under such conditions (i.e. presence of light source in the incubator). As control, I used cells grown on a plate that was shielded from light and was kept in the same incubator with the light-exposed one to ensure identical conditions of temperature, CO_2 and humidity. These tests showed that under these conditions I could obtain a reduction of 661W cell viability comparable to that reported in

literature (*185*). Specifically, the cell viability decreased by ~20% compared to the control cells in dark conditions (Figure 21). Other combinations of cell density and light exposure induced even higher damage (data not shown). I considered that this moderate damage was appropriate to reveal the fine modulation that I expected since I preferred to use a mild concentration of miRNAs in the screening.

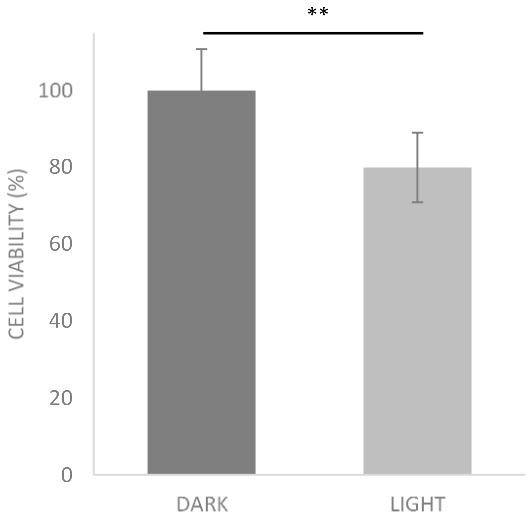

Figure 21. Cell death after 4 hours of light exposure of 661W cells transfected with negative mimics.

Cells were transfected with 25 nM of negative mimics and cultured in a clear 96-well plate at a density of ~2700cellsl/well. Cell viability was assessed by an MTT assay. The absorbance readings of the blue formazan product were carried out at 570 nm and plotted as percent ratio of the light-exposed cells to the dark-grown ones (mean± SEM), set as 100% viable.

**p<0.01, two-tailed t-student's test.

3.8 High-content screening of a miRNA mimic library using the light-induced damage model

To test the effect of a large number of miRNAs on the viability of 661W cells exposed to light stress I implemented a high-content screening approach in collaboration with Medina's research group at TIGEM. The microscopy-based high-throughput screen allowed us to visualize and better control key features of the sample preparation (e.g. cell density, spatial distribution into the well) that could impact the screening efficiency and outcome. Moreover, the high-content approach enabled the simultaneous, automated and robust analysis of multiple phenotypic parameters within a single experiment. For the screening, I used a 384-well format library of human miRNAs (miRIDIAN miRNA Mimic Library, Dharmacon) which contains mimics for every human miRNA annotated in the miRBase sequence database v.21.0. I then screened the first two plates of the library which contain 560 miRNAs, highly conserved across evolution. The workflow adopted for the high-content screening is illustrated in Figure 22.

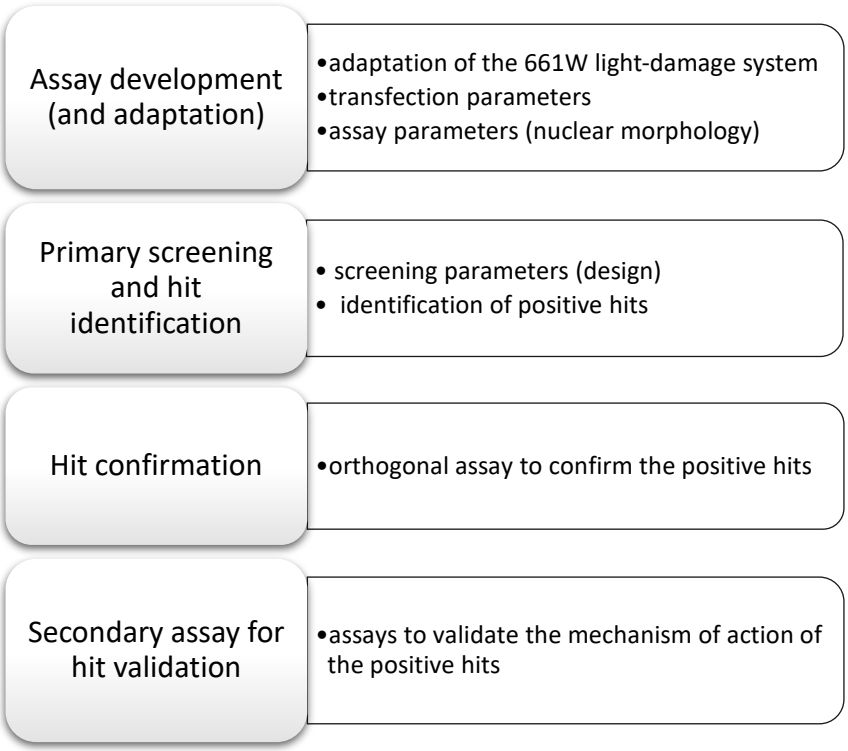

Figure 22. Workflow for the high-content screening of a miRNA library based on light-induced damage in 661W cells.

3.8.1 Assay development: adaptation of the *in vitro* system (i.e. light-induced damage in 661W cells) and transfection conditions

The high-content screening was developed in 384-well plates. Compared to the 96-well plates used in the pilot assay, the 384-well format reduces the inter-plate variability given that a larger number of test samples can be compared to each other within the same plate. Furthermore, the total amount of required reagent is significantly optimized. I therefore adapted the cell seeding density and the amount of transfection reagent used per well, accordingly. Adjusting the cell number (~ 650 cells/well) required various tests, because the bottom of the well in the 384-well black plates used for imaging has a different cell adherence

compared to the multi-well plates routinely used for cell culture. Moreover, I also extended light-exposure to 6 h to reach the same amount of cell damage achieved during the pilot experiments using the 96-well clear plates. Finally, using a non-targeting miRNA mimic transfection control labeled with Dy547 (absorbance/emission max: 557/570 nm), I verified that the average transfection efficiency was approximately 50% (Figure 23).

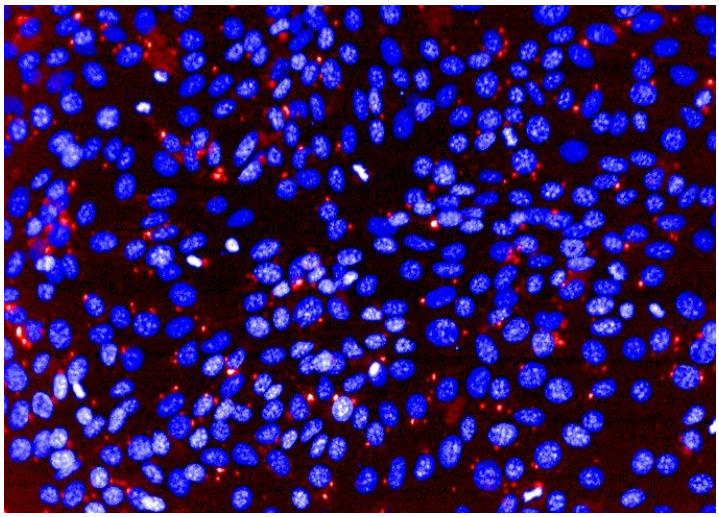

Figure 23. Representative image of 661W cells transfected with microRNA mimic control Dy547.

The cells were plated at the optimized conditions (650 cells/well, cultured for ~ 60 h in a 37°C and 5% CO_2 incubator), stained with Hoechst 33342 dye (shown in blue) and visualized under the high-content microscope. The red spots correspond to the signal of the red-fluorescent dye (Dy547)-labeled mimic.

3.8.2 Assay development: assay parameters

To assess the percentage of dying cells as a read-out of the damage induced by the light stimulus in 661W cells (transfected with control or test samples), I analysed the nuclear morphology using Hoechst 33342 staining in collaboration with Angela Panarella. Nuclear features (e.g. chromatin condensation, reduced nuclear size) were shown to be reliable indicators of dying cells (*208, 209*). Therefore, the quantitation of nuclear size and

condensation status using Hoechst 33342 staining is a straightforward assay of cell viability, particularly suitable for large-scale screenings. Hoechst is a fluorescent, non-intercalating dye that binds the A-T regions of the DNA minor groove. It penetrates both healthy and dying cells. However, its fluorescent intensity is increased due to nuclear condensation, a characteristic morphological change that occurs following cell injury.

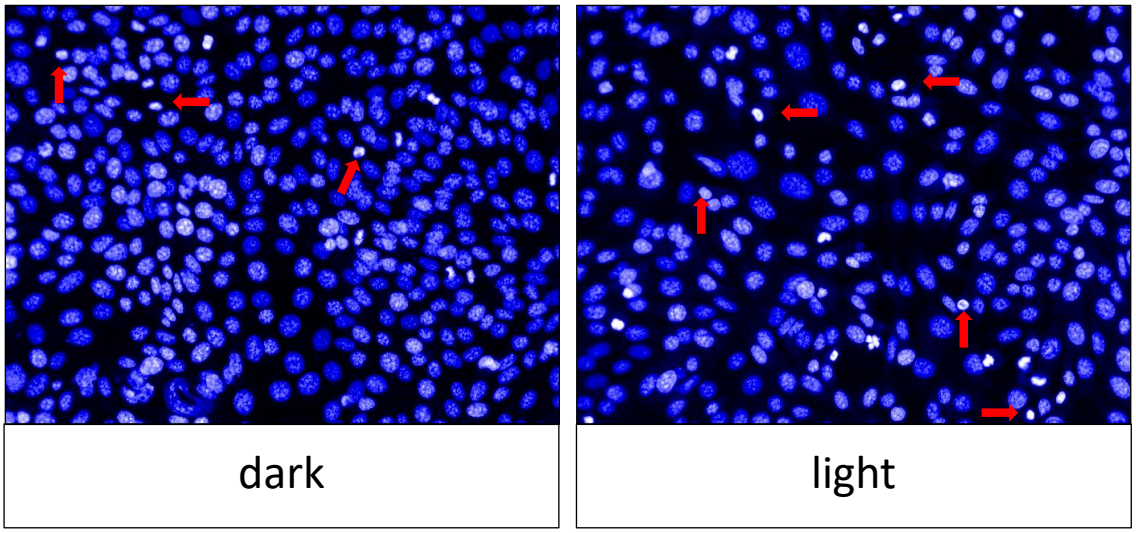

Figure 24. Hoechst 33342 staining of 661W cells transfected with negative mimics and kept in dark (dark) or exposed to light (light)).

Representative images of wells from 384-format plates containing 661W cells transfected with negative mimics and kept in dark (dark) or exposed to light (light). The red arrows indicate nuclei with the typical morphology found in dying cells. Cells transfected with negative mimic controls and exposed to light show a higher frequency of reduced nuclear size and brighter Hoechst staining.

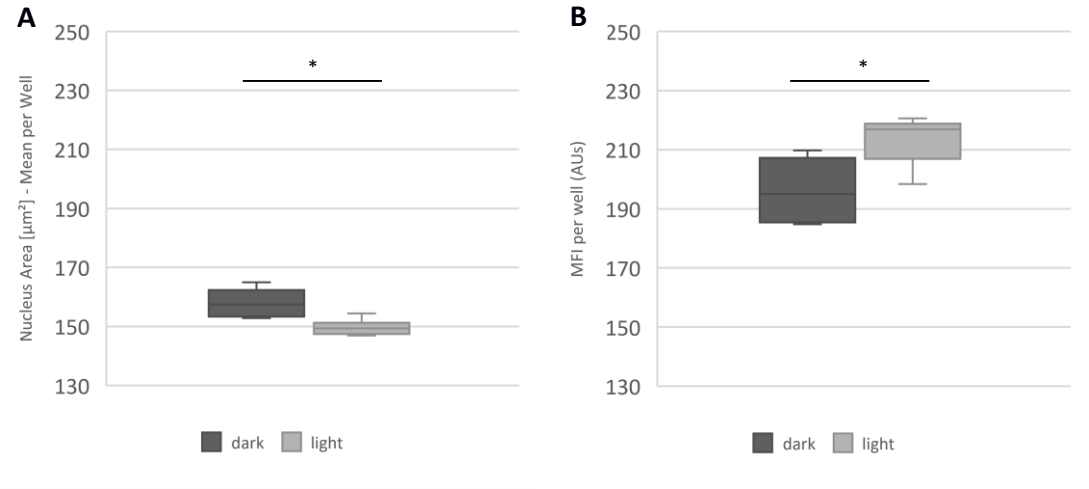

Figure 25. Boxplot showing the distribution of the nuclear parameters analysed for the control groups.

The plots show a decrease of the mean nuclear area (A) and the increase of the mean fluorescence intensity (MFI; B) within the wells in dark (n=10) compared to those exposed to light (n=10), as expected for dying cells. *p <0.05, Mann-Whitney test

To assess whether measurements of the nuclear area and Hoechst 33342 fluorescence intensity were suitable morphological readouts of the cell damage in our system, we looked at their mean values among the cells exposed to light-damage compared to those kept in the dark.

We set thresholds (also validated by visual inspection) for nuclear size and Hoechst 33342 staining intensity to define a subpopulation of dying cells (Figure 24). We then quantified their percentage in the overall population in each sample. The Columbus 2.6 software was then used for the automated analysis of the images acquired by the Opera HTS imaging system. The resulting analysis showed significant differences between the cells exposed to light-damage and those maintained in dark conditions. Specifically, I detected both a reduction of the

nuclear area (Figure 25A) as well as increased Hoechst fluorescence intensity (Figure 25B) in light-exposed cells, indicating the prevalence of a phenotype typical of damaged cells.

The experimental setting used for the HCS experiments is recapitulated in Figure 26.

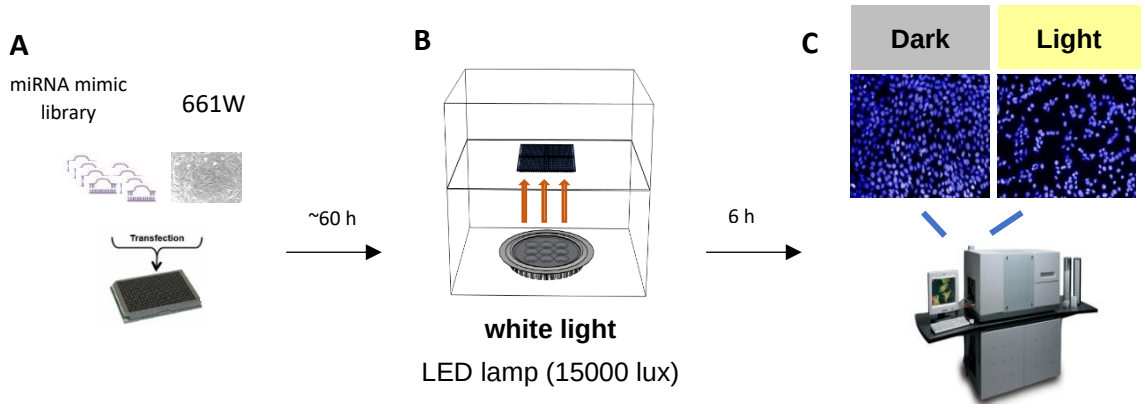

Figure 26. Schematic representation of the experimental set up used for the HCS experiments.

The HCS experiments consisted of the following stages. A) 661W (650 cell/well) were retro-transfected with miRNA mimics (25 nM) in a black 384-well plate with clear bottom which is adequate for imaging. B) The cells were exposed to light in dedicated humified incubator (37 °C, 5% CO_2) containing a LED lamp placed on the bottom. The plate laid on a plexiglass plane that was placed above the lamp at such a distance so that the plate was reached by an illumination intensity of 15000 lux. The first two column of the plated where shielded to generate the controls in dark conditions. C) Following 6 h of light-exposure, Hoechst 33342 was added to the media and the cells were imaged by using the Opera live imaging system to assess changes in nucleus area and MFI.

3.8.3 Primary screening: quality control (QC) of the assay

Assessing assay performance is a fundamental prerequisite for the up-scaling of an *in vitro* assay. For this reason, quality control (QC) criteria have been defined to evaluate the performance of the controls and inform about the variability and reliability of the results. In my case, I used the Strictly Standardized Mean Difference (SSMD) which is the reference QC

parameter for miRNA screenings (*210*). It evaluates the degree of difference between positive and negative controls considering also their variability, with a solid probabilistic and statistical interpretation. According to the SSMD equation (Figure 27), an SSMD value of 1, 2, or 3 indicates that the probabilities that a value from the positive control population is greater than a value from the negative control population are respectively about 0.5, 0.95, and 0.975, when the difference shows a symmetric unimodal distribution with finite variance (*211*). This defines good quality for an assay with controls of moderate strength.

$$SSMD = \frac{mean(C_{pos}) - mean(C_{neg})}{\sqrt{std(C_{pos})^2 + std(C_{neg})^2}}$$

Figure 27. Equation of the SSMD parameter.

To perform the QC assay I considered the percentage of dying cells in the wells exposed to light (positive control , C_{pos}) or in dark conditions (negative control, C_{neg}). The resulting SSMDs of each replicate ranged between 2 and 3, indicating the good quality of the assay.

3.8.4 Primary screening: screening parameters and hit identification

I screened a subset of the human miRIDIAN mimic library consisting of the first 560 miRNAs that are among the most conserved across evolution (Figure 28). The screen was performed using 384-well plates in which the test miRNAs were arranged in the same positions as in the original 384-well plate of the library. The two first and the two last columns of the plate were used to test control conditions (Figure 29). In particular, the two first columns of each plate contained an equal quantity of 661W cells transfected with the negative mimics and shielded

from light to represent controls kept in dark conditions (Figure 29). The rest of the plate was exposed to light. The last two columns contained the 661W cells transfected with the negative mimics and were used as controls of cell death upon light exposure (Figure 29). Controls of transfection efficiency were also added in each control column.

miRNA mature name
let-7a-3p, let-7d-3p, let-7e-3p, let-7f-2-3p, let-7g-3p, let-7i-3p, miR-7-1-3p, miR-7-2-3p, miR-7-5p, miR-9-3p, miR-9-5p, miR-10a-3p, miR-10a-5p, miR-10b-3p, miR-10b-5p, miR-15a-3p, miR-15b-3p, miR-16-1-3p, miR-16-2-3p, miR-18a-5p, miR-18b-3p, miR-18b-5p, miR-19a-3p, miR-19a-5p, miR-19b-1-5p, miR-19b-2-5p, miR-19b-3p, miR-20a-3p, miR-20a-5p, miR-20b-3p, miR-20b-5p, miR-21-3p, miR-21-5p, miR-22-3p, miR-22-5p, miR-23a-3p, miR-23a-5p, miR-23b-3p, miR-23b-5p, miR-24-1-5p, miR-24-2-5p, miR-24-3p, miR-25-3p, miR-25-5p, miR-26a-1-3p, miR-26a-2-3p, miR-26a-5p, miR-26b-3p, miR-26b-5p, miR-27a-3p, miR-27a-5p, miR-27b-3p, miR-27b-5p, miR-28-3p, miR-28-5p, miR-296-3p, miR-296-5p, miR-299-3p, miR-29a-3p, miR-29a-5p, miR-29b-1-5p, miR-29b-2-5p, miR-29b-3p, miR-29c-3p, miR-29c-5p, miR-30a-3p, miR-30a-5p, miR-30b-3p, miR-30b-5p, miR-30c-2-3p, miR-30c-5p, miR-30d-3p, miR-30d-5p, miR-30e-3p, miR-30e-5p, miR-31-3p, miR-31-5p, miR-32-3p, miR-32-5p, miR-33a-3p, miR-33a-5p, miR-33b-3p, miR-34a-3p, miR-34a-5p, miR-34b-3p, miR-34b-5p, miR-34c-3p, miR-34c-5p, miR-92a-1-5p, miR-92a-2-5p, miR-92a-3p, miR-93-5p, miR-95, miR-96-5p, miR-98-5p, miR-99a-3p, miR-99a-5p, miR-99b-3p, miR-99b-5p, miR-100-3p, miR-100-5p, miR-101-3p, miR-101-5p, miR-103a-3p, miR-105-5p, miR-106a-3p, miR-106a-5p, miR-106b-3p, miR-106b-5p, miR-107, miR-122-3p, miR-122-5p, miR-124-3p, miR-124-5p, miR-125a-3p, miR-125a-5p, miR-125b-1-3p, miR-125b-2-3p, miR-125b-5p, miR-126-3p, miR-126-5p, miR-127-3p, miR-127-5p, miR-128, miR-129-2-3p, miR-129-5p, miR-130a-3p, miR-130a-5p, miR-130b-3p, miR-132-3p, miR-132-5p, miR-133a, miR-133b, miR-134, miR-135a-3p, miR-135a-5p, miR-135b-5p, miR-136-3p, miR-136-5p, miR-137, miR-138-1-3p, miR-138-2-3p, miR-138-5p, miR-139-3p, miR-139-5p, miR-140-3p, miR-140-5p, miR-141-3p, miR-141-5p, miR-142-3p, miR-142-5p, miR-143-3p, miR-143-5p, miR-144-3p, miR-144-5p, miR-145-3p, miR-145-5p, miR-146a-3p, miR-146a-5p, miR-146b-3p, miR-147a, miR-148a-3p, miR-148b-3p, miR-148b-5p, miR-149-3p, miR-149-5p, miR-150-3p, miR-150-5p, miR-151a-3p, miR-151a-5p, miR-152, miR-153, miR-154-3p, miR-154-5p, miR-155-3p, miR-155-5p, miR-181a-3p, miR-181a-5p, miR-181b-5p, miR-181c-3p, miR-181c-5p, miR-181d, miR-182-3p, miR-182-5p, miR-183-3p, miR-183-5p, miR-184, miR-185-3p, miR-185-5p, miR-186-3p, miR-186-5p, miR-187-3p, miR-187-5p, miR-188-3p, miR-188-5p, miR-190a, miR-191-3p, miR-191-5p, miR-192-3p, miR-192-5p, miR-193a-3p, miR-193a-5p, miR-193b-3p, miR-193b-5p, miR-194-3p, miR-194-5p, miR-195-3p, miR-195-5p, miR-196a-3p, miR-196a-5p, miR-196b-5p, miR-197-3p, miR-198, miR-199a-3p, miR-199a-5p, miR-199b-3p, miR-199b-5p, miR-200a-3p, miR-200a-5p, miR-200b-5p, miR-200c-3p, miR-200c-5p, miR-202-3p, miR-203a, miR-204-5p, miR-205-5p, miR-206, miR-208a, miR-210, miR-211-5p, miR-212-3p, miR-214-3p, miR-214-5p, miR-215, miR-216a-5p, miR-217, miR-218-1-3p, miR-218-2-3p, miR-218-5p, miR-219-2-3p, miR-221-5p, miR-222-5p, miR-301a-3p, miR-302a-3p, miR-302a-5p, miR-302b-3p, miR-302b-5p, miR-302c-3p, miR-302c-5p, miR-302d-3p, miR-302d-5p, miR-320a, miR-323a-3p, miR-323a-5p, miR-324-3p, miR-324-5p, miR-325, miR-326, miR-328, miR-329, miR-330-3p, miR-330-5p,

miR-331-3p, miR-331-5p, miR-335-3p, miR-335-5p, miR-337-3p, miR-337-5p, miR-338-3p, miR-338-5p, miR-339-3p, miR-339-5p, miR-340-3p, miR-340-5p, miR-342-3p, miR-342-5p, miR-345-5p, miR-346, miR-361-3p, miR-361-5p, miR-362-5p, miR-363-3p, miR-365a-3p, miR-367-3p, miR-367-5p, miR-369-3p, miR-369-5p, miR-370, miR-371a-3p, miR-371a-5p, miR-372, miR-373-3p, miR-373-5p, miR-374a-3p, miR-374a-5p, miR-375, miR-376a-3p, miR-376b-3p, miR-376c-3p, miR-377-3p, miR-377-5p, miR-378a-3p, miR-378a-5p, miR-379-3p, miR-379-5p, miR-380-3p, miR-380-5p, miR-381-3p, miR-382-5p, miR-383, miR-384, miR-409-3p, miR-409-5p, miR-410, miR-411-3p, miR-411-5p, miR-412, miR-421, miR-422a, miR-423-3p, miR-423-5p, miR-424-3p, miR-424-5p, miR-425-3p, miR-425-5p, miR-429, miR-431-3p, miR-431-5p, miR-432-3p, miR-432-5p, miR-433, miR-448, miR-449a, miR-449b-5p, miR-450a-5p, miR-451a, miR-452-3p, miR-452-5p, miR-454-3p, miR-454-5p, miR-455-3p, miR-483-3p, miR-483-5p, miR-484, miR-485-5p, miR-488-3p, miR-490-5p, miR-491-3p, miR-492, miR-493-5p, miR-494, miR-495-3p, miR-496, miR-497-3p, miR-497-5p, miR-498, miR-499a-3p, miR-499a-5p, miR-500a-3p, miR-500a-5p, miR-501-3p, miR-501-5p, miR-502-3p, miR-502-5p, miR-503-5p, miR-504, miR-505-3p, miR-505-5p, miR-506-3p, miR-507, miR-508-3p, miR-508-5p, miR-509-3p, miR-509-5p, miR-512-3p, miR-512-5p, miR-513a-3p, miR-513a-5p, miR-515-3p, miR-515-5p, miR-516a-5p, miR-516b-3p, miR-516b-5p, miR-517-5p, miR-517a-3p, miR-517b-3p, miR-517c-3p, miR-518a-3p, miR-518a-5p, miR-518b, miR-518c-3p, miR-518c-5p, miR-518d-3p, miR-518d-5p, miR-518e-3p, miR-518e-5p, miR-518f-3p, miR-518f-5p, miR-519a-3p, miR-519a-5p, miR-519b-3p, miR-519b-5p, miR-519c-3p, miR-519c-5p, miR-519d, miR-519e-3p, miR-519e-5p, miR-520a-3p, miR-520a-5p, miR-520b, miR-520c-3p, miR-520c-5p, miR-520d-3p, miR-520d-5p, miR-520e, miR-520f, miR-520g, miR-520h, miR-521, miR-522-3p, miR-522-5p, miR-523-3p, miR-523-5p, miR-524-3p, miR-524-5p, miR-525-3p, miR-525-5p, miR-526a, miR-526b-3p, miR-526b-5p, miR-527, miR-532-3p, miR-545-5p, miR-548a-3p, miR-548a-5p, miR-548b-3p, miR-548c-3p, miR-548c-5p, miR-548d-3p, miR-548d-5p, miR-549a, miR-550a-3p, miR-551b-3p, miR-555, miR-556-5p, miR-557, miR-558, miR-559, miR-561-3p, miR-562, miR-563, miR-564, miR-566, miR-567, miR-568, miR-569, miR-570-3p, miR-571, miR-572, miR-573, miR-574-3p, miR-575, miR-576-5p, miR-577, miR-578, miR-579, miR-580, miR-581, miR-582-5p, miR-583, miR-584-5p, miR-585, miR-586, miR-587, miR-588, miR-589-3p, miR-590-5p, miR-591, miR-592, miR-593-3p, miR-593-5p, miR-595, miR-596, miR-597, miR-598, miR-599, miR-600, miR-601, miR-602, miR-603, miR-604, miR-605, miR-606, miR-607, miR-608, miR-609, miR-610, miR-611, miR-612, miR-613, miR-614, miR-615-3p, miR-615-5p, miR-616-3p, miR-616-5p, miR-617, miR-618, miR-619, miR-620, miR-621, miR-622, miR-624-3p, miR-625-3p, miR-628-5p, miR-629-5p, miR-632, miR-633, miR-634, miR-635, miR-636, miR-637, miR-638, miR-639, miR-640, miR-641, miR-642a-5p, miR-643, miR-644a, miR-645, miR-646, miR-647, miR-648, miR-649, miR-650, miR-651, miR-652-3p, miR-653, miR-654-3p, miR-654-5p, miR-655, miR-656, miR-657, miR-658, miR-659-3p, miR-660-5p, miR-661, miR-662, miR-663a, miR-668, miR-671-5p, miR-675-5p, miR-758-3p, miR-765, miR-766-3p, miR-767-3p, miR-767-5p, miR-769-3p, miR-769-5p, miR-770-5p, miR-802

Figure 28. List of miRNAs used in the HCS.

The table shows the 560 miRNAs that were screened in the HCS experiments. They represent a subset of the most conserved miRNAs contained in the human miRIDIAN mimic library.

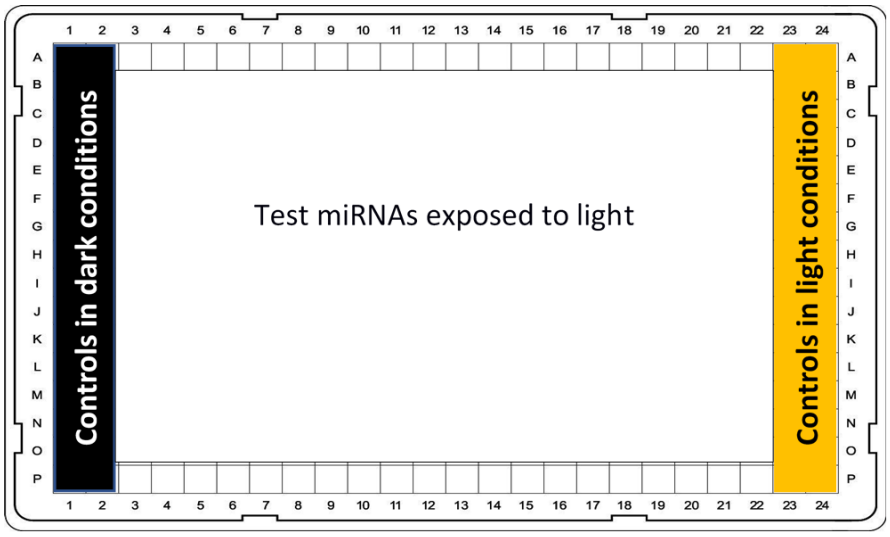

Figure 29. Arrangement of the 384-well plate used for the assay.

The test miRNAs were plated at the same position as in the original 384-plate of the miRNA library. Control columns contained 661W cells transfected with the negative mimics and the Dy547-labeled miRNA as control of the transfection efficiency. The upper and lower edge rows contained only medium and un-transfected cells to minimize medium evaporation within the wells of the adjacent test rows.

In order to compare the effect of each miRNA treatment to control mimics, the percentage of dying cells in each sample well was converted into a z score using the formula shown in Figure 30.

$$\text{z score} = \frac{Y\text{-mean } Y_N}{SD_N}$$

Figure 30. Equation for calculating z score.

Y = percentage of dying cells in the sample well; Y_N = percentage of dying cells in the negative mimic wells exposed to light; SDN = standard deviation of the percentage of dying cells in 661W transfected with neg mimic and exposed to light.

I ranked the z score obtained for each miRNA and arbitrarily defined an average z score lower or equal to -2 as threshold (dashed red line in Figure 31). From this analysis, I selected the miRNAs that showed the lowest variability among replicates, namely miR-429 and miR-218-5p (depicted in red in Figure 31), as positive hits for further confirmation.

Z score values equal or higher than 2 indicated miRNAs that exacerbated the percentage of dying 661W cells upon light exposure compared to the negative mimics (threshold indicated by the black dashed line in Figure 31). For instance, miR-9-5p was among the miRNAs that exacerbated the light-induced damage in 661W cells. Interestingly, miR-9 was found to be up-regulated in the serum of patients with age-related macular degeneration (AMD) and has been proposed as a biomarker for AMD (*141, 212*). The retinal degeneration associated with AMD shares common mechanisms of cell death with the degeneration observed in the 661W cells exposed to light (i.e. ROS production). Therefore, the finding related to miR-9 corroborates the reliability of the system used for the screening.

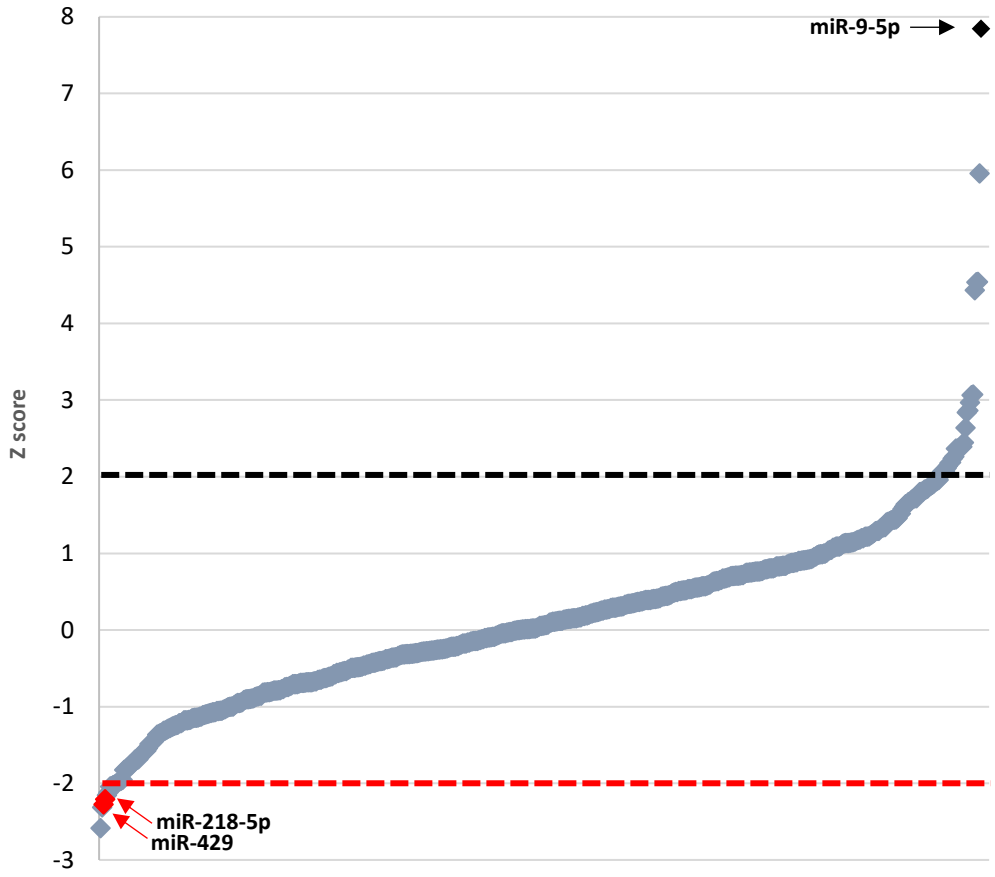

Figure 31. Plot showing the outcome of the primary screening.

The red dashed line indicates the threshold used to select the positive hits with a protective effect i.e. a z score < - 2 in at least two replicates. miR-429 and miR-218-5 (red arrows) are two positive hits. The diamonds above the black dashed line represent the miRNAs that exacerbated the light-induced damage in 661W compared to the control mimics, as indicated by z scores ≥ 2. miR-9-5p (black arrow) induced the highest degree of damage in 661W cells exposed to light.

3.8.5 Confirmation of positive hits

To confirm the positive hits identified in the primary screening, it is essential to perform an orthogonal assay that relies on a detection technology different from that of the primary screening. To this aim, I performed a metabolic assay of cell viability (namely, the MTT assay)

with a spectrophotometric read-out using the set-up of the pilot experiments. For these independent validation experiments I used new batches of test miRNA mimics. I assessed the effect of each miRNA on the viability of the 661W cells exposed to light as a percentage of the viability measured for the 661W cells transfected with the corresponding miRNA and kept in dark (considered as 100% viable).

The results of the MTT assay showed that the viability of 661W cells transfected with the negative mimics (ctl mimic) was significantly reduced (20%) after light exposure. Instead, the viability of 661W transfected with miR-218-5p or miR-429 did not show significant changes between the conditions of photo-stress or darkness (Figure 32).

These data confirmed that both positive hits from the primary screening were able to counteract the light-induced damage in 661W. Therefore, these two miRNAs were further tested in a validation assay to determine their possible mechanism of action.

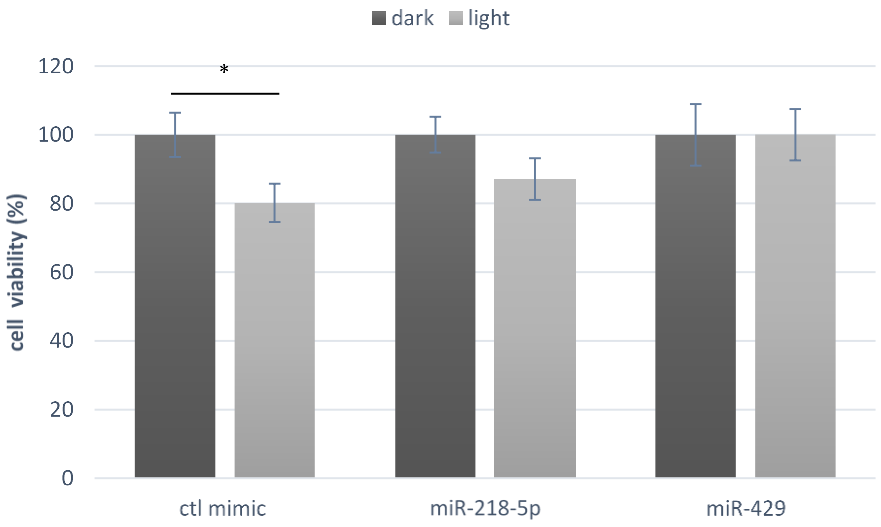

Figure 32. Confirmation of the positive hits from the primary screen using an MTT assay.

An MTT assay was used to assess cell viability. Cell viability of 661W transfected with ctl mimic resulted significantly reduced after light exposure, while cell viability of 661W transfected with miR-218-5p and miR-429 did not change significantly between dark and light conditions. These results showed that both the primary selected hits, miR-218-5p and miR-429 can protect the 661W cells from light-induced damage The absorbance readings of the blue formazan product were carried out at 570 nm and plotted as percentage of light-exposed cells relative to those kept in dark condition (mean± SEM), considered as 100% viable. The cells transfected with negative control mimics were referred to as 'ctl mimic'. *p<0.05

3.8.6 Hit validation: miR-429 reduces ROS levels in 661W cells exposed to H_2O_2

Reactive Oxygen Species (ROS) are radical and non-radical oxygen species whose excessive accumulation leads to molecular modifications of cellular components (e.g. protein oxidation, lipid peroxidation). These modifications can, in turn, result in dysfunction and severe damage (*49, 50*). Light-induced damage in the retina is tightly associated with the increase of ROS levels. In fact, ROS-induced oxidative stress is considered as a major player in the retinal degeneration induced by intense and prolonged light exposure (*213-215*). Therefore, in order

to get insights into the possible mechanisms underlying the activity of the confirmed hits, I assessed the effect of miR-429 and miR-218-5p on the accumulation of intracellular ROS levels. To this end, 661W cells transfected with both miRNA mimics or negative control mimics were exposed to hydrogen peroxide (H_2O_2), a commonly used and well-characterized inducer of oxidative stress. By visual inspection under the light microscope, I first determined a dose of H_2O_2 and an exposure time (200 µM for 3 h and 15') that induced a cellular morphology typical of stressed cells (e.g. reduced cell size), without causing extensive cell detachment and death. I then used the CM-H_2DCFDA ROS sensor to detect intracellular ROS levels. CM-H_2DCFDA passively diffuses into the cells where it undergoes cleavage by the intracellular esterase and oxidation resulting in a green fluorescent adduct that is retained inside the cell. To improve sensitivity, labeled cells were visualized by fluorescence microscopy using the Operetta live imaging system. The fluorescence levels and spatial distribution of the green signal were then analysed with the Columbus 6.0 software.

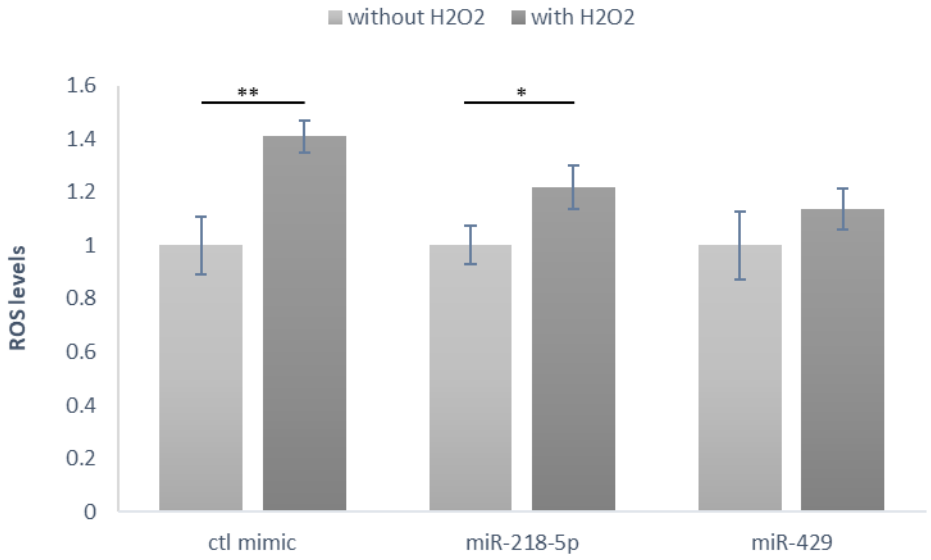

Figure 33. ROS levels in 661W cells transfected with miR-429 did not increase significantly upon exposure to H_2O_2.

The fluorescence and spatial distribution of the green signal emitted by the ROS-sensitive probe was quantified to assess ROS levels. The data are plotted as a ratio of H_2O_2-treated cells (dark grey bars) compared to untreated control cells (ctrl mimic; light grey bar) (mean ± SEM). A nonparametric test for the interaction in two-way factorial designs was used to compare the groups. Data are represented as mean ± SEM. * $p<0.05$, ** $p<0.01$

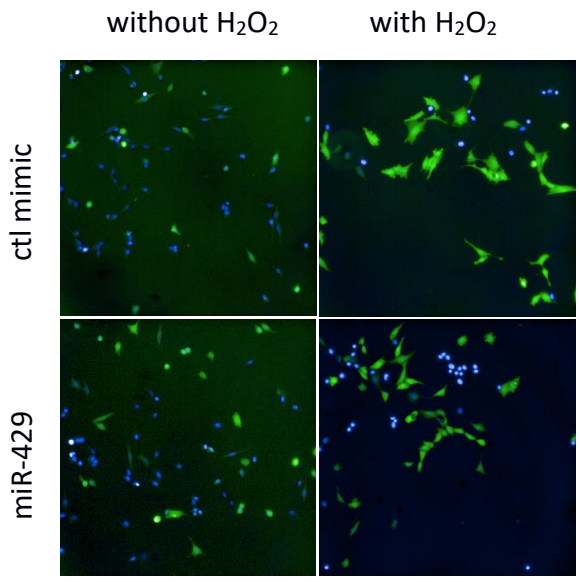

Figure 34. 661W cells transfected with miR-429 show reduced fluorescence of the ROS-sensitive probe after treatment with H_2O_2.

661W cells transfected with miR-429 or control mimics (ctl mimic) were treated with H_2O_2 (200 µM for 2 h 30 min) and loaded with a ROS-sensitive probe (green fluorescent signal). Untreated cells (without H_2O_2) were used as controls. Cells were also stained with the DAPI nuclear dye (shown in blue). Images were acquired by using the Operetta live imaging system at a 20X magnification.

I found that the 661W cells transfected with control mimics and exposed to H_2O_2 showed a significantly higher and more diffuse green fluorescence signal compared to untreated cells, indicating higher ROS levels (Figure 33; Figure 34, upper panel). In contrast, the cells overexpressing miR-429 showed a small increase in the green signal following H_2O_2 treatment compared to control cells, indicating low and non-significant ROS levels (Figure 33; Figure 34 lower panels). Furthermore, the ROS levels in 661W cells transfected with miR-429 and treated with H_2O_2 were significantly lower compared to cells transfected with control mimics. On the contrary, the 661W cells transfected with miR-218-5p mimic still showed a significant increase of ROS levels upon treatment with H_2O_2. The visual inspection of the automatically acquired images corroborated the outcome of the above analysis (Figure 34). Taken together, these

findings indicate that the transfection of miR-429 in 661W cells is able to control the increase of ROS levels, without resetting them completely. A plausible explanation could be that the overexpression of miR-429 prevents the excessive accumulation of ROS during photo-stress, while preserving a minimal ROS quantity that can elicit a potential antioxidant response (*216*) favoring cell protection.

Additional secondary assays should be performed to study the effect of the selected miRNAs on concomitant pathological mechanisms associated with light-induced retinal damage. For example, evaluating the effect of miR-218 and miR-429 overexpression on Ca^{++} mobilization, mitochondrial features and adenosine triphosphate (ATP) levels after light exposure could provide valuable insights on the precise role of the selected protective hits (*217*).

3.9 miR-429 overexpression enhances AMPK activation in 661W cells exposed to light damage

To better characterise the protective effect of miR-429 overexpression against light-induced damage in 661W cells, I sought to identify the molecular pathways involved. After combining data from literature and miRNA target-prediction databases (e.g. microTCDS, TargetScan) I looked into a possible link between the activation of the adenosine monophosphate (AMP)-activated protein kinase (AMPK) pathway and the effect of miR-429 in 661W cells exposed to light-induced damage. Recent studies demonstrated a role of AMPK activation in the neuroprotection and amelioration of visual activity in retinas under photo-stress (*217, 218*).

In particular, while photo-stress reduced mitochondrial respiratory function and ATP levels, pharmacological activation of the AMPK pathway promoted neuronal survival and retained visual function, stabilizing ATP levels through the preservation of mitochondrial enzyme

activity (*217*). Moreover, activated AMPK appears to be essential in maintaining the intracellular redox status, as emerged in endothelial cells, by inhibiting oxidant production from mitochondria, NADPH oxidases, etc. or by increasing the expression of antioxidant enzymes such as SOD2 (*219*).

AMPK is ubiquitously expressed and is considered a key energy sensor, fundamental to maintain proper energetic cellular conditions during environmental stress. In particular, it monitors changes in ATP levels and increases the rate of ATP-producing pathways in response to an increase in adenosine monophosphate (AMP)/ adenosine diphosphate (ADP) relative to ATP (*220*). AMPK comprises a catalytic α-subunit associated with β and γ regulatory subunits. AMPK signalling is initiated by the binding of AMP to the AMPKγ subunit. It is positively regulated by phosphorylation of the amino acid Thr172 of its α-subunit, which is the major phosphorylation site of AMPK, and is negatively regulated by phosphatases (*220*). Interestingly, the catalytic subunit of the key AMPK phosphatase, namely PP2A, is a predicted and experimentally validated target of miR-429 (*221*). As a consequence, miR-429 could positively modulate the activation of AMPK pathway by reducing the expression of the catalytic subunit of PP2A (PP2Ac).

Based on this evidence, I performed a western blot analysis to assess the levels of AMPK phosphorylation (Thr172) in 661W cells transfected with miR-429 or control mimics and either exposed to light for 6 h or kept in dark (Figure 35A). I observed a significant increase of the p-AMPK/AMPK ratio in the 661W cells overexpressing miR-429 and exposed to light compared to the cells transfected with control negative mimic (ctl mimic) and kept in dark, thus indicating the activation of the AMPK pathway (Figure 35B).

It has also been reported that retinas exposed to photo-stress can generate an initial, transient, protective cellular response that subsequently declines, leaving the cell exposed to damage (*217*). Based on this theory, it would be tempting to hypothesize that the 661W cells transfected with control mimics and exposed to light-damage try to activate a pro-survival response, as suggested by the slight increase of p-AMPK levels. Instead, the miR-429 overexpression appears to significantly strengthen and prolong the activation of AMPK pro-survival pathway.

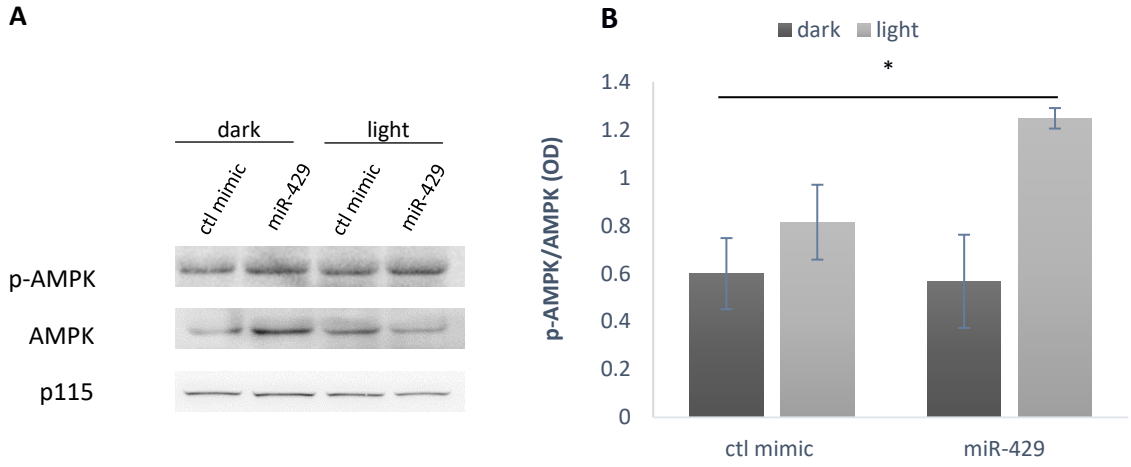

Figure 35. Activation of the AMPK pathway in 661W cells transfected with miR-429 and exposed to light damage.

A) Western blot (WB) analysis of total cell lysates from 661W cells transfected with negative control mimic (ctl mimic) or miR-429. Transfected cells were either kept in darkness or exposed to light-stress. Lysates were immunoblotted with antibodies to p-AMPKα (Thr 172), AMPK and p115.

B) Optical densities (OD) of the bands from three independent experiments were quantified and plotted as mean ± SEM. The 661W cells transfected with miR-429 and exposed to light damage showed a significant increase in the p-AMPK/AMPK compared to the cells transfected with the ctl mimic and kept in dark. ANOVA and multiple pairwise tests against a reference group were used for the comparisons. * $p<0.05$

To assess whether there is a link between the protective activity of miR-429 in light-injured 661W cells and AMPK activation, I assessed the viability of the 661W cells transfected with miR-429 or control mimics and exposed to light after pharmacological inhibition of the AMPK activity. To this aim, I used the SBI-0206965 molecule which was shown to be a potent and more selective inhibitor of the AMPK activity compared to the commonly used Compound C (*222*).

I did not find significant changes in viability between 661W cells transfected with miR-429 or control mimics and kept in dark, regardless of the SBI-0206965 treatment (data not shown). I then evaluated whether AMPK inhibition in 661W cells transfected with miR-429 or negative mimics could affect cell viability after 4 h of light exposure. I found that the inhibition of AMPK activity by SBI-0206965 at both tested concentrations (i.e. 1 µM and 5 µM) was associated with a reduction of viability upon light-exposure that resulted comparable to the one observed in the 661W transfected with control mimics in the absence of SBI-0206965 (Figure 36A). On the contrary, the transfection of 661W cells with miR-429 confirmed the ability of this miRNA to preserve cell viability upon light exposure (Figure 36B), as shown in the confirmation experiments of the primary hits (section 3.8.5). This response was not affected by SBI-0206965 pre-treatment at the lower concentration tested (1 µM). Instead, when cells overexpressing miR-429 were treated with a higher concentration of SBI-0206965 (5 µM) and exposed to light, I detected a notable decrease of cell viability, suggesting that the AMPK activity contributes to the protective effect mediated by miR-429. Taken together, these data indicate that the protective effect of the miR-429 overexpression in this *in vitro* model of photo-stress is, at least in part, mediated by the activation of the AMPK pro-survival pathway. Our results are in agreement with recent studies that describe the activation of the AMPK pathway as a key

protective mechanism in mouse models of light induced damage (*217, 218*) and suggest a possible link between miR-429 and AMPK activation in different models involving oxidative stress (e.g. the Dexamethasone-induced death in osteoblastic cells) (*221*).

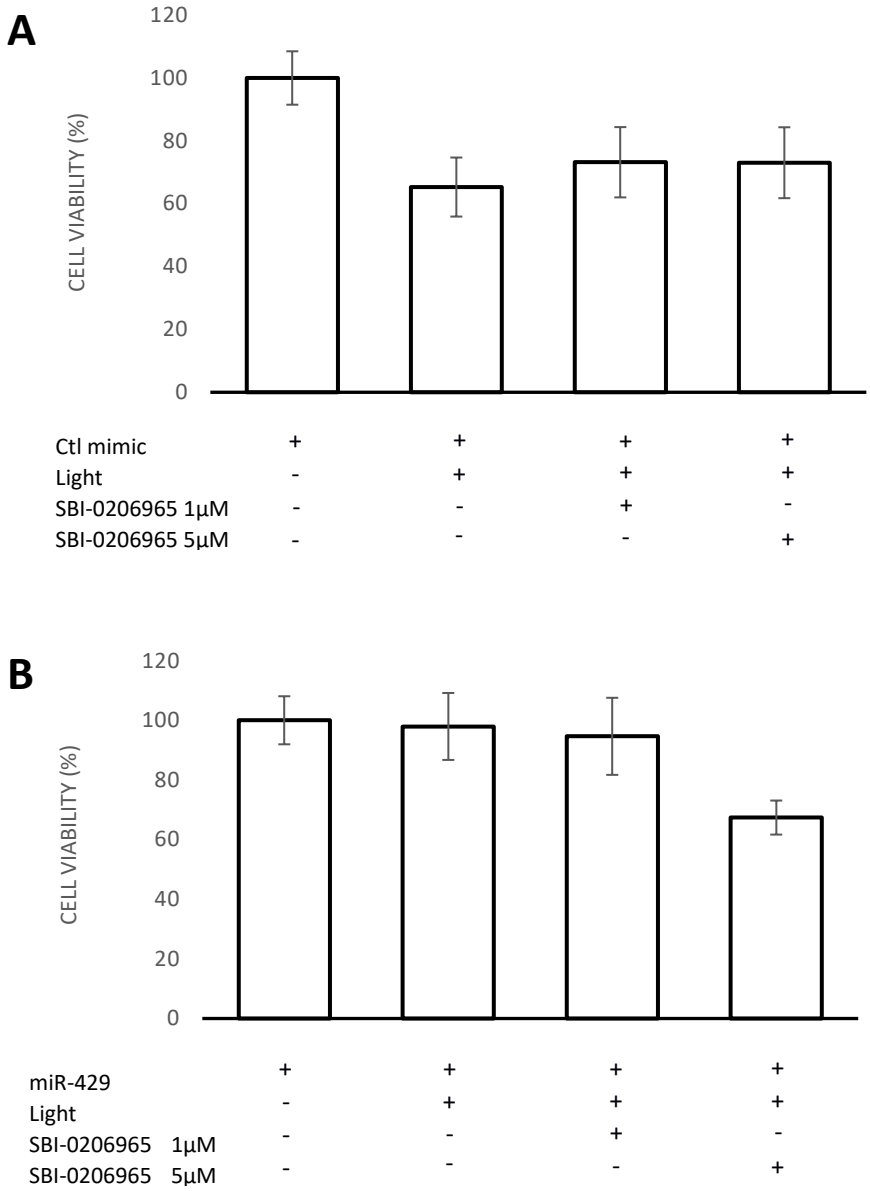

Figure 36. Pharmacological inhibition of AMPK abolishes the protective effect of miR-429 in light-stressed 661W cells

The 661W cells transfected with negative mimics (ctl mimic) (A) or miR-429 (B) were pre-treated with the pharmacological inhibitor of AMPK activity (SBI-0206965) for 90 min prior to light exposure for 4 h. Cell viability was assessed by an MTT assay. The absorbance readings of the blue formazan product were carried out at 570 nm and were plotted as percentage of light-exposed conditions compared to the dark control, considered as 100% viable (mean± SEM).

Finally, to understand whether the effect of miR-429 on AMPK activation could be mediated by the regulation of the gene that encodes *PP2Ac*, analysis of the transcripts, protein levels and post-transcriptional modifications will be necessary.

4 DISCUSSION AND CONCLUSIONS

The results of the first part of my thesis work confirms our hypothesis that miR-204 is able to slow down retinal degeneration when administered at advanced stages of the disease in a relevant murine model of IRD, the *RHO*-P347S mice. I recorded a long-lasting improvement of retinal function upon subretinal delivery of miR-204 both at PN14 and PN24, when the adult retinas already exhibit signs of degeneration. The observed increase in the a- and b-wave amplitudes of the ERG response, albeit moderate, indicated a protective effect on rod and cone photoreceptor function as well as on the synaptic connectivity in the inner retina. Further enhancements could derive from testing higher vector doses and inoculations in multiple injection spots with the aim to increase the number of transduced cells. Importantly, the ability of miR-204 to preserve retinal function by injections after the disease onset supports the clinical potential of the approach at patient-relevant stages of disease progression. In that respect, it should be underlined that the effect of miR-204 was tested using a retinal delivery system with proven safety and efficacy for clinical use (i.e. by subretinal injection of AAV vectors carrying the sequence of interest). Further experiments using alternative IRD models, including larger animals, are needed to corroborate the clinical potential of the proposed approach.

The use of a relevant murine model, like the *RHO*-P347S mice, enabled us to explore the pathways related to the miR-204 overexpression and the functional response associated with different timings of intervention in a significant number of animals. The latter aspect is indeed crucial for assessing the effect of novel treatments. The advantage of using larger animal models, instead, is that the eyes have similar size to the human one, thus allowing a more accurate testing of dosage studies and delivery routes. In addition, the structural composition

of the retina of larger animal models (e.g. rod:cone ratio in pigs) is more similar to that of humans. In *RHO*-P347S mice I did not detect significant morphological improvements at P30 or P60 after injection of AAV.miR-204 vector at PN14 and PN24. Future experiments in larger animals that combine the aforementioned structural features with a longer life-span and a slower rate of degeneration, could better clarify the relation between functional and structural preservation following miR-204 delivery at advanced stages of degeneration.

Dysregulated innate immune response and inflammation have emerged as relevant pathological processes associated with IRDs both in preclinical models (*41*) and patients(*37, 40*). Importantly, their deleterious effect is common to various IRDs models bearing different disease-causing mutations. In particular, microglia activation represents a prominent non-cell autonomous pathological mechanism that accompanies different forms of IRDs (*48*).

Microglia are the main immune effector cells in the CNS as well as in the retina. Their activation under conditions of tissue damage is fundamental to maintain the integrity of the retinal milieu by removing cell debris, promoting tissue repair and restoring homeostasis. However, when the triggering insult is excessive or prolonged, activated microglia contribute to the initiation and/or exacerbation of retinal degeneration in IRDs. They can phagocytose living PRs (*41*), proliferate and release a large amount of pro-inflammatory and potentially cytotoxic compounds (*35*) (e.g. TNF-α, IL-1β, ROS, NO) that sustain the inflammatory processes leading to deleterious effects. Increased microglia proliferation and elevated levels of pro-inflammation factors are associated with PR dysfunction and death not only during degeneration, but even at disease stages that precede PR degeneration (*48*). Protective approaches that are based on limiting microglia activation and innate immune response in IRDs

have indeed showed promising results. Such strategies should however be designed in a way that does not interfere with the homeostatic function of the retinal immune effectors.

miRNAs are attractive therapeutic tools as they can control functionally correlated pathways allowing a fine-tuning of the related processes. In agreement with these principles, the results of our transcriptomic analysis indicated that miR-204 overexpression is able to influence multiple processes in *RHO*-P347S mice already at a pre-degenerative stage, particularly those related to the innate immunity and inflammatory responses. The modulation of these pathways, therefore, more likely represents a primary mechanism underlying the miR-204 protective effect rather than an indirect response to reduced triggering signals from the degenerating PRs. In particular, our *in vitro* study suggested a direct activity of miR-204 on microglia activation in IRDs, taking into account the reduction of *TNF-α* and *iNOS* expression in BV-2 cells overexpressing miR-204 and exposed to LPS-mediated activation. Importantly, miR-204 overexpression does not suppress completely the expression of these mediators, endorsing the possibility that miR-204 prevents the exacerbation of retinal damage mediated by microglia overactivation without suppressing completely their activity. To fully address this aspect, it will be interesting to test the effects of the microglial-specific delivery of miR-204 in *RHO*-P347S retinas. However, the transduction of microglial cells by AAV vectors is still particularly challenging with only one study reporting a successful outcome (*206*).

Nonetheless, the administration of miR-204 under a ubiquitous promoter showed a stronger effect than the one obtained with the use of the rod-specific *RHO* promoter. This evidence supports the idea that the protective effect of miR-204 in IRD models is presumably due to the pleiotropic action of this miRNA on multiple cell targets (e.g. RPE, photoreceptors, microglia). Therefore, as also suggested by the *in vitro* evidence, the dampening of microglial reactivity

observed upon AAV.CMV.miR204 delivery is most likely due to a direct role of this miRNA on microglia activation rather than secondary to events occurring in PRs.

It is known that miR-204 plays a pivotal role in retinal development and function, as well as in the pathogenesis of IRDs when mutated (*169*). The effects of modulating miR-204 expression in IRDs was never reported prior to a recently published study by the Banfi's research team (*177*). In the first part of my PhD thesis, which is included in the above-mentioned manuscript, I showed that miR-204 overexpression at post-developmental stages exert protective effects in a preclinical model of IRD, supporting its translational potential for the development of therapeutic approaches. In fact, both the described administration system (i.e. subretinal injection of AAV) and disease stage of intervention (i.e. PN24, advanced postnatal stages) were compatible with the development of a clinical protocol for human translational purposes (e.g. subretinal delivery in patients). In light of the effect of miR-204 on disease mechanisms common to genetically different IRDs, this miRNA can represent a mutation-independent therapeutic agent that dampens disease-amplifying processes.

Strategies to halt or slow down the IRD progression irrespectively of the specific pathological mutation are particularly relevant to the development of therapeutic approaches intended for a large population of IRD patients. To date, the only treatment available on the market for IRDs is based on gene replacement therapy and destined to patients with an autosomal dominant form of LCA associated with mutations in *RPE65*. Considering that gene replacement strategies are not suitable for the treatment of dominant conditions due to the gain-of-function/dominant-negative effects of the mutated allele, the gene-independent approach that I am pursuing with this study is particularly appealing. Eventually, it will be interesting to study the association of mutation-independent treatments based on miRNAs with gene-

specific replacement approaches with the ultimate aim to improve their efficiency. Finally, it is worth exploring the therapeutic potential of the proposed strategy also in the context of multifactorial forms of retinopathies in which dysregulated innate immunity response exerts a pathogenic role (i.e. AMD and diabetic retinopathy).

The results of the second part of my thesis suggest that the development of miRNA-based approaches for IRDs could be useful to modulate additional mechanisms that participate to the disease progression in a mutation-independent manner, such as oxidative stress. In particular, oxidative stress is considered a major contributor in the secondary cone demise that occurs during the progression of RP regardless of the disease-causing mutation (*21*). Oxidative stress occurs when the cell produces excessive oxidant agents that overwhelm its intrinsic capacity to neutralize them through endogenous antioxidants (*52*). ROS constitute a highly reactive oxidant species that is produced both as a by-product of cellular metabolism as well as by dedicated enzymes such as those of the NOX family (*54*). Oxidative stress leads to modifications of cellular components (e.g. protein oxidation, lipid peroxidation) that can, in turn, result in cell dysfunction (*29, 223*) and severe damage (*49*). However, it was demonstrated that low and controlled levels of ROS take part to physiological cell signalling (*224*) and can promote cell survival in response to various detrimental stimuli (*56*). Several studies reported that strategies to counteract oxidative stress hold promise for developing treatments to delay retinal degeneration (*74*), especially by preserving cones PRs (*67, 73*). In this regard, beneficial approaches for delaying cones demise should not aim to completely abolish ROS, but merely to reduce their levels preserving their physiological, protective activity.

The light-induced damage in 661W cone-like cells is an appropriate model of PRs degeneration involving oxidative stress (*225*) allowed us to identify miRNAs that could be particularly valuable to target secondary cone degeneration in IRDs. I found that overexpression of miR-429 prevents the damage induced in 661W cone-like cells upon prolonged exposure to intense light, as indicated by the results of the primary screening (HCS) of 560 miRNAs. Our results show that miR-429 overexpression in 661W cells also prevents the accumulation of intracellular ROS following the treatment with exogenous H_2O_2 (Figure 33). In particular, the ROS levels upon H_2O_2 exposure were significantly lower in 661W cells overexpressing miR-429 compared to those of cells transfected with the control mimic, while being higher than those detected in basal conditions (Figure 34). These results suggest that miR-429 can act as a fine modulator of ROS levels in 661W cells, preventing their excessive accumulation, while preserving a minimal increase as adaptive response to the stress stimulus. It is therefore plausible that a fine-tuning of ROS levels could contribute to the protective effect exerted by miR-429 against photo-stress in 661W.

Interestingly, studies conducted both in mice retinas (*218*) as well as in endhotelial (*219*) and osteoblastic cells (*226, 227*), indicate that the activation of the AMPK pathway is essential in maintaining the intracellular redox status, with one report pointing out also a role of miR-429 (*221*). In the study by Guo *et al.*, miR-429 was shown to protect osteoblastic cells from the damage associated with dexamethasone treatment and to attenuate the related production of ROS levels *via* the activation of AMPK (*221*). More interestingly, a recent study reported that the activation of the AMPK pathway prevents photoreceptor degeneration in different models of retinal degeneration, such as RP and light damage (*218*). In the mouse model of light-induced damage the protection was associated with an increased mitochondrial DNA copy

number, increased levels of ATP, and a reduction in oxidative stress and oxidative DNA damage.

Taken together, our experiments in the 661W cells are in accordance with the above-mentioned evidence and indicate that miR-429 is able to prevent the light-induced damage in 661W cells by activating the AMPK pro-survival pathway. To assess the extent to which the modulation of cellular ROS levels participates to such effect and to identify the molecular mediators involved, experiments measuring ROS levels in 661W cells overexpressing miR-429 and exposed to light will be necessary. This notwithstanding, our results represent an encouraging premise to investigate whether the miR-429 retinal delivery can prevent or delay the cone degeneration also in preclinical *in vivo* model of RP regardless of the causative mutation that primarily affects rods. This kind of studies are particularly relevant to address the need for therapies that counteract the most severe visual impairment, that deriving from cone demise.

As fine modulators acting on multiple functionally correlated pathways, miRNAs are attractive therapeutic targets and tools for human conditions. miRNA-based therapeutics are in the clinical phase of development for various diseases, e.g. liver cancer, heart failure and mesothelioma (*228*). My thesis work underscores the potential of miRNAs as molecular tools for gene-independent protective approaches in IRDs, expanding our knowledge on their mechanisms of action in preclinical models of retinal degeneration and paving the way to future translational studies.

5 REFERENCES

1. T. D. Lamb, S. P. Collin, E. N. Pugh, Evolution of the vertebrate eye: opsins, photoreceptors, retina and eye cup. *Nat Rev Neurosci* **8**, 960-976 (2007).
2. P. Gaspar, I. Almudi, M. D. S. Nunes, A. P. McGregor, Human eye conditions: insights from the fly eye. *Hum Genet* **138**, 973-991 (2019).
3. E. A. Bassett, V. A. Wallace, Cell fate determination in the vertebrate retina. *Trends Neurosci* **35**, 565-573 (2012).
4. V. García-Marín, P. García-López, M. Freire, Cajal's contributions to glia research. *Trends Neurosci* **30**, 479-487 (2007).
5. H. Holländer *et al.*, Structure of the macroglia of the retina: sharing and division of labour between astrocytes and Müller cells. *J Comp Neurol* **313**, 587-603 (1991).
6. E. Vecino, F. D. Rodriguez, N. Ruzafa, X. Pereiro, S. C. Sharma, Glia-neuron interactions in the mammalian retina. *Prog Retin Eye Res* **51**, 1-40 (2016).
7. O. Strauss, The retinal pigment epithelium in visual function. *Physiol Rev* **85**, 845-881 (2005).
8. R. H. Steinberg, Interactions between the retinal pigment epithelium and the neural retina. *Doc Ophthalmol* **60**, 327-346 (1985).
9. S. Beatty, M. Boulton, D. Henson, H. H. Koh, I. J. Murray, Macular pigment and age related macular degeneration. *Br J Ophthalmol* **83**, 867-877 (1999).
10. F. P. M. Cremers, C. J. F. Boon, K. Bujakowska, C. Zeitz, Special Issue Introduction: Inherited Retinal Disease: Novel Candidate Genes, Genotype-Phenotype Correlations, and Inheritance Models. *Genes (Basel)* **9**, (2018).
11. J. S. Rahi, N. Cable, B. C. V. I. S. Group, Severe visual impairment and blindness in children in the UK. *Lancet* **362**, 1359-1365 (2003).
12. L. S. Sullivan, S. P. Daiger, Inherited retinal degeneration: exceptional genetic and clinical heterogeneity. *Mol Med Today* **2**, 380-386 (1996).
13. R. G. Weleber, R. E. Carr, W. H. Murphey, V. C. Sheffield, E. M. Stone, Phenotypic variation including retinitis pigmentosa, pattern dystrophy, and fundus flavimaculatus in a single family with a deletion of codon 153 or 154 of the peripherin/RDS gene. *Arch Ophthalmol* **111**, 1531-1542 (1993).
14. C. E. Keeler, The Inheritance of a Retinal Abnormality in White Mice. *Proc Natl Acad Sci U S A* **10**, 329-333 (1924).
15. C. Bowes *et al.*, Retinal degeneration in the rd mouse is caused by a defect in the beta subunit of rod cGMP-phosphodiesterase. *Nature* **347**, 677-680 (1990).
16. B. Chang *et al.*, Retinal degeneration mutants in the mouse. *Vision Res* **42**, 517-525 (2002).
17. C. Gargini, E. Terzibasi, F. Mazzoni, E. Strettoi, Retinal organization in the retinal degeneration 10 (rd10) mutant mouse: a morphological and ERG study. *J Comp Neurol* **500**, 222-238 (2007).

18. V. Ramamurthy, G. A. Niemi, T. A. Reh, J. B. Hurley, Leber congenital amaurosis linked to AIPL1: a mouse model reveals destabilization of cGMP phosphodiesterase. *Proc Natl Acad Sci U S A* **101**, 13897-13902 (2004).
19. E. L. Berson, B. Rosner, M. A. Sandberg, C. Weigel-DiFranco, T. P. Dryja, Ocular findings in patients with autosomal dominant retinitis pigmentosa and rhodopsin, proline-347-leucine. *Am J Ophthalmol* **111**, 614-623 (1991).
20. T. Li, W. K. Snyder, J. E. Olsson, T. P. Dryja, Transgenic mice carrying the dominant rhodopsin mutation P347S: evidence for defective vectorial transport of rhodopsin to the outer segments. *Proc Natl Acad Sci U S A* **93**, 14176-14181 (1996).
21. P. A. Campochiaro, T. A. Mir, The mechanism of cone cell death in Retinitis Pigmentosa. *Prog Retin Eye Res* **62**, 24-37 (2018).
22. M. R. al-Ubaidi *et al.*, Bilateral retinal and brain tumors in transgenic mice expressing simian virus 40 large T antigen under control of the human interphotoreceptor retinoid-binding protein promoter. *J Cell Biol* **119**, 1681-1687 (1992).
23. E. Tan *et al.*, Expression of cone-photoreceptor-specific antigens in a cell line derived from retinal tumors in transgenic mice. *Invest Ophthalmol Vis Sci* **45**, 764-768 (2004).
24. Y. Kanan *et al.*, Retinoid processing in cone and Müller cell lines. *Exp Eye Res* **86**, 344-354 (2008).
25. R. R. Krishnamoorthy *et al.*, Photo-oxidative stress down-modulates the activity of nuclear factor-kappaB via involvement of caspase-1, leading to apoptosis of photoreceptor cells. *J Biol Chem* **274**, 3734-3743 (1999).
26. D. M. Paskowitz, M. M. LaVail, J. L. Duncan, Light and inherited retinal degeneration. *Br J Ophthalmol* **90**, 1060-1066 (2006).
27. Y. Kuse, K. Ogawa, K. Tsuruma, M. Shimazawa, H. Hara, Damage of photoreceptor-derived cells in culture induced by light emitting diode-derived blue light. *Sci Rep* **4**, 5223 (2014).
28. Y. Inoue *et al.*, RS9, a novel Nrf2 activator, attenuates light-induced death of cells of photoreceptor cells and Müller glia cells. *J Neurochem* **141**, 750-765 (2017).
29. J. Sancho-Pelluz *et al.*, Photoreceptor cell death mechanisms in inherited retinal degeneration. *Mol Neurobiol* **38**, 253-269 (2008).
30. D. S. Narayan, J. P. Wood, G. Chidlow, R. J. Casson, A review of the mechanisms of cone degeneration in retinitis pigmentosa. *Acta Ophthalmol* **94**, 748-754 (2016).
31. T. Harada *et al.*, Microglia-Muller glia cell interactions control neurotrophic factor production during light-induced retinal degeneration. *J Neurosci* **22**, 9228-9236 (2002).
32. R. M. Ferrer-Martin *et al.*, Microglial Activation Promotes Cell Survival in Organotypic Cultures of Postnatal Mouse Retinal Explants. *PLoS One* **10**, e0135238 (2015).
33. H. Y. Zeng *et al.*, Identification of sequential events and factors associated with microglial activation, migration, and cytotoxicity in retinal degeneration in rd mice. *Invest Ophthalmol Vis Sci* **46**, 2992-2999 (2005).
34. L. P. Yang, Y. Li, X. A. Zhu, M. O. Tso, Minocycline delayed photoreceptor death in rds mice through iNOS-dependent mechanism. *Mol Vis* **13**, 1073-1082 (2007).

35. T. Rana, P. Kotla, R. Fullard, M. Gorbatyuk, TNFa knockdown in the retina promotes cone survival in a mouse model of autosomal dominant retinitis pigmentosa. *Biochim Biophys Acta Mol Basis Dis* **1863**, 92-102 (2017).

36. T. Langmann, Microglia activation in retinal degeneration. *J Leukoc Biol* **81**, 1345-1351 (2007).

37. N. Yoshida *et al.*, Clinical evidence of sustained chronic inflammatory reaction in retinitis pigmentosa. *Ophthalmology* **120**, 100-105 (2013).

38. N. Yoshida *et al.*, Laboratory evidence of sustained chronic inflammatory reaction in retinitis pigmentosa. *Ophthalmology* **120**, e5-12 (2013).

39. M. Karlstetter *et al.*, Disruption of the retinitis pigmentosa 28 gene Fam161a in mice affects photoreceptor ciliary structure and leads to progressive retinal degeneration. *Hum Mol Genet* **23**, 5197-5210 (2014).

40. N. Gupta, K. E. Brown, A. H. Milam, Activated microglia in human retinitis pigmentosa, late-onset retinal degeneration, and age-related macular degeneration. *Exp Eye Res* **76**, 463-471 (2003).

41. L. Zhao *et al.*, Microglial phagocytosis of living photoreceptors contributes to inherited retinal degeneration. *EMBO Mol Med* **7**, 1179-1197 (2015).

42. R. Sudharsan, D. P. Beiting, G. D. Aguirre, W. A. Beltran, Involvement of Innate Immune System in Late Stages of Inherited Photoreceptor Degeneration. *Sci Rep* **7**, 17897 (2017).

43. C. J. Zeiss, E. A. Johnson, Proliferation of microglia, but not photoreceptors, in the outer nuclear layer of the rd-1 mouse. *Invest Ophthalmol Vis Sci* **45**, 971-976 (2004).

44. B. Peng *et al.*, Suppression of microglial activation is neuroprotective in a mouse model of human retinitis pigmentosa. *J Neurosci* **34**, 8139-8150 (2014).

45. S. L. Roche *et al.*, Progesterone Attenuates Microglial-Driven Retinal Degeneration and Stimulates Protective Fractalkine-CX3CR1 Signaling. *PLoS One* **11**, e0165197 (2016).

46. S. K. Wang, Y. Xue, C. L. Cepko, Microglia modulation by TGF-β1 protects cones in mouse models of retinal degeneration. *J Clin Invest*, (2020).

47. A. I. Arroba, N. Alvarez-Lindo, N. van Rooijen, E. J. de la Rosa, Microglia-mediated IGF-I neuroprotection in the rd10 mouse model of retinitis pigmentosa. *Invest Ophthalmol Vis Sci* **52**, 9124-9130 (2011).

48. K. Rashid, I. Akhtar-Schaefer, T. Langmann, Microglia in Retinal Degeneration. *Front Immunol* **10**, 1975 (2019).

49. E. Niki, Lipid peroxidation: physiological levels and dual biological effects. *Free Radic Biol Med* **47**, 469-484 (2009).

50. M. M. Gaschler, B. R. Stockwell, Lipid peroxidation in cell death. *Biochem Biophys Res Commun* **482**, 419-425 (2017).

51. R. V. Lloyd, P. M. Hanna, R. P. Mason, The origin of the hydroxyl radical oxygen in the Fenton reaction. *Free Radic Biol Med* **22**, 885-888 (1997).

52. T. Masuda, M. Shimazawa, H. Hara, Retinal Diseases Associated with Oxidative Stress and the Effects of a Free Radical Scavenger (Edaravone). *Oxid Med Cell Longev* **2017**, 9208489 (2017).

53. M. P. Murphy, How mitochondria produce reactive oxygen species. *Biochem J* **417**, 1-13 (2009).
54. K. Bedard, K. H. Krause, The NOX family of ROS-generating NADPH oxidases: physiology and pathophysiology. *Physiol Rev* **87**, 245-313 (2007).
55. H. Sies, D. P. Jones, Reactive oxygen species (ROS) as pleiotropic physiological signalling agents. *Nat Rev Mol Cell Biol* **21**, 363-383 (2020).
56. C. Nathan, A. Cunningham-Bussel, Beyond oxidative stress: an immunologist's guide to reactive oxygen species. *Nat Rev Immunol* **13**, 349-361 (2013).
57. N. Bashan, J. Kovsan, I. Kachko, H. Ovadia, A. Rudich, Positive and negative regulation of insulin signaling by reactive oxygen and nitrogen species. *Physiol Rev* **89**, 27-71 (2009).
58. Y. Bhootada *et al.*, Limited ATF4 Expression in Degenerating Retinas with Ongoing ER Stress Promotes Photoreceptor Survival in a Mouse Model of Autosomal Dominant Retinitis Pigmentosa. *PLoS One* **11**, e0154779 (2016).
59. E. B Domènech, G. Marfany, The Relevance of Oxidative Stress in the Pathogenesis and Therapy of Retinal Dystrophies. *Antioxidants (Basel)* **9**, (2020).
60. M. Manevski *et al.*, Cellular stress responses and dysfunctional Mitochondrial-cellular senescence, and therapeutics in chronic respiratory diseases. *Redox Biol* **33**, 101443 (2020).
61. A. Bill, G. Sperber, K. Ujiie, Physiology of the choroidal vascular bed. *Int Ophthalmol* **6**, 101-107 (1983).
62. C. Espinós *et al.*, Oxidative Stress, a Crossroad Between Rare Diseases and Neurodegeneration. *Antioxidants (Basel)* **9**, (2020).
63. C. Martínez-Fernández de la Cámara *et al.*, Altered antioxidant-oxidant status in the aqueous humor and peripheral blood of patients with retinitis pigmentosa. *PLoS One* **8**, e74223 (2013).
64. M. M. Sanz *et al.*, Significant photoreceptor rescue by treatment with a combination of antioxidants in an animal model for retinal degeneration. *Neuroscience* **145**, 1120-1129 (2007).
65. K. Komeima, B. S. Rogers, P. A. Campochiaro, Antioxidants slow photoreceptor cell death in mouse models of retinitis pigmentosa. *J Cell Physiol* **213**, 809-815 (2007).
66. K. Komeima, S. Usui, J. Shen, B. S. Rogers, P. A. Campochiaro, Blockade of neuronal nitric oxide synthase reduces cone cell death in a model of retinitis pigmentosa. *Free Radic Biol Med* **45**, 905-912 (2008).
67. K. Komeima, B. S. Rogers, L. Lu, P. A. Campochiaro, Antioxidants reduce cone cell death in a model of retinitis pigmentosa. *Proc Natl Acad Sci U S A* **103**, 11300-11305 (2006).
68. J. Shen *et al.*, Oxidative damage is a potential cause of cone cell death in retinitis pigmentosa. *J Cell Physiol* **203**, 457-464 (2005).
69. M. Haruta *et al.*, Depleting Rac1 in mouse rod photoreceptors protects them from photo-oxidative stress without affecting their structure or function. *Proc Natl Acad Sci U S A* **106**, 9397-9402 (2009).

70. D. Y. Yu, S. J. Cringle, E. N. Su, P. K. Yu, Intraretinal oxygen levels before and after photoreceptor loss in the RCS rat. *Invest Ophthalmol Vis Sci* **41**, 3999-4006 (2000).

71. D. Y. Yu *et al.*, Photoreceptor death, trophic factor expression, retinal oxygen status, and photoreceptor function in the P23H rat. *Invest Ophthalmol Vis Sci* **45**, 2013-2019 (2004).

72. S. Usui *et al.*, NADPH oxidase plays a central role in cone cell death in retinitis pigmentosa. *J Neurochem* **110**, 1028-1037 (2009).

73. S. Y. Lee *et al.*, N-Acetylcysteine promotes long-term survival of cones in a model of retinitis pigmentosa. *J Cell Physiol* **226**, 1843-1849 (2011).

74. L. Fernández-Sánchez *et al.*, Safranal, a saffron constituent, attenuates retinal degeneration in P23H rats. *PLoS One* **7**, e43074 (2012).

75. S. Usui *et al.*, Increased expression of catalase and superoxide dismutase 2 reduces cone cell death in retinitis pigmentosa. *Mol Ther* **17**, 778-786 (2009).

76. S. Usui *et al.*, Overexpression of SOD in retina: need for increase in H2O2-detoxifying enzyme in same cellular compartment. *Free Radic Biol Med* **51**, 1347-1354 (2011).

77. A. M. Maguire *et al.*, Efficacy, Safety, and Durability of Voretigene Neparvovec-rzyl in RPE65 Mutation-Associated Inherited Retinal Dystrophy: Results of Phase 1 and 3 Trials. *Ophthalmology* **126**, 1273-1285 (2019).

78. D. T. Hartong, E. L. Berson, T. P. Dryja, Retinitis pigmentosa. *Lancet* **368**, 1795-1809 (2006).

79. H. P. Scholl *et al.*, Emerging therapies for inherited retinal degeneration. *Sci Transl Med* **8**, 368rv366 (2016).

80. M. Kutluer, L. Huang, V. Marigo, Targeting molecular pathways for the treatment of inherited retinal degeneration. *Neural Regen Res* **15**, 1784-1791 (2020).

81. J. Bennett, Immune response following intraocular delivery of recombinant viral vectors. *Gene Ther* **10**, 977-982 (2003).

82. N. Kumaran, M. Michaelides, A. J. Smith, R. R. Ali, J. W. B. Bainbridge, Retinal gene therapy. *Br Med Bull* **126**, 13-25 (2018).

83. F. M. Dyka, S. L. Boye, V. A. Chiodo, W. W. Hauswirth, S. E. Boye, Dual adeno-associated virus vectors result in efficient in vitro and in vivo expression of an oversized gene, MYO7A. *Hum Gene Ther Methods* **25**, 166-177 (2014).

84. A. Maddalena *et al.*, Triple Vectors Expand AAV Transfer Capacity in the Retina. *Mol Ther* **26**, 524-541 (2018).

85. J. H. Wilson, T. G. Wensel, The nature of dominant mutations of rhodopsin and implications for gene therapy. *Mol Neurobiol* **28**, 149-158 (2003).

86. M. Diakatou, G. Manes, B. Bocquet, I. Meunier, V. Kalatzis, Genome Editing as a Treatment for the Most Prevalent Causative Genes of Autosomal Dominant Retinitis Pigmentosa. *Int J Mol Sci* **20**, (2019).

87. M. L. Maeder *et al.*, Development of a gene-editing approach to restore vision loss in Leber congenital amaurosis type 10. *Nat Med* **25**, 229-233 (2019).

88. H. P. Scholl *et al.*, Safety and Proof-of-Concept Study of Oral QLT091001 in Retinitis Pigmentosa Due to Inherited Deficiencies of Retinal Pigment Epithelial 65 Protein (RPE65) or Lecithin:Retinol Acyltransferase (LRAT). *PLoS One* **10**, e0143846 (2015).

89. N. Aït-Ali *et al.*, Rod-derived cone viability factor promotes cone survival by stimulating aerobic glycolysis. *Cell* **161**, 817-832 (2015).

90. L. C. Byrne *et al.*, Viral-mediated RdCVF and RdCVFL expression protects cone and rod photoreceptors in retinal degeneration. *J Clin Invest* **125**, 105-116 (2015).

91. M. Cayouette, S. B. Smith, S. P. Becerra, C. Gravel, Pigment epithelium-derived factor delays the death of photoreceptors in mouse models of inherited retinal degenerations. *Neurobiol Dis* **6**, 523-532 (1999).

92. Y. Wang *et al.*, Pigment epithelium-derived factor reduces apoptosis and pro-inflammatory cytokine gene expression in a murine model of focal retinal degeneration. *ASN Neuro* **5**, e00126 (2013).

93. J. Kenealey *et al.*, Small Retinoprotective Peptides Reveal a Receptor-binding Region on Pigment Epithelium-derived Factor. *J Biol Chem* **290**, 25241-25253 (2015).

94. A. Comitato *et al.*, Pigment epithelium-derived factor hinders photoreceptor cell death by reducing intracellular calcium in the degenerating retina. *Cell Death Dis* **9**, 560 (2018).

95. D. A. Fox, A. T. Poblenz, L. He, Calcium overload triggers rod photoreceptor apoptotic cell death in chemical-induced and inherited retinal degenerations. *Ann N Y Acad Sci* **893**, 282-285 (1999).

96. M. Power *et al.*, Cellular mechanisms of hereditary photoreceptor degeneration - Focus on cGMP. *Prog Retin Eye Res* **74**, 100772 (2020).

97. P. A. Campochiaro *et al.*, Oral N-acetylcysteine improves cone function in retinitis pigmentosa patients in phase I trial. *J Clin Invest* **130**, 1527-1541 (2020).

98. J. Duebel, K. Marazova, J. A. Sahel, Optogenetics. *Curr Opin Ophthalmol* **26**, 226-232 (2015).

99. M. P. Simunovic *et al.*, Optogenetic approaches to vision restoration. *Exp Eye Res* **178**, 15-26 (2019).

100. M. H. Berry *et al.*, Restoration of high-sensitivity and adapting vision with a cone opsin. *Nat Commun* **10**, 1221 (2019).

101. I. Vázquez-Domínguez, A. Garanto, R. W. J. Collin, Molecular Therapies for Inherited Retinal Diseases-Current Standing, Opportunities and Challenges. *Genes (Basel)* **10**, (2019).

102. F. Osakada *et al.*, In vitro differentiation of retinal cells from human pluripotent stem cells by small-molecule induction. *J Cell Sci* **122**, 3169-3179 (2009).

103. F. Osakada *et al.*, Toward the generation of rod and cone photoreceptors from mouse, monkey and human embryonic stem cells. *Nat Biotechnol* **26**, 215-224 (2008).

104. F. Giordano, A. De Marzo, F. Vetrini, V. Marigo, Fibroblast growth factor and epidermal growth factor differently affect differentiation of murine retinal stem cells in vitro. *Mol Vis* **13**, 1842-1850 (2007).

105. G. C. Demontis, C. Aruta, A. Comitato, A. De Marzo, V. Marigo, Functional and molecular characterization of rod-like cells from retinal stem cells derived from the adult ciliary epithelium. *PLoS One* **7**, e33338 (2012).

106. S. D. Schwartz *et al.*, Human embryonic stem cell-derived retinal pigment epithelium in patients with age-related macular degeneration and Stargardt's macular dystrophy: follow-up of two open-label phase 1/2 studies. *Lancet* **385**, 509-516 (2015).

107. R. C. Friedman, K. K. Farh, C. B. Burge, D. P. Bartel, Most mammalian mRNAs are conserved targets of microRNAs. *Genome Res* **19**, 92-105 (2009).

108. Y. K. Kim, V. N. Kim, Processing of intronic microRNAs. *EMBO J* **26**, 775-783 (2007).

109. D. de Rie *et al.*, An integrated expression atlas of miRNAs and their promoters in human and mouse. *Nat Biotechnol* **35**, 872-878 (2017).

110. M. Ha, V. N. Kim, Regulation of microRNA biogenesis. *Nat Rev Mol Cell Biol* **15**, 509-524 (2014).

111. A. Rodriguez, S. Griffiths-Jones, J. L. Ashurst, A. Bradley, Identification of mammalian microRNA host genes and transcription units. *Genome Res* **14**, 1902-1910 (2004).

112. D. L. Corcoran *et al.*, Features of mammalian microRNA promoters emerge from polymerase II chromatin immunoprecipitation data. *PLoS One* **4**, e5279 (2009).

113. S. Baskerville, D. P. Bartel, Microarray profiling of microRNAs reveals frequent coexpression with neighboring miRNAs and host genes. *RNA* **11**, 241-247 (2005).

114. Y. Tay, J. Zhang, A. M. Thomson, B. Lim, I. Rigoutsos, MicroRNAs to Nanog, Oct4 and Sox2 coding regions modulate embryonic stem cell differentiation. *Nature* **455**, 1124-1128 (2008).

115. J. R. Lytle, T. A. Yario, J. A. Steitz, Target mRNAs are repressed as efficiently by microRNA-binding sites in the 5' UTR as in the 3' UTR. *Proc Natl Acad Sci U S A* **104**, 9667-9672 (2007).

116. J. P. Broughton, M. T. Lovci, J. L. Huang, G. W. Yeo, A. E. Pasquinelli, Pairing beyond the Seed Supports MicroRNA Targeting Specificity. *Mol Cell* **64**, 320-333 (2016).

117. M. J. Moore *et al.*, miRNA-target chimeras reveal miRNA 3'-end pairing as a major determinant of Argonaute target specificity. *Nat Commun* **6**, 8864 (2015).

118. J. Krol, I. Loedige, W. Filipowicz, The widespread regulation of microRNA biogenesis, function and decay. *Nat Rev Genet* **11**, 597-610 (2010).

119. M. H. Jo *et al.*, Human Argonaute 2 Has Diverse Reaction Pathways on Target RNAs. *Mol Cell* **59**, 117-124 (2015).

120. H. C. Martin *et al.*, Imperfect centered miRNA binding sites are common and can mediate repression of target mRNAs. *Genome Biol* **15**, R51 (2014).

121. S. Jonas, E. Izaurralde, Towards a molecular understanding of microRNA-mediated gene silencing. *Nat Rev Genet* **16**, 421-433 (2015).

122. A. Eulalio, E. Huntzinger, E. Izaurralde, GW182 interaction with Argonaute is essential for miRNA-mediated translational repression and mRNA decay. *Nat Struct Mol Biol* **15**, 346-353 (2008).

123. A. Fukao *et al.*, MicroRNAs trigger dissociation of eIF4AI and eIF4AII from target mRNAs in humans. *Mol Cell* **56**, 79-89 (2014).

124. S. S. Truesdell *et al.*, MicroRNA-mediated mRNA translation activation in quiescent cells and oocytes involves recruitment of a nuclear microRNP. *Sci Rep* **2**, 842 (2012).

125. S. Vasudevan, J. A. Steitz, AU-rich-element-mediated upregulation of translation by FXR1 and Argonaute 2. *Cell* **128**, 1105-1118 (2007).

126. U. A. Ørom, F. C. Nielsen, A. H. Lund, MicroRNA-10a binds the 5'UTR of ribosomal protein mRNAs and enhances their translation. *Mol Cell* **30**, 460-471 (2008).

127. L. P. Lim *et al.*, Microarray analysis shows that some microRNAs downregulate large numbers of target mRNAs. *Nature* **433**, 769-773 (2005).

128. M. S. Ebert, P. A. Sharp, Roles for microRNAs in conferring robustness to biological processes. *Cell* **149**, 515-524 (2012).

129. H. Herranz, S. M. Cohen, MicroRNAs and gene regulatory networks: managing the impact of noise in biological systems. *Genes Dev* **24**, 1339-1344 (2010).

130. E. Andrés-León, D. González Peña, G. Gómez-López, D. G. Pisano, miRGate: a curated database of human, mouse and rat miRNA-mRNA targets. *Database (Oxford)* **2015**, bav035 (2015).

131. V. Ambros, MicroRNAs and developmental timing. *Curr Opin Genet Dev* **21**, 511-517 (2011).

132. H. Y. Cheng *et al.*, microRNA modulation of circadian-clock period and entrainment. *Neuron* **54**, 813-829 (2007).

133. A. Shenoy, R. H. Blelloch, Regulation of microRNA function in somatic stem cell proliferation and differentiation. *Nat Rev Mol Cell Biol* **15**, 565-576 (2014).

134. K. N. Ivey, D. Srivastava, MicroRNAs as regulators of differentiation and cell fate decisions. *Cell Stem Cell* **7**, 36-41 (2010).

135. P. Xu, M. Guo, B. A. Hay, MicroRNAs and the regulation of cell death. *Trends Genet* **20**, 617-624 (2004).

136. C. Z. Chen, L. Li, H. F. Lodish, D. P. Bartel, MicroRNAs modulate hematopoietic lineage differentiation. *Science* **303**, 83-86 (2004).

137. V. Ambros, The functions of animal microRNAs. *Nature* **431**, 350-355 (2004).

138. T. Y. Ha, MicroRNAs in Human Diseases: From Cancer to Cardiovascular Disease. *Immune Netw* **11**, 135-154 (2011).

139. S. Sharma, H. C. Lu, microRNAs in Neurodegeneration: Current Findings and Potential Impacts. *J Alzheimers Dis Parkinsonism* **8**, (2018).

140. X. Chen *et al.*, Characterization of microRNAs in serum: a novel class of biomarkers for diagnosis of cancer and other diseases. *Cell Res* **18**, 997-1006 (2008).

141. G. L. Romano *et al.*, Retinal and Circulating miRNAs in Age-Related Macular Degeneration: An. *Front Pharmacol* **8**, 168 (2017).

142. J. D. Arroyo *et al.*, Argonaute2 complexes carry a population of circulating microRNAs independent of vesicles in human plasma. *Proc Natl Acad Sci U S A* **108**, 5003-5008 (2011).

143. A. Machida, T. Ohkubo, T. Yokota, Circulating microRNAs in the cerebrospinal fluid of patients with brain diseases. *Methods Mol Biol* **1024**, 203-209 (2013).

144. Y. F. Xiao *et al.*, microRNA detection in feces, sputum, pleural effusion and urine: novel tools for cancer screening (Review). *Oncol Rep* **30**, 535-544 (2013).

145. M. Ragusa *et al.*, MicroRNAs in vitreus humor from patients with ocular diseases. *Mol Vis* **19**, 430-440 (2013).

146. H. Iftikhar, G. E. Carney, Evidence and potential in vivo functions for biofluid miRNAs: From expression profiling to functional testing: Potential roles of extracellular miRNAs as indicators of physiological change and as agents of intercellular information exchange. *Bioessays* **38**, 367-378 (2016).

147. T. R. Sundermeier, K. Palczewski, The physiological impact of microRNA gene regulation in the retina. *Cell Mol Life Sci* **69**, 2739-2750 (2012).

148. M. Karali *et al.*, miRNeye: a microRNA expression atlas of the mouse eye. *BMC Genomics* **11**, 715 (2010).

149. M. Karali *et al.*, High-resolution analysis of the human retina miRNome reveals isomiR variations and novel microRNAs. *Nucleic Acids Res* **44**, 1525-1540 (2016).

150. E. Bernstein *et al.*, Dicer is essential for mouse development. *Nat Genet* **35**, 215-217 (2003).

151. D. Damiani *et al.*, Dicer inactivation leads to progressive functional and structural degeneration of the mouse retina. *J Neurosci* **28**, 4878-4887 (2008).

152. R. Pinter, R. Hindges, Perturbations of microRNA function in mouse dicer mutants produce retinal defects and lead to aberrant axon pathfinding at the optic chiasm. *PLoS One* **5**, e10021 (2010).

153. A. Iida, T. Shinoe, Y. Baba, H. Mano, S. Watanabe, Dicer plays essential roles for retinal development by regulation of survival and differentiation. *Invest Ophthalmol Vis Sci* **52**, 3008-3017 (2011).

154. S. A. Georgi, T. A. Reh, Dicer is required for the transition from early to late progenitor state in the developing mouse retina. *J Neurosci* **30**, 4048-4061 (2010).

155. N. Davis, E. Mor, R. Ashery-Padan, Roles for Dicer1 in the patterning and differentiation of the optic cup neuroepithelium. *Development* **138**, 127-138 (2011).

156. M. Zuzic, J. E. Rojo Arias, S. G. Wohl, V. Busskamp, Retinal miRNA Functions in Health and Disease. *Genes (Basel)* **10**, (2019).

157. T. R. Sundermeier *et al.*, DICER1 is essential for survival of postmitotic rod photoreceptor cells in mice. *FASEB J* **28**, 3780-3791 (2014).

158. V. Busskamp *et al.*, miRNAs 182 and 183 are necessary to maintain adult cone photoreceptor outer segments and visual function. *Neuron* **83**, 586-600 (2014).

159. E. Z. Aldunate *et al.*, Conditional Dicer1 depletion using Chrnb4-Cre leads to cone cell death and impaired photopic vision. *Sci Rep* **9**, 2314 (2019).

160. A. La Torre, S. Georgi, T. A. Reh, Conserved microRNA pathway regulates developmental timing of retinal neurogenesis. *Proc Natl Acad Sci U S A* **110**, E2362-2370 (2013).

161. M. Karali, I. Peluso, V. Marigo, S. Banfi, Identification and characterization of microRNAs expressed in the mouse eye. *Invest Ophthalmol Vis Sci* **48**, 509-515 (2007).

162. R. Sanuki *et al.*, miR-124a is required for hippocampal axogenesis and retinal cone survival through Lhx2 suppression. *Nat Neurosci* **14**, 1125-1134 (2011).

163. S. Lumayag *et al.*, Inactivation of the microRNA-183/96/182 cluster results in syndromic retinal degeneration. *Proc Natl Acad Sci U S A* **110**, E507-516 (2013).

164. Q. Zhu *et al.*, Sponge transgenic mouse model reveals important roles for the microRNA-183 (miR-183)/96/182 cluster in postmitotic photoreceptors of the retina. *J Biol Chem* **286**, 31749-31760 (2011).

165. J. H. Wu *et al.*, Altered microRNA expression profiles in retinas with diabetic retinopathy. *Ophthalmic Res* **47**, 195-201 (2012).

166. C. J. Loscher *et al.*, Altered retinal microRNA expression profile in a mouse model of retinitis pigmentosa. *Genome Biol* **8**, R248 (2007).

167. C. J. Loscher *et al.*, A common microRNA signature in mouse models of retinal degeneration. *Exp Eye Res* **87**, 529-534 (2008).

168. A. Anasagasti *et al.*, Expression Profiling Analysis Reveals Key MicroRNA-mRNA Interactions in Early Retinal Degeneration in Retinitis Pigmentosa. *Invest Ophthalmol Vis Sci* **59**, 2381-2392 (2018).

169. I. Conte *et al.*, MiR-204 is responsible for inherited retinal dystrophy associated with ocular coloboma. *Proc Natl Acad Sci U S A* **112**, E3236-3245 (2015).

170. S. Xu, P. D. Witmer, S. Lumayag, B. Kovacs, D. Valle, MicroRNA (miRNA) transcriptome of mouse retina and identification of a sensory organ-specific miRNA cluster. *J Biol Chem* **282**, 25053-25066 (2007).

171. M. Deo, J. Y. Yu, K. H. Chung, M. Tippens, D. L. Turner, Detection of mammalian microRNA expression by in situ hybridization with RNA oligonucleotides. *Dev Dyn* **235**, 2538-2548 (2006).

172. I. Conte *et al.*, miR-204 is required for lens and retinal development via Meis2 targeting. *Proc Natl Acad Sci U S A* **107**, 15491-15496 (2010).

173. R. Avellino *et al.*, miR-204 targeting of Ankrd13A controls both mesenchymal neural crest and lens cell migration. *PLoS One* **8**, e61099 (2013).

174. F. Q. Liang, V. Anand, A. M. Maguire, J. Bennett, Intraocular delivery of recombinant virus. *Methods Mol Med* **47**, 125-139 (2001).

175. S. Barbato *et al.*, MiR-211 is essential for adult cone photoreceptor maintenance and visual function. *Sci Rep* **7**, 17004 (2017).

176. M. Hildinger *et al.*, Hybrid vectors based on adeno-associated virus serotypes 2 and 5 for muscle-directed gene transfer. *J Virol* **75**, 6199-6203 (2001).

177. M. Karali *et al.*, AAV-miR-204 Protects from Retinal Degeneration by Attenuation of Microglia Activation and Photoreceptor Cell Death. *Mol Ther Nucleic Acids* **19**, 144-156 (2020).

178. M. Allocca *et al.*, Novel adeno-associated virus serotypes efficiently transduce murine photoreceptors. *J Virol* **81**, 11372-11380 (2007).

179. J. G. Flannery *et al.*, Efficient photoreceptor-targeted gene expression in vivo by recombinant adeno-associated virus. *Proc Natl Acad Sci U S A* **94**, 6916-6921 (1997).

180. M. A. Denti, A. Rosa, O. Sthandier, F. G. De Angelis, I. Bozzoni, A new vector, based on the PolII promoter of the U1 snRNA gene, for the expression of siRNAs in mammalian cells. *Mol Ther* **10**, 191-199 (2004).

181. M. Pinelli *et al.*, An atlas of gene expression and gene co-regulation in the human retina. *Nucleic Acids Res* **44**, 5773-5784 (2016).

182. d. W. Huang, B. T. Sherman, R. A. Lempicki, Systematic and integrative analysis of large gene lists using DAVID bioinformatics resources. *Nat Protoc* **4**, 44-57 (2009).

183. S. Botta *et al.*, Targeting and silencing of rhodopsin by ectopic expression of the transcription factor KLF15. *JCI Insight* **2**, (2017).

184. R. Scholz *et al.*, Minocycline counter-regulates pro-inflammatory microglia responses in the retina and protects from degeneration. *J Neuroinflammation* **12**, 209 (2015).

185. Y. Kanan, G. Moiseyev, N. Agarwal, J. X. Ma, M. R. Al-Ubaidi, Light induces programmed cell death by activating multiple independent proteases in a cone photoreceptor cell line. *Invest Ophthalmol Vis Sci* **48**, 40-51 (2007).

186. C. A. Grant, S. Ponnazhagan, X. S. Wang, A. Srivastava, T. Li, Evaluation of recombinant adeno-associated virus as a gene transfer vector for the retina. *Curr Eye Res* **16**, 949-956 (1997).

187. H. Kolb, E. Fernandez, R. Nelson. (1995).

188. N. Cuenca *et al.*, Cellular responses following retinal injuries and therapeutic approaches for neurodegenerative diseases. *Prog Retin Eye Res* **43**, 17-75 (2014).

189. G. C. Brown, J. J. Neher, Microglial phagocytosis of live neurons. *Nat Rev Neurosci* **15**, 209-216 (2014).

190. S. M. Peterson *et al.*, Common features of microRNA target prediction tools. *Front Genet* **5**, 23 (2014).

191. M. D. Paraskevopoulou *et al.*, DIANA-microT web server v5.0: service integration into miRNA functional analysis workflows. *Nucleic Acids Res* **41**, W169-173 (2013).

192. B. P. Lewis, C. B. Burge, D. P. Bartel, Conserved seed pairing, often flanked by adenosines, indicates that thousands of human genes are microRNA targets. *Cell* **120**, 15-20 (2005).

193. V. A. Gennarino *et al.*, HOCTAR database: a unique resource for microRNA target prediction. *Gene* **480**, 51-58 (2011).

194. V. A. Gennarino *et al.*, MicroRNA target prediction by expression analysis of host genes. *Genome Res* **19**, 481-490 (2009).

195. H. Rempel, C. Calosing, B. Sun, L. Pulliam, Sialoadhesin expressed on IFN-induced monocytes binds HIV-1 and enhances infectivity. *PLoS One* **3**, e1967 (2008).

196. T. K. van den Berg *et al.*, Sialoadhesin on macrophages: its identification as a lymphocyte adhesion molecule. *J Exp Med* **176**, 647-655 (1992).

197. J. Groh *et al.*, Sialoadhesin promotes neuroinflammation-related disease progression in two mouse models of CLN disease. *Glia* **64**, 792-809 (2016).

198. M. Yabal *et al.*, XIAP restricts TNF- and RIP3-dependent cell death and inflammasome activation. *Cell Rep* **7**, 1796-1808 (2014).

199. Y. Xia, R. Novak, J. Lewis, C. S. Duckett, A. C. Phillips, Xaf1 can cooperate with TNFalpha in the induction of apoptosis, independently of interaction with XIAP. *Mol Cell Biochem* **286**, 67-76 (2006).

200. K. C. Leonard *et al.*, XIAP protection of photoreceptors in animal models of retinitis pigmentosa. *PLoS One* **2**, e314 (2007).

201. D. Petrin *et al.*, Structural and functional protection of photoreceptors from MNU-induced retinal degeneration by the X-linked inhibitor of apoptosis. *Invest Ophthalmol Vis Sci* **44**, 2757-2763 (2003).

202. T. Clément, V. Salone, M. Rederstorff, Dual luciferase gene reporter assays to study miRNA function. *Methods Mol Biol* **1296**, 187-198 (2015).

203. M. Karlstetter *et al.*, Retinal microglia: just bystander or target for therapy? *Prog Retin Eye Res* **45**, 30-57 (2015).

204. A. Henn *et al.*, The suitability of BV2 cells as alternative model system for primary microglia cultures or for animal experiments examining brain inflammation. *ALTEX* **26**, 83-94 (2009).

205. C. Martínez-Fernández de la Cámara *et al.*, Adalimumab Reduces Photoreceptor Cell Death in A Mouse Model of Retinal Degeneration. *Sci Rep* **5**, 11764 (2015).

206. A. M. Rosario *et al.*, Microglia-specific targeting by novel capsid-modified AAV6 vectors. *Mol Ther Methods Clin Dev* **3**, 16026 (2016).

207. M. R. Al-Ubaidi, H. Matsumoto, S. Kurono, A. Singh, Proteomics profiling of the cone photoreceptor cell line, 661W. *Adv Exp Med Biol* **613**, 301-311 (2008).

208. I. M. Helmy, A. M. Azim, Efficacy of ImageJ in the assessment of apoptosis. *Diagn Pathol* **7**, 15 (2012).

209. J. R. Eidet, L. Pasovic, R. Maria, C. J. Jackson, T. P. Utheim, Objective assessment of changes in nuclear morphology and cell distribution following induction of apoptosis. *Diagn Pathol* **9**, 92 (2014).

210. X. D. Zhang, A pair of new statistical parameters for quality control in RNA interference high-throughput screening assays. *Genomics* **89**, 552-561 (2007).

211. X. D. Zhang, Novel analytic criteria and effective plate designs for quality control in genome-scale RNAi screens. *J Biomol Screen* **13**, 363-377 (2008).

212. W. J. Lukiw, B. Surjyadipta, P. Dua, P. N. Alexandrov, Common micro RNAs (miRNAs) target complement factor H (CFH) regulation in Alzheimer's disease (AD) and in age-related macular degeneration (AMD). *Int J Biochem Mol Biol* **3**, 105-116 (2012).

213. D. T. Organisciak, D. K. Vaughan, Retinal light damage: mechanisms and protection. *Prog Retin Eye Res* **29**, 113-134 (2010).

214. N. Sanvicens, V. Gómez-Vicente, I. Masip, A. Messeguer, T. G. Cotter, Oxidative stress-induced apoptosis in retinal photoreceptor cells is mediated by calpains and caspases and blocked by the oxygen radical scavenger CR-6. *J Biol Chem* **279**, 39268-39278 (2004).

215. V. E. Baksheeva *et al.*, Suppression of Light-Induced Oxidative Stress in the Retina by Mitochondria-Targeted Antioxidant. *Antioxidants (Basel)* **8**, (2018).

216. N. Di Marzo, E. Chisci, R. Giovannoni, The Role of Hydrogen Peroxide in Redox-Dependent Signaling: Homeostatic and Pathological Responses in Mammalian Cells. *Cells* **7**, (2018).

217. H. Kawashima *et al.*, Neuroprotective and vision-protective effect of preserving ATP levels by AMPK activator. *FASEB J* **34**, 5016-5026 (2020).

218. L. Xu, L. Kong, J. Wang, J. D. Ash, Stimulation of AMPK prevents degeneration of photoreceptors and the retinal pigment epithelium. *Proc Natl Acad Sci U S A* **115**, 10475-10480 (2018).

219. S. Wang, P. Song, M. H. Zou, AMP-activated protein kinase, stress responses and cardiovascular diseases. *Clin Sci (Lond)* **122**, 555-573 (2012).

220. D. Garcia, R. J. Shaw, AMPK: Mechanisms of Cellular Energy Sensing and Restoration of Metabolic Balance. *Mol Cell* **66**, 789-800 (2017).

221. S. Guo, C. Chen, F. Ji, L. Mao, Y. Xie, PP2A catalytic subunit silence by microRNA-429 activates AMPK and protects osteoblastic cells from dexamethasone. *Biochem Biophys Res Commun* **487**, 660-665 (2017).

222. T. A. Dite *et al.*, AMP-activated protein kinase selectively inhibited by the type II inhibitor SBI-0206965. *J Biol Chem* **293**, 8874-8885 (2018).

223. D. Vlachantoni *et al.*, Evidence of severe mitochondrial oxidative stress and a protective effect of low oxygen in mouse models of inherited photoreceptor degeneration. *Hum Mol Genet* **20**, 322-335 (2011).

224. J. T. Hancock, R. Desikan, S. J. Neill, Role of reactive oxygen species in cell signalling pathways. *Biochem Soc Trans* **29**, 345-350 (2001).

225. R. Natoli *et al.*, The Role of Pyruvate in Protecting 661W Photoreceptor-Like Cells Against Light-Induced Cell Death. *Curr Eye Res* **41**, 1473-1481 (2016).

226. S. Guo *et al.*, Activating AMP-activated protein kinase by an α1 selective activator compound 13 attenuates dexamethasone-induced osteoblast cell death. *Biochem Biophys Res Commun* **471**, 545-552 (2016).

227. W. Liu *et al.*, Targeted activation of AMPK by GSK621 ameliorates H2O2-induced damages in osteoblasts. *Oncotarget* **8**, 10543-10552 (2017).

228. J. Hanna, G. S. Hossain, J. Kocerha, The Potential for microRNA Therapeutics and Clinical Research. *Front Genet* **10**, 478 (2019).